Chen

Princeton University
PLASMA PHYSICS LABORATORY
Princeton, New Jersey

Preliminary Studies of a Reflex Arc

R. L. Bingham, F. F. Chen,
and W. L. Harries

MATT-63

February 1, 1962

PLASMA PHYSICS LABORATORY

Contract AT(30-1)—1238 with the
US Atomic Energy Commission

PRINCETON UNIVERSITY

PRINCETON, NEW JERSEY

Princeton University
PLASMA PHYSICS LABORATORY
Princeton, New Jersey

Preliminary Studies of a Reflex Arc

R. L. Bingham, F. F. Chen,
and W. L. Harries

MATT-63 February 1, 1962

AEC Research and Development Report

This work was supported under Contract AT(30-1)-1238 with the Atomic Energy Commission.

CONTENTS

Preliminary Studies of a Reflex Arc

R. L. Bingham, F. F. Chen, and W. L. Harries
Plasma Physics Laboratory, Princeton University
Princeton, New Jersey

ABSTRACT

The operation of a 5-to 11-foot long 2 in. diameter hot-cathode helium discharge in a strong magnetic field has been investigated. The geometry is that of a Philips Ionization Gauge, and the cathode was a solid slab of tungsten heated to emission by electron bombardment. Because of the reduction in transverse diffusion of electrons caused by the magnetic field, the potential in the center of the discharge was found to be depressed to nearly the cathode potential. Consequently, most of the ionization occurs near the edge of the discharge, and the density and electron temperature on the axis are also somewhat lower than at larger radii. Since enhanced diffusion is likely to be important in the operation of such a discharge, the characteristics of the potential fluctuations in the plasma were studied as well as the time-averaged characteristics of the arc. The frequency spectrum was found to be concentrated at very low frequencies, and rms values of the hash followed the radial variation of electron temperature. An azimuthal asymmetry and rotation of the arc column were discovered which made quantitative comparison with theory difficult. However, what theoretical progress has been made has been included in this report. Partly because of difficulties with maintaining a stable discharge over a large range of pressures and fields, this preliminary study was largely confined to a standard operating condition of 4000 gauss, 15 ampere discharge current, and 3 microns pressure.

I. Introduction

In an attempt to develop a steady d.c. plasma source, we have studied Phillips Ionization Gauge (PIG) type discharges. From unpublished data obtained from our L-1 machine, operated as a cold cathode PIG, several disadvantages of this approach are evident.

1) In order to obtain sufficient emission from the cold cathode, high electric fields and hence high operating potentials are required. This has two undesirable effects, namely the need to couple the diagnostic apparatus to these high voltages and also the fact that any potential fluctuations on the electrodes, even if small compared to the d.c. voltages, generate large signals which tend to mask plasma oscillations under study.

2) The cathode surface plays an important part in discharges of this type. With aluminum cathodes, for example, the emission depended on the oxide coating of the surface, and as the oxide wore off the emissivity decreased until strong filamentary arcs developed and stable discharges could not be maintained. The average aluminum cathode had a lifetime of about 50 10-sec discharges. An aging effect could also be observed with pure tungsten or molybdenum cathodes. If the discharge was left on, the current would gradually drop as the cathode heated up[1]. The original operating characteristic would again be seen, however, if the machine were turned off for a few minutes. This drift of the discharge conditions was unsuitable for detailed plasma studies.

3) In order to obtain sufficiently high plasma densities (approx. 10^{13} cm^{-3}), it was necessary to have a neutral helium pressure of 75 to 100

microns. At this pressure the ionization was less than 1%, and the plasma was completely dominated by the presence of the neutral particles. When attempts were made to increase the ionization by discharging a condenser bank across the PIG, filamentary arcs appeared. Reducing the neutral pressure changed the whole character of the discharge without increasing the percentage ionization.

As a result of these observations, it was felt that a thermionically emitting cathode would be desirable. In particular, if emission could be maintained at a high enough level to provide a space charge cloud of electrons in front of the cathode, variations in cathode surface properties would no longer be important. Furthermore, with an emitting cathode the potentials applied to the plasma could be very much lower. If the temperature of the cathode is high enough, there will be sufficient primary emission to draw substantial discharge currents at these lower potentials so that there will be less likelihood for arcing while still allowing the possibility of higher percentage ionization than in the cold cathode case. Should these expectations be fulfilled, it would be possible to use a lower neutral gas pressure to obtain a given plasma density. In this way a hot cathode could be expected to give considerable improvement in all three areas where the cold cathodes were deficient.

It was decided to use a pure tungsten cathode heated to emission temperatures rather than a coated cathode for several reasons. Coated cathodes are difficult to handle and require long and careful outgassing procedures. As

our machine would be opened up to air for changes in diagnostics etc. quite frequently, some types of coated cathodes would have to be replaced while others would require reactivation. In contrast, the hot tungsten cathode would be unaffected by exposure to air and require no activation, although, of course, it would have to be heated to a higher temperature than the coated cathodes. It was also difficult to predict in advance the damage that ion bombardment from the discharge might do to a coated cathode.

This report will describe our preliminary studies on the L-2 device using a hot tungsten cathode. Precise measurements have so far not been possible because of a basic inhomogeneity which our survey has revealed. It is felt at present that this is a dense rotating plasma filament, somehow connected with the sheath at the hot cathode. As long as this persists, definitive conclusions are difficult to attain. Nevertheless enough work has been done to give some understanding of the processes involved and permit use of our plasma for further experiments.

Section II gives a description of the L-2 plasma source, and Section III will summarize the experiments performed and the results obtained. For convenience this chapter has been divided into two major parts; the first half gives a review of the time average experiments while the remainder discusses results having variations in time. Section IV presents qualitative explanations for the experimental observations. In an Appendix we discuss our probes and the techniques we have learned in their use.

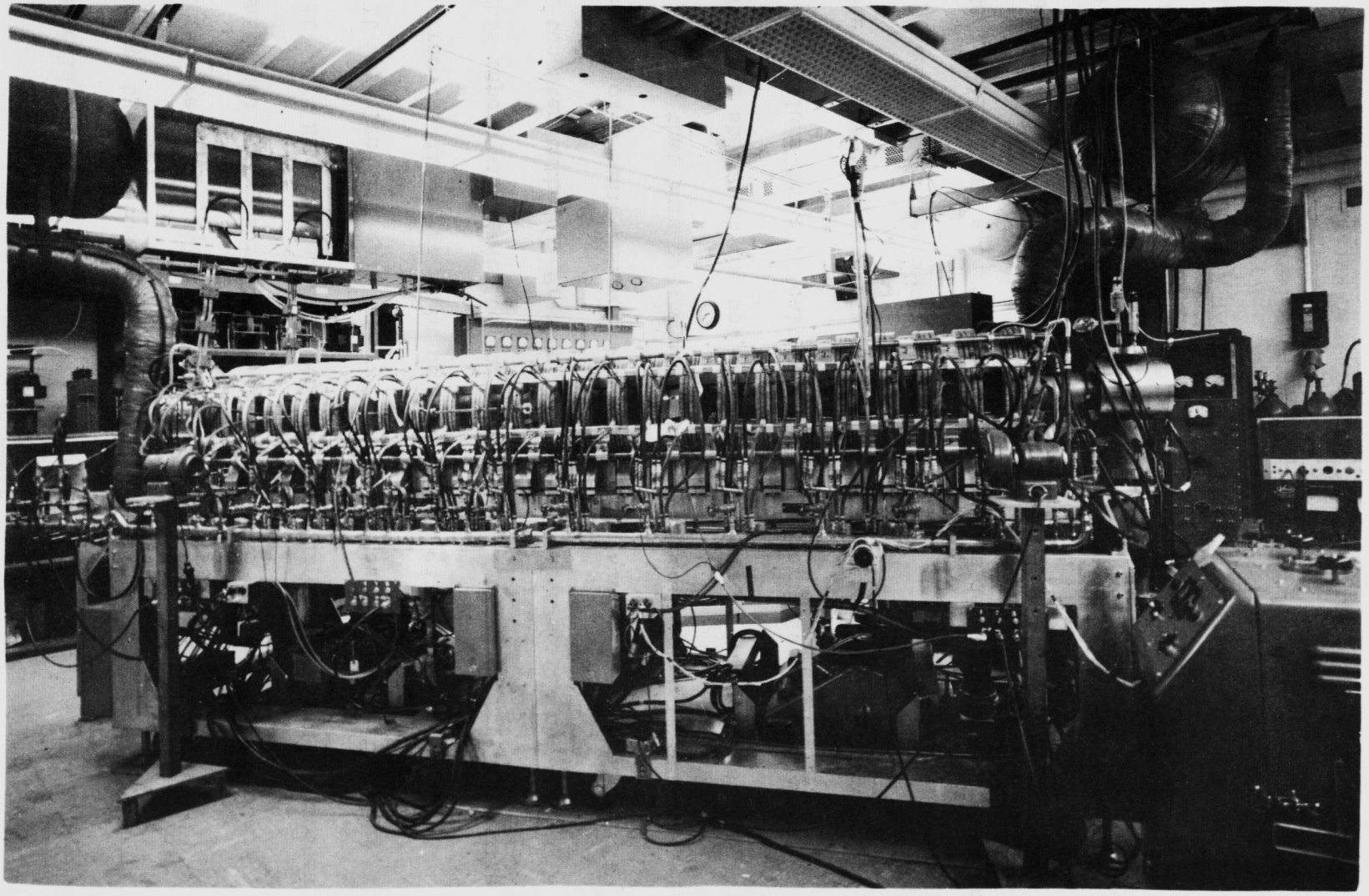

FIG. 2.1 THE L-2 MACHINE

II. Physical Description of Machine

A physical description of the L-2 device has been given previously.[2] Figure 2.1 shows the machine as it stands in the laboratory. In the indicated coil geometry of equal lengths of coil and gap a steady magnetic field of 5000 gauss uniform to ± 1% can be maintained.

A diagram of the stainless steel vacuum chamber is given in Figure 2.2. The end sections are grounded and contain both the cathodes for the discharge and the pumping ports. The insulated center section of the tube serves as the anode. At five locations along the anode section there are ports for diagnostic equipment, three ports around the circumference at each location. These ports have been used principally for probes and, near the center, for a microwave density measuring apparatus. Also shown in Figure 2.2 is the 100 KW discharge supply with its filtering circuits to eliminate the three-phase ripple. The series resistors give an essentially constant direct current source across the machine.

One of our two cathodes is a tungsten disc, supported on 3 spring loaded tungsten legs, which is heated by electron bombardment to a temperature of about 2700°K. In order to have the discharge side of the cathode at a uniform temperature, the disc thickness was chosen as 1/4", a length about equal to the spacing of the wires in the spiral filament providing the bombarding current. The cathode diameter is 2.2". The filament is heated by an 800 cycle supply, well above the mechanical resonsance frequency, to prevent deformation in the magnetic field and is biased negative with respect to the cathode so as to provide 6 KW to the cathode. Behind the filament are

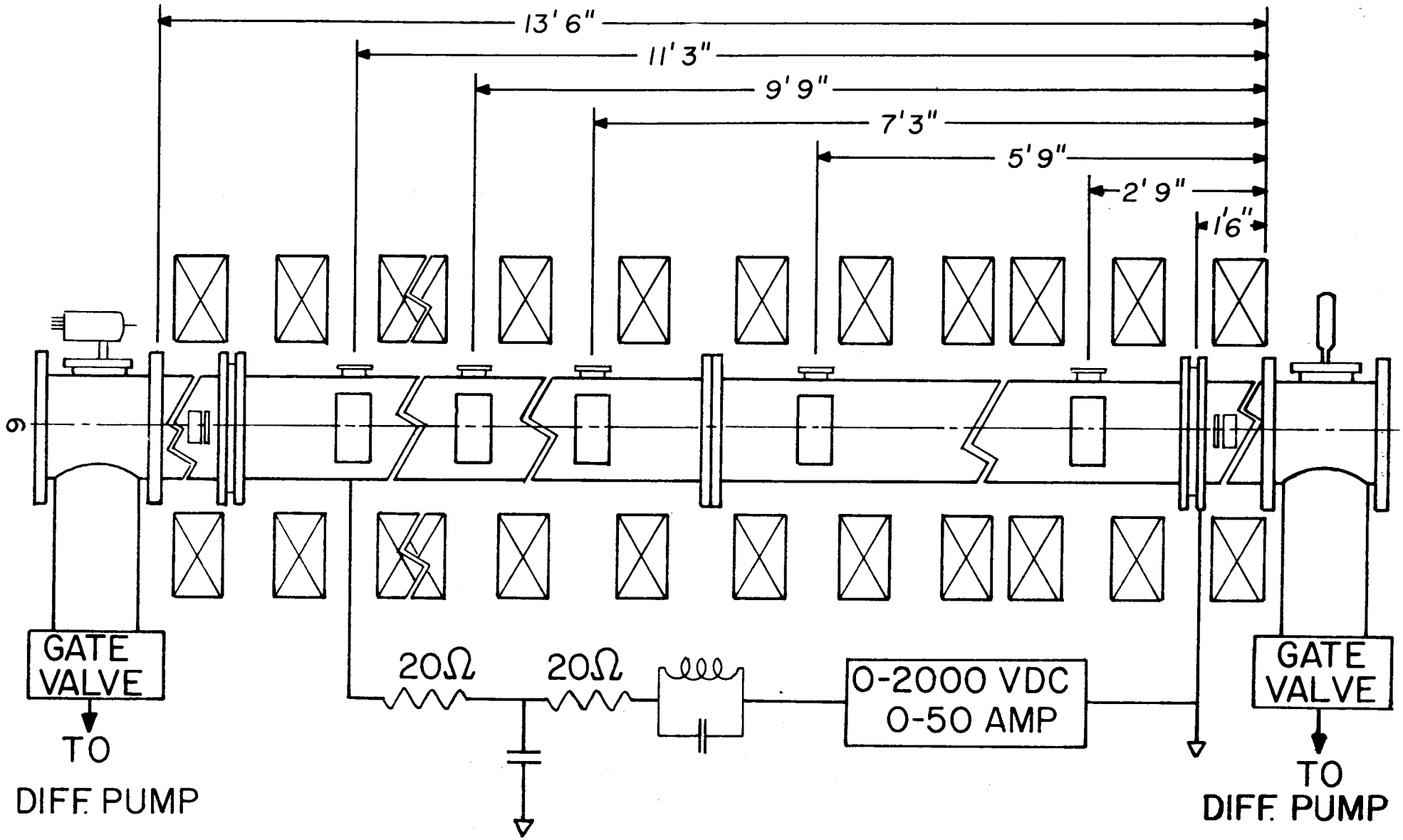

FIG. 2.2 DIAGRAM OF STAINLESS STEEL VACUUM CHAMBER

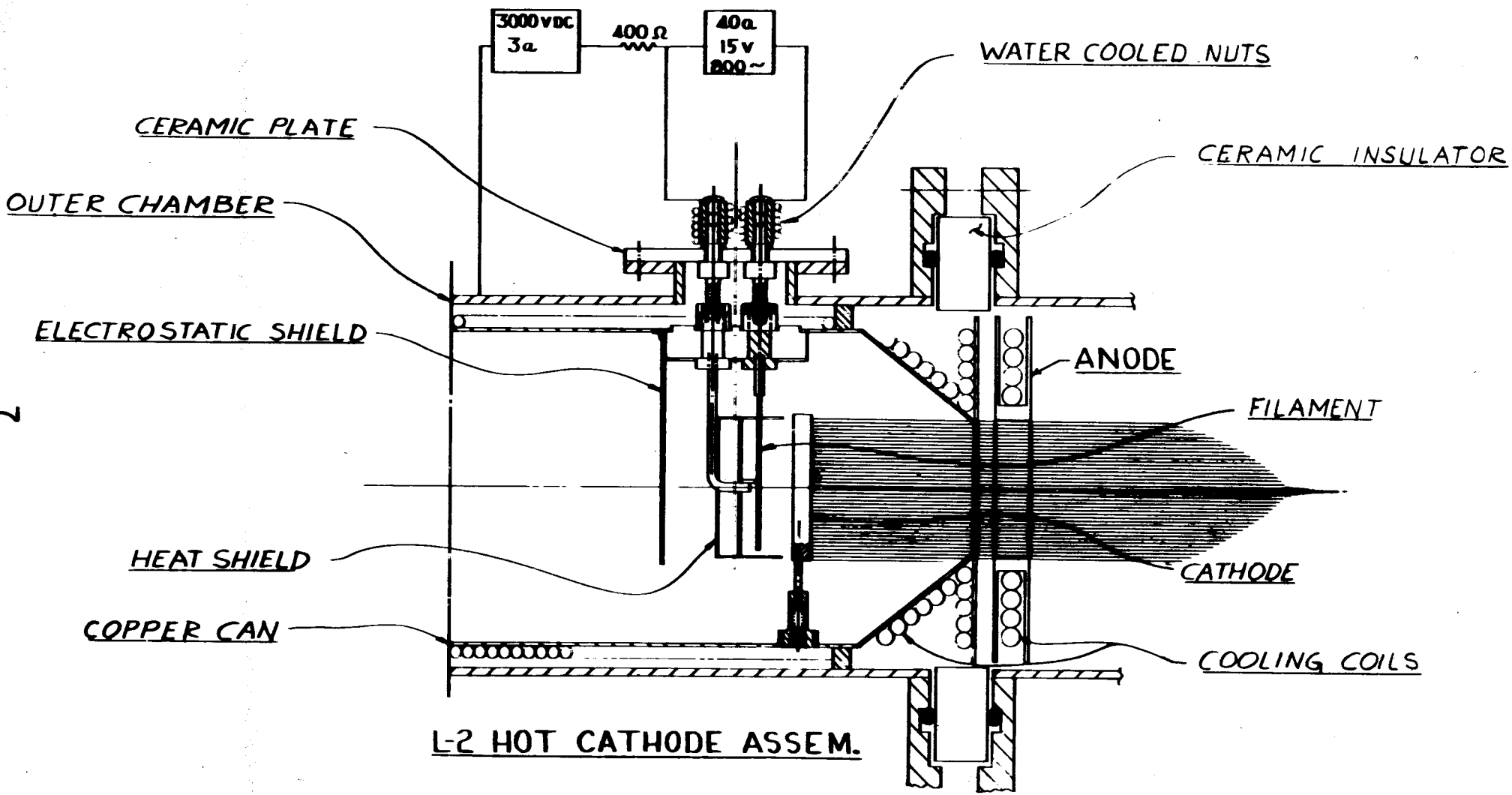

FIG. 2.3 DIAGRAM OF THE HOT CATHODE ASSEMBLY

BN insulators
Reason for top-mounting
Hole thru cathode

heat and electrostatic shields. Figure 2.3 is a diagram of the entire hot cathode assembly as enclosed in its water-cooled copper jacket, the hole in which defines the edge of the discharge. The other cathode, 11 feet away, is a similar tungsten disc but not heated.

III. Measurements on the Plasma

Section 3.1 - D. C. Measurements

We turn now to a consideration of the experimental results obtained on L-2. These can be divided into two major classifications: the d. c. and the a.c. experiments. In this section only the d. c. results will be considered. For our purpose we shall class as d. c. those measurements which are made in a time long compared to the characteristic times of the various oscillations and rotations. This then gives us the time-averaged properties of our plasma.

3.1.1 Current-Voltage Characteristics

The first property to become apparent is the current-voltage characteristic of the discharge. Figures 3.1.1 and 3.1.2 show plots of the discharge current as a function of discharge voltage for different values of the magnetic confining field and the neutral gas pressure. These plots are taken on an x-y recorder connected to the discharge through a voltage dividing network. It will be noticed that the discharge appears much more stable in the middle region of the curve than at the ends. The greatest

Not in drawing

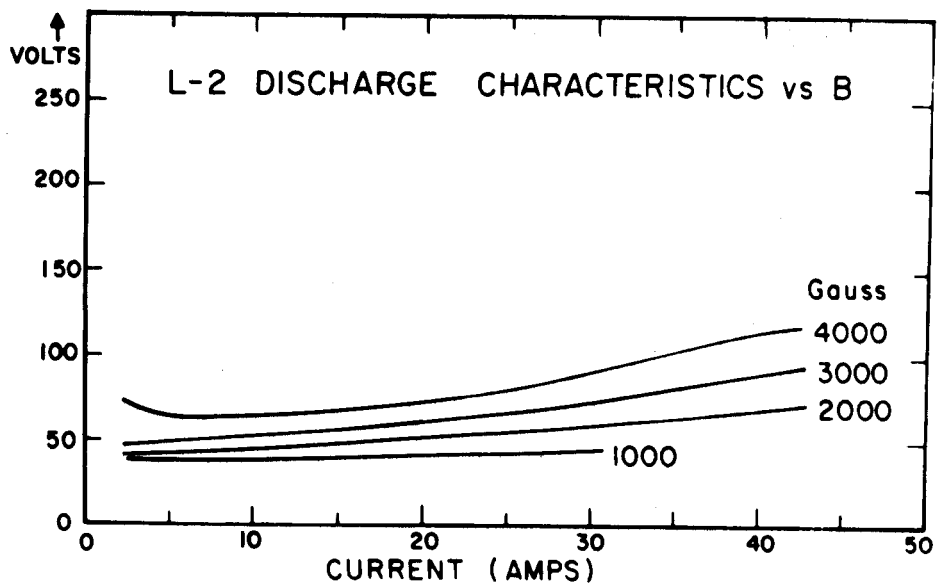

FIG. 3.1.1 CURRENT-VOLTAGE CHARACTERISTICS AT DIFFERENT MAGNETIC FIELDS

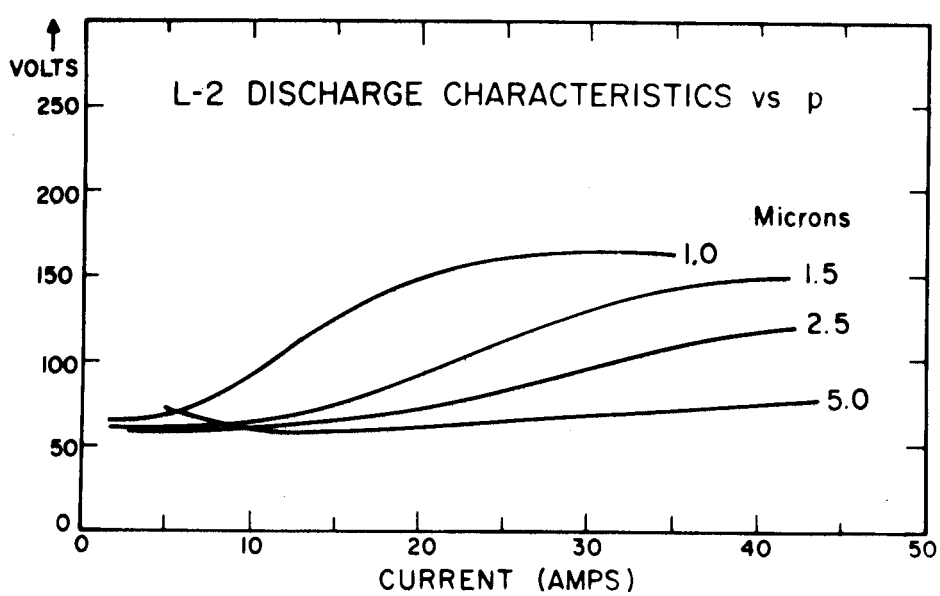

FIG. 3.1.2 CURRENT-VOLTAGE CHARACTERISTICS AT DIFFERENT NEUTRAL GAS PRESSURE

instability occurs at the low current end, where the curve frequently has a negative slope. Both these sets of curves can be understood intuitively when it is realized that electrons must cross magnetic field lines in getting from the cathode to the anode, since the diffusion process would be expected to vary inversely with some power of B.

Our base pressure is about 2×10^{-6} mm of Hg with the cathode cold and 2×10^{-5} mm of Hg with the hot cathode at operating temperature.

Under normal operation the L-2 machine has a continuous flow of helium at a pressure of 2-3 microns. Empirically this was found to be the best operating pressure. Below 1 micron the noise as seen on the anode increases very rapidly with decreasing pressure, arcing occurs, and the discharge characteristic shown on the x-y recorder becomes very unstable. At helium pressures above 10 microns other undesirable affects occur. In the case of the long machine the primary electron mean free path is much shorter than the machine which then behaves like a single ended device with the discharge getting fainter with increasing distance from the hot cathode. For a shortened machine (see Section 3.1.6) the discharge merely became faint and more hollow as the pressure increased.

Initially, at our usual operating pressure considerable difficulty was encountered in starting the discharge when the anode voltage was applied. This effect was not understood but has been circumvented by using a Tesla coil to initiate the discharge. With a high frequency pulse from the Tesla

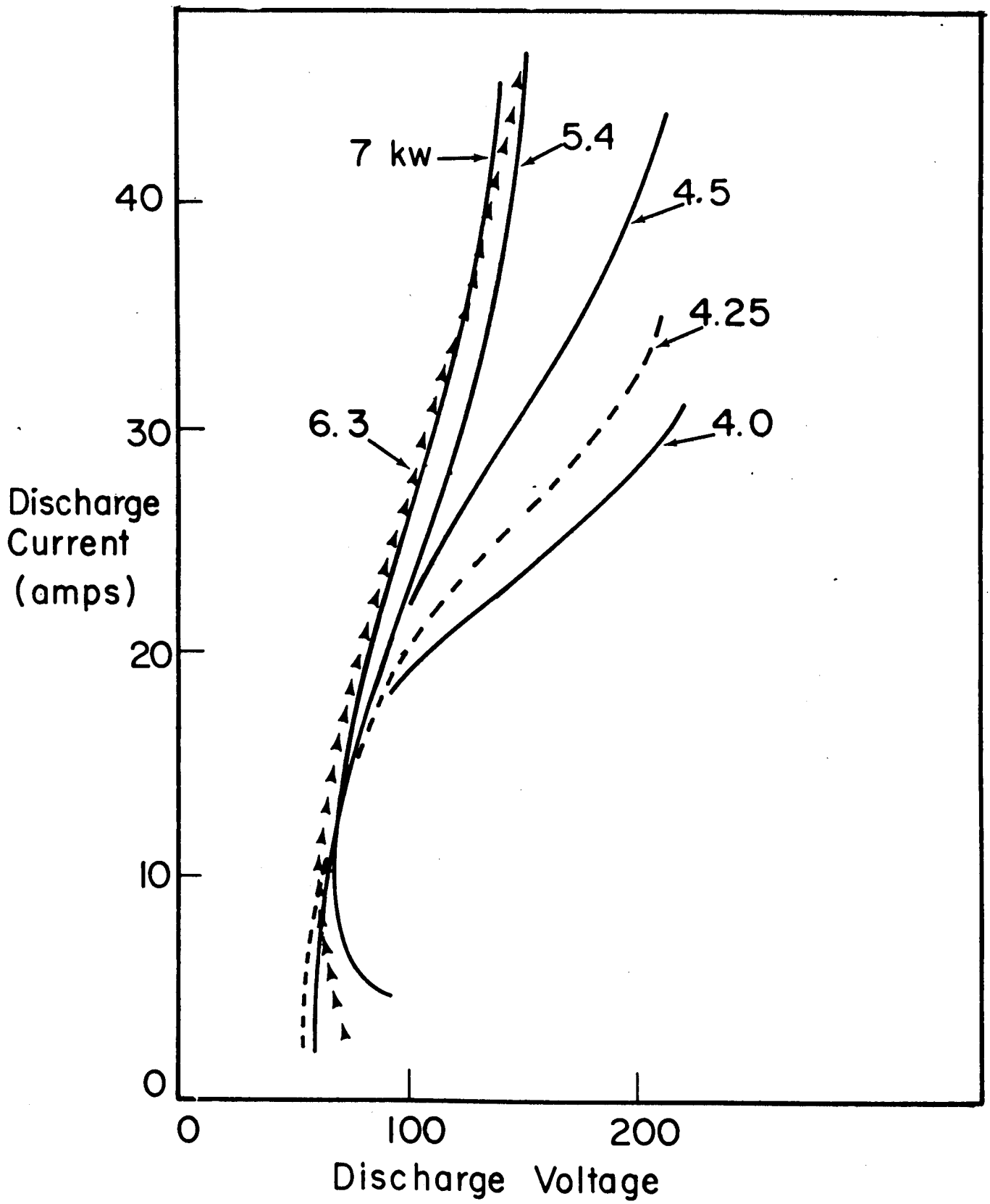

FIG. 3.1.3 CURRENT-VOLTAGE CHARACTERISTICS AS A FUNCTION OF CATHODE HEATING POWER

coil after application of the anode potential, reliable starting has been obtained.

The standard conditions of magnetic field and discharge current under which most experiments have been performed have been 4000 gauss and 15 amperes. Although the generator will provide current for a field of 5000 gauss the coil themselves are only designed for 4000 gauss and hence operation has been limited to this value, except for brief periods. If the field is lowered below 2000 gauss, the noise in the anode voltage rises considerably. The discharge also begins to become unstable. At still lower confining fields big negative spikes appear in the anode voltage as displayed on an oscilloscope. The 15 amp discharge current standard was also chosen empirically for stability reasons. From Figures 3.1.1 and 3.1.2 it will be seen that this current value corresponds to a point between the unstable operating point for low currents and the much more noisy discharges at higher currents. It was also found, as will be discussed further later, that in many cases the density was already an appreciable fraction of the maximum obtainable in the machine.

In order to avoid cathode surface effects, the cathode was heated until the operating characteristic showed no further change. As a check the discharge characteristic was taken as a function of the cathode heating power. From Figure 3.1.3 it will be seen that for input powers above 5.4 KW the discharge is essentially unchanged. Normal operation is therefore chosen to be at a cathode heating power between 5.5 and 6 kilowatts.

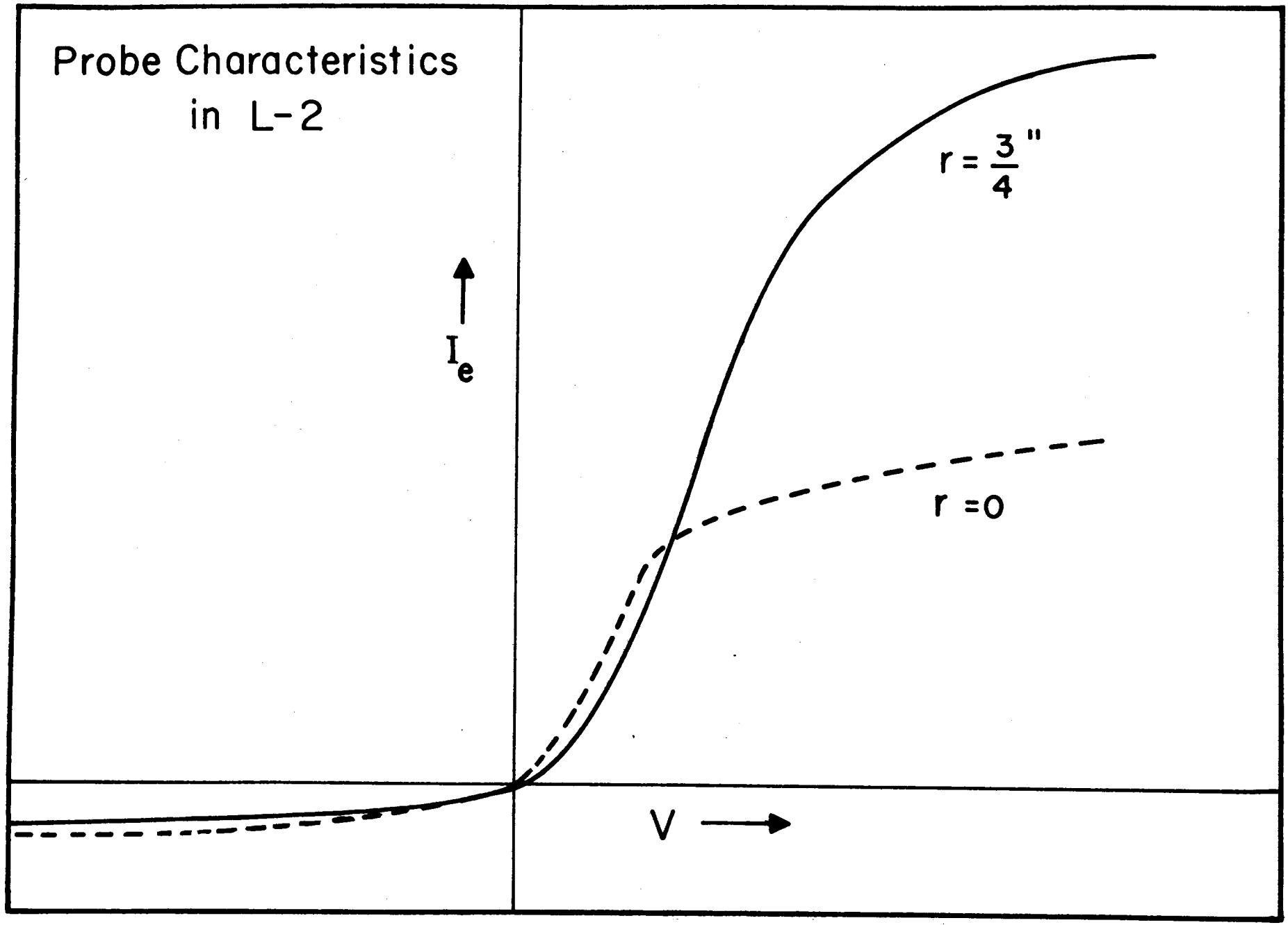

FIG. 3.1.4 TYPICAL LANGMUIR PROBE CURVE

3.1.2 Probe Data

An important method for obtaining data on the L-2 machine was the use of Langmuir probes. (See Appendix) Figure 3.1.4 shows typical probe curves, one of which is replotted on semi-logarithmic paper in Figure 3.1.5. From these curves one can obtain the average electron temperature, the floating potential of the plasma, and the relative plasma density as given by the saturation ion current.

One of the most noticeable and significant, as well as one of the most reproducible, results obtained in this way is the floating potential distribution shown in Figure 3.1.6 giving the floating potential as a function of radius. This result is essentially independent of position along the axis of the machine. We note that the voltage rises from a slightly negative potential at the axis to the full applied voltage at the edge of the discharge. There are three principal implications of this distribution. First, the sheath drop at the cathode must vary with radius; second, the discharge will be less dense at the center because there is no field to accelerate the primary electrons and hence no ionization. The center of the discharge will thus be filled only by particles diffusing into it across the magnetic field. The third implication is that the plasma will rotate due to the $\underset{\sim}{E} \times \underset{\sim}{B}$ drift velocity caused by the indicated radial electric field. As will become apparent later, this rotation is one of the most dominant features of our plasma.

From Figure 3.1.5 we see that the sloping portion of our probe curve

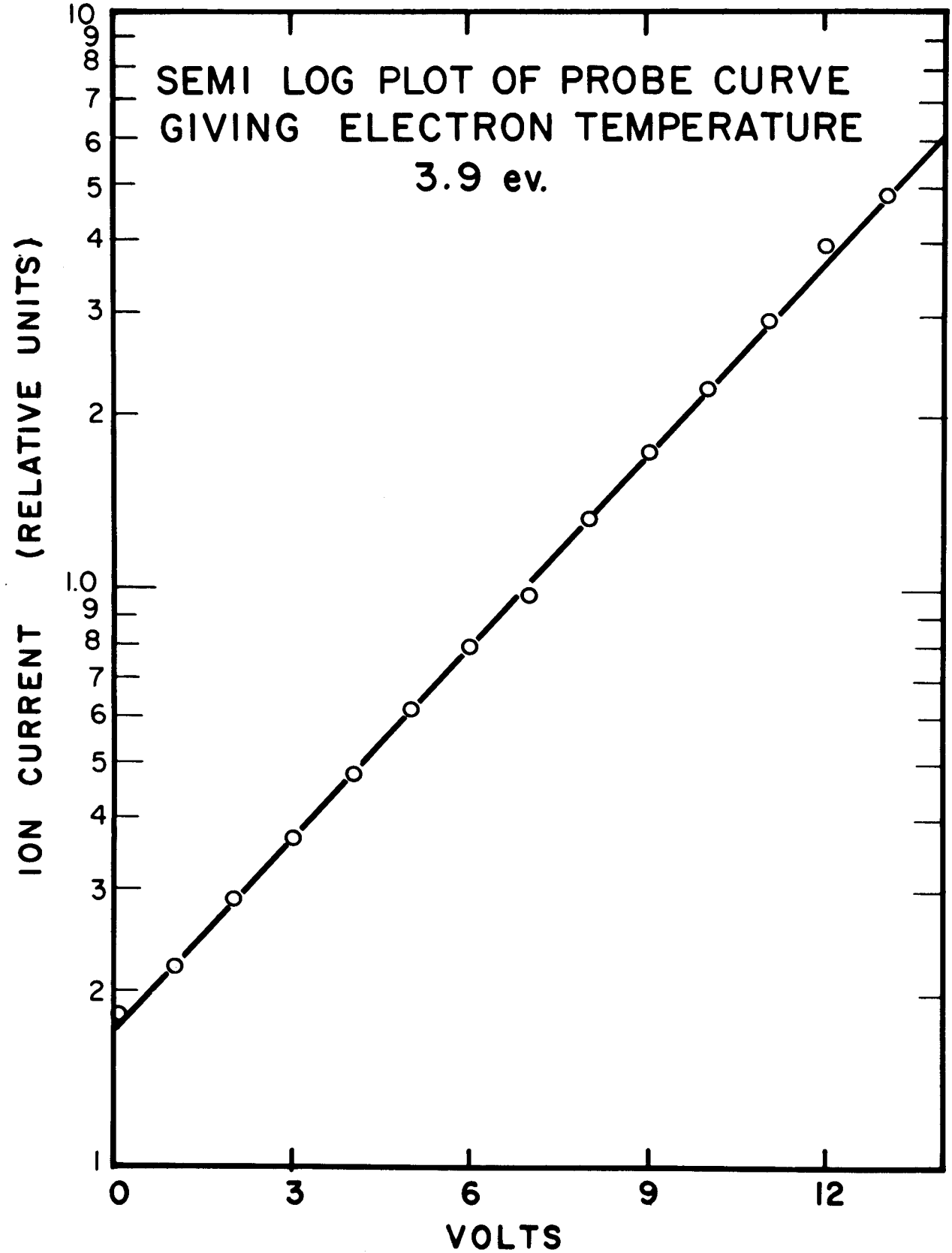

FIG. 3.1.5 PROBE CURVE PLOTTED ON SEMI-LOG PAPER

indicates a Maxwellian electron velocity distribution corresponding to an electron temperature of 3.9 ev. The straight line in the figure is typical of the results obtained in the interior regions of the plasma, the outer regions not always being quite as good. Typically the electron temperature measured in this way will vary from about 3 ev in the center of the discharge to about 6 or 8 ev near the edge. Figure 3.1.7 gives typical radial temperature distributions.

In order to get a picture of the plasma density as a function of radius, the probe ion saturation current was studied. For the sake of standardization, readings were taken at 20 volts negative with respect to floating potential. The ion density is then obtained by dividing the saturation ion current by the square root of the electron temperature.[3] The absolute value of the density cannot be obtained from the probe current unless this has been independently calibrated, by a microwave bridge, for instance. This situation arises because in our machine the ion larmor radius and probe size are of the same order of magnitude while the ion-neutral mean free path is two orders of magnitude larger. No suitable theory of probe collection exists for this situation at the present time. Nevertheless, the information obtained about the relative densities is of considerable interest.

In Figure 3.1.8 two typical density profiles have been plotted. It should be remembered that the zero density point is at the bottom of the graph for both curves and only the shape has meaning; the absolute values do not. In

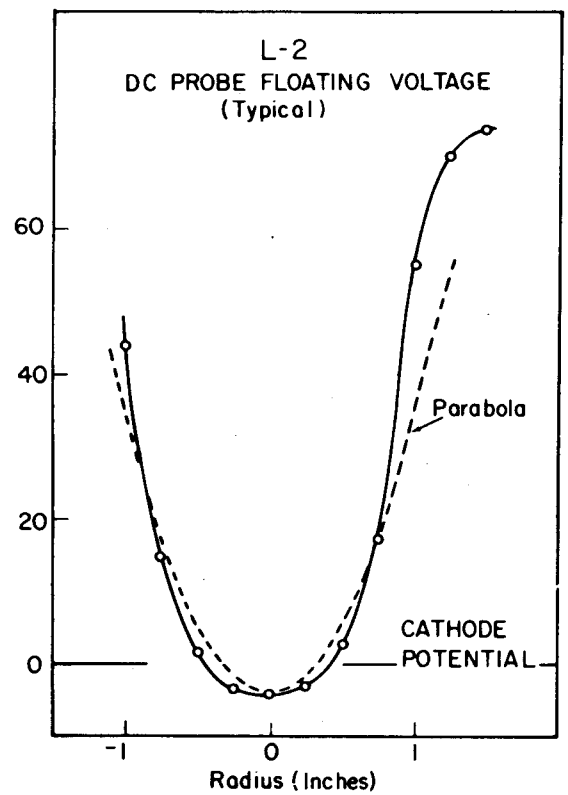

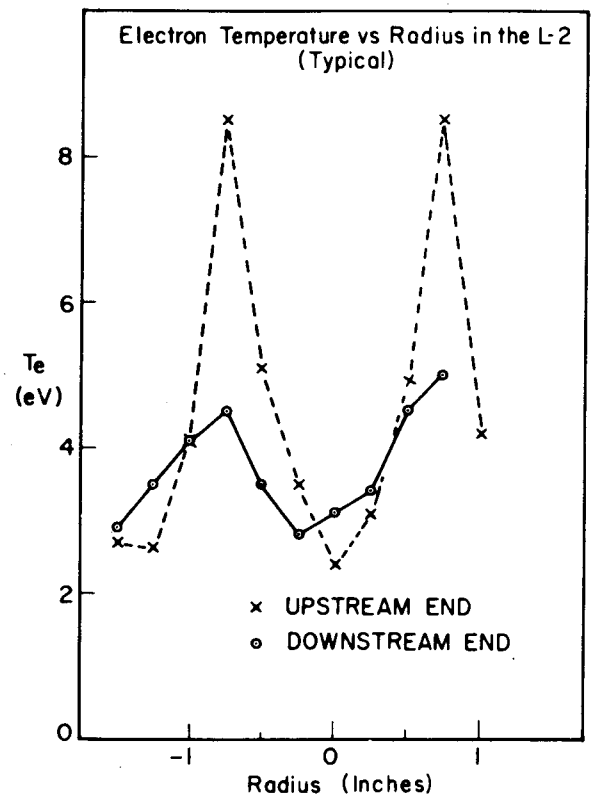

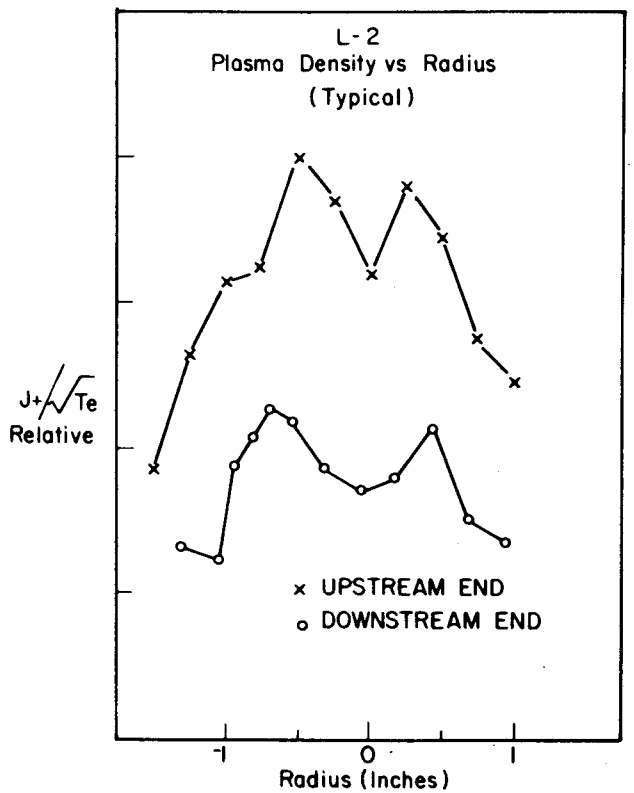

FIG. 3.1.6 FLOATING POTENTIAL AS A FUNCTION OF RADIAL POSITION

FIG. 3.1.7 ELECTRON TEMPERATURE AS A FUNCTION OF RADIAL POSITION

FIG. 3.1.8 PLASMA DENSITY AS A FUNCTION OF RADIAL POSITION

each case it will be observed that there is roughly a 20% dip in density at the center of the discharge. At the present time it is not possible to say whether or not this "hollowness" of the discharge varies with distance along the axis of the machine, due to the uncertainty of the measurements and the difficulty of keeping the discharge constant during the considerable time interval needed to make the necessary measurements.

3.1.3 - Segmented and Biased Cathodes

In order to further investigate the phenomenon associated with the negative floating potential along the axis of the machine, the cold cathode was electrically insulated from the vacuum chamber. This made possible a study of the current collected and also permitted biasing the cathode with respect to ground and observing the effect on the discharge. A quick check then revealed that the net current to the cathode was an electron current. To get more information a segmented cathode, shown in Figure 3.1.9, was installed at the cold end. This cathode, made of stainless steel segments mounted in boron nitride, is so constructed that all the segments have equal area and are all independently floating. As shown in Figure 3.1.10, the floating potential thus obtained matches that obtained by the probes. It will also be noted that there is considerable net electron collection in the center segments and an even greater net ion collection in the outer segments. This makes the total net cathode current an ion current, contrary to our earlier result. A likely cause for this is the effect

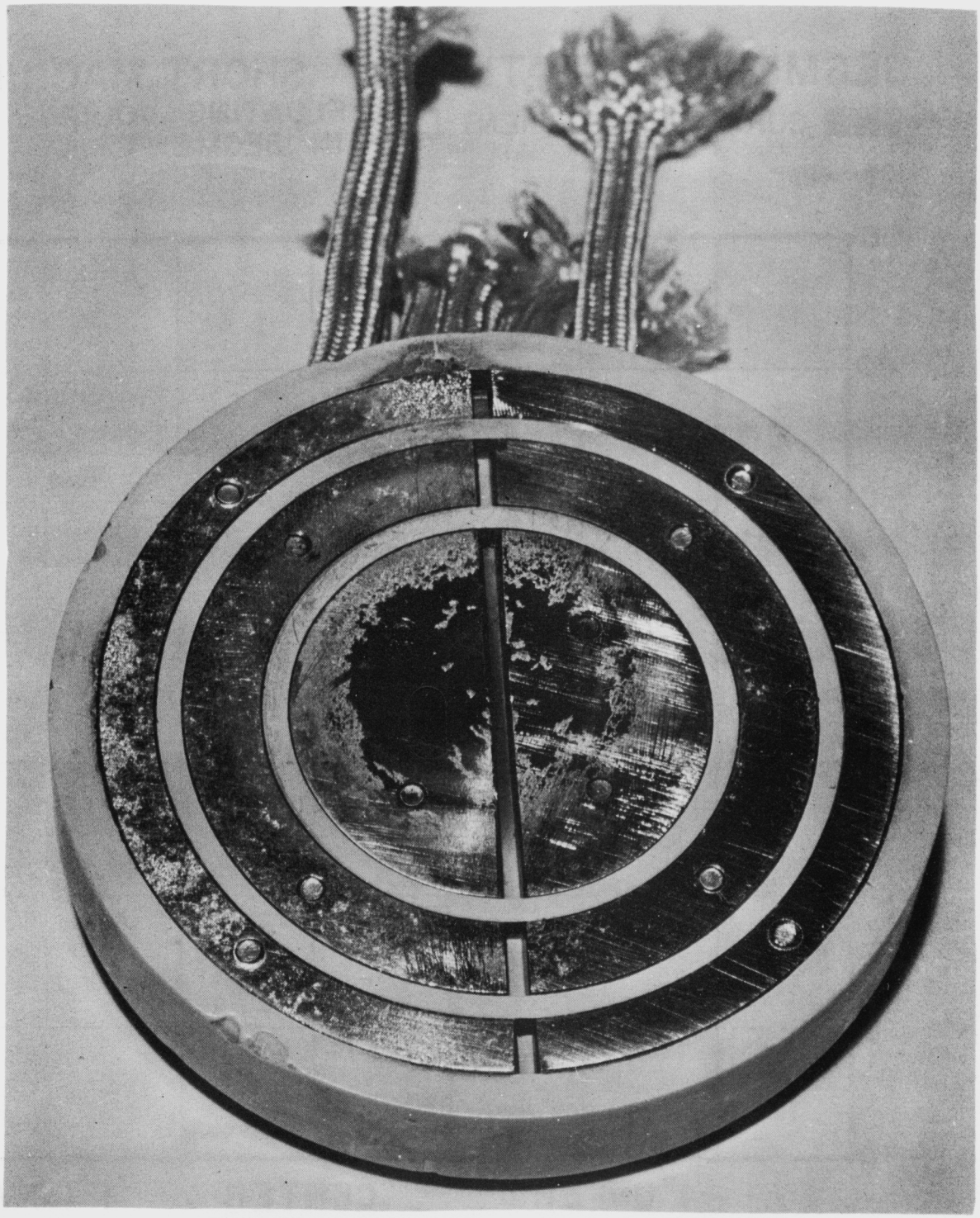

FIG. 3.1.9 PHOTO OF SEGMENTED CATHODE

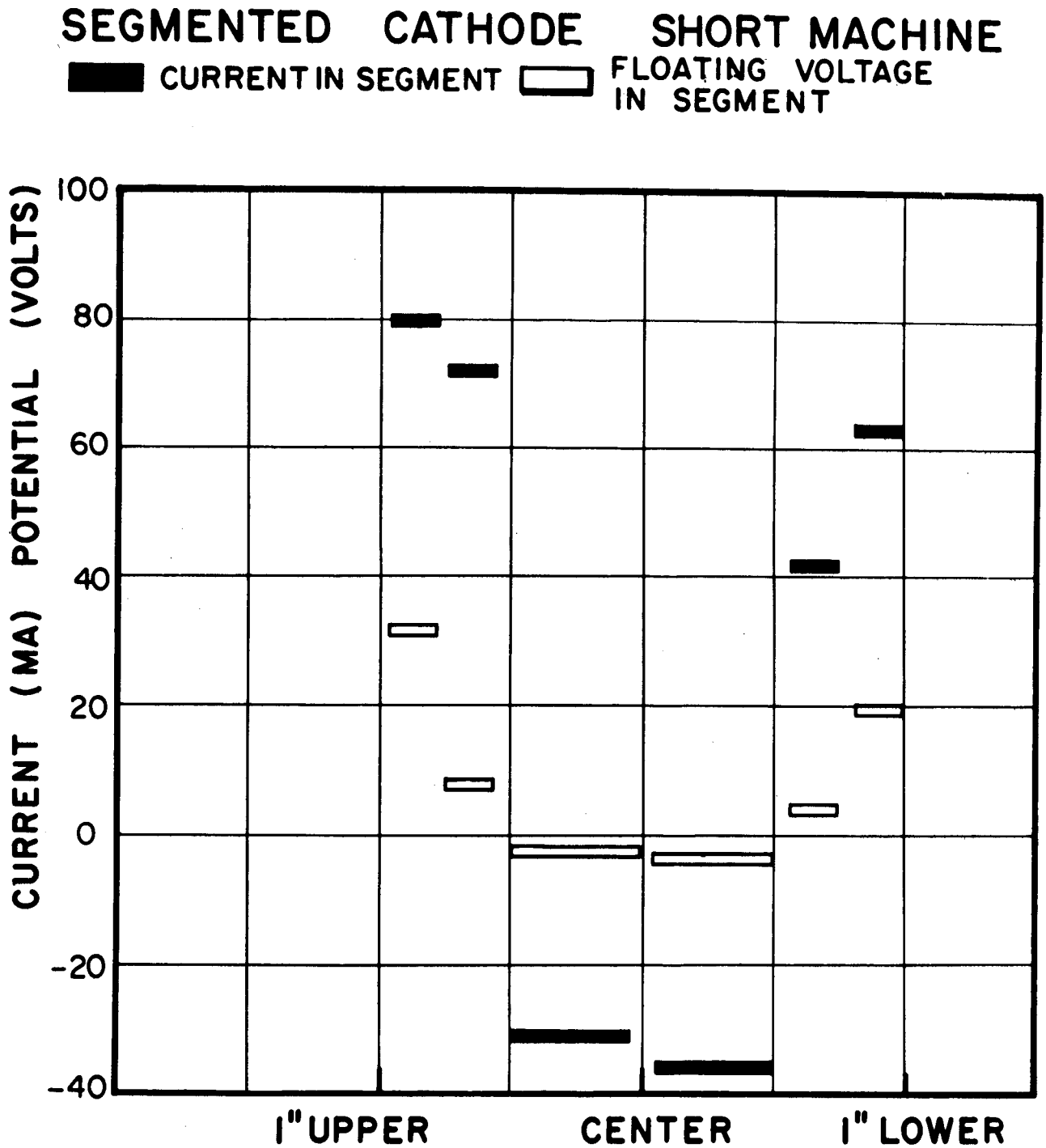

FIG. 3.1.10 RADIAL CURRENT AND FLOATING POTENTIAL DISTRIBUTIONS OBTAINED BY SEGMENTED CATHODE

elim. details + photo + graph

of the boron nitride mounting for the cathode segments. It was observed while this segmented cathode was in use that the discharge characteristic drifted somewhat and, if the discharge was left on too long arcing occurred. This is felt to be due to the impurities driven off the ceramic surface by the bombardment from the discharge. Such impurities could then cause electron attachment by the electrons which would otherwise go to the cathode, thus decreasing the net cathode electron current, due to space charge effects.

When the cold tungsten cathode on the long machine was biased negatively with respect to ground, no observable difference was found in the probe data. For biases of 6 and 12 volts the temperature, density and floating potentials distributions were not affected within the reproducibility of our data.

3.1.4 - Microwave Density Measurements

The plasma density in these experiments was monitored by an eight millimeter microwave density measuring system. This system has been described in detail in Technical Memorandum No. 92.[4] In Figure 3.1.11 the electron density, as measured on the microwave system, is shown as a function of the discharge current. For this particular case maximum density is reached for 20 amps of discharge current, but this point varies considerably since for some discharges the density is still a linear function of current at 40 amps. In the latter case it was noted that the machine was exceptionally clean and impurity free,

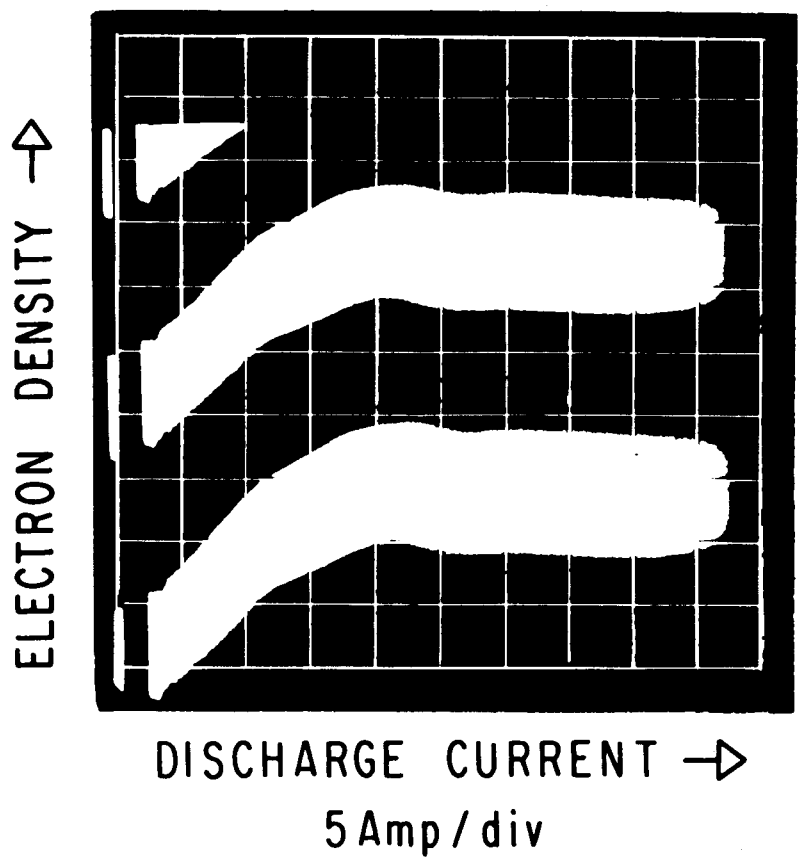

FIG. 3.1.11 ELECTRON DENSITY AS A FUNCTION OF DISCHARGE CURRENT

judging from the base pressures and color of the discharge. It is therefore felt that leveling off of the density-current curve is due to the rate of loss due to recombination becoming equal to the rate of plasma creation, and that this loss mechanism increases substantially with the presence of impurity ions, which have been shown, by spectroscopic analysis, to be present.

By use of the plasma density profile given by the probe curves, it is possible to relate the total phase shift given by the microwave display to the electron-density at some given part of the discharge. This gives the result that the central part of the discharge has a density of 1×10^{12} to 2×10^{12} electrons/cm^3 with 15 amps discharge current.

3.1.5 - Crowbarred Discharge

By observing the fringe shift as a function of time it is possible to study the decay of the plasma after crowbarring the discharge. When the density, as shown by the fringe shift, was plotted as a function of time on semi logarithmic paper, it was seen that the plasma decayed expontentially with a lifetime of 850 microseconds. This decay cannot de due principally to classical electron-ion recombinations as this would be mainly by radiative recombination, which for our 3-8 eV electrons would have a coefficient $\alpha \sim 10^{-13}$. This is four orders of magnitude too low and furthermore this process would not be expected to give an exponential decay. We can also rule out effects due to the molecular ion He_2^+ as this only becomes a significant factor in the discharge at pressures

above 1 mm. of Hg.[5]

Electron attachment to impurity atoms followed by recombination of the negative ion with positive helium ions would give an exponential decay if the latter process were faster than the former. However, even if the discharge gas were 10% air, the attachment rate would be more than an order of magnitude too low.

Ambipolar diffusion along the field to the cathodes would give both an exponential decay and approximately the right rate. However, previous measurements with a cold-cathode discharge at 100μ showed that the density profile in the Z-direction was inconsistent with this process. This measurement has not been made in the hot-cathode 3μ discharge here, so that diffusion remains a possibility. Classical diffusion across the field is of course too slow. Bohm diffusion is ruled out because the hash on a floating probe after crowbar was undetectably small.

The mechanism of three-body recombination suggested by D'Angelo[6] would also give the right order of magnitude for the decay time if the electron temperature decayed rapidly to below 0.1 volt. Although the decay is not strictly exponential, the falling temperature can cause it to look exponential over a decade in density. This phenomenon has been observed[7] in a stellarator, and it is not unlikely that a similar recombination mechanism occurs in our discharge.

Probe current measurements at various radii after crowbar indicated that the inhomogeneity and rotation described in Section 3.2 persisted, although at a lower frequency. In using a probe to investigate the quiescence of the plasma after crowbar, it was discovered that it was necessary to use a triggered semi-conductor diode for a crowbar, since an ignitron, being itself a gas discharge, imposes oscillations on the anode.

3.1.6 - Other Machine Configurations

The first modification was to insert a grid with approximately 1/8" spacing in the middle of the discharge tube to see if the potential gradients could be altered. An insulating break in the middle of the steel tube enabled the grid and the whole cold cathode half of the machine to be grounded. This modification made no change on the operating characteristics of the device. In particular the radial potential was the same in both halves of the tube. This can be understood when one realizes that for our plasma the Debye length is less than 0.1 mm and hence our grid is more than 90% open electrostatically. Most of the particles in the discharge, being tied to the magnetic field lines, thus do not see the grid and are unaffected by it.

When the grid was removed from the machine, it was observed (Figure 3.1.12) that blackening had occurred on a ring corresponding to the outer regions of the discharge, giving further evidence that the plasma is hotter and denser near the edge.

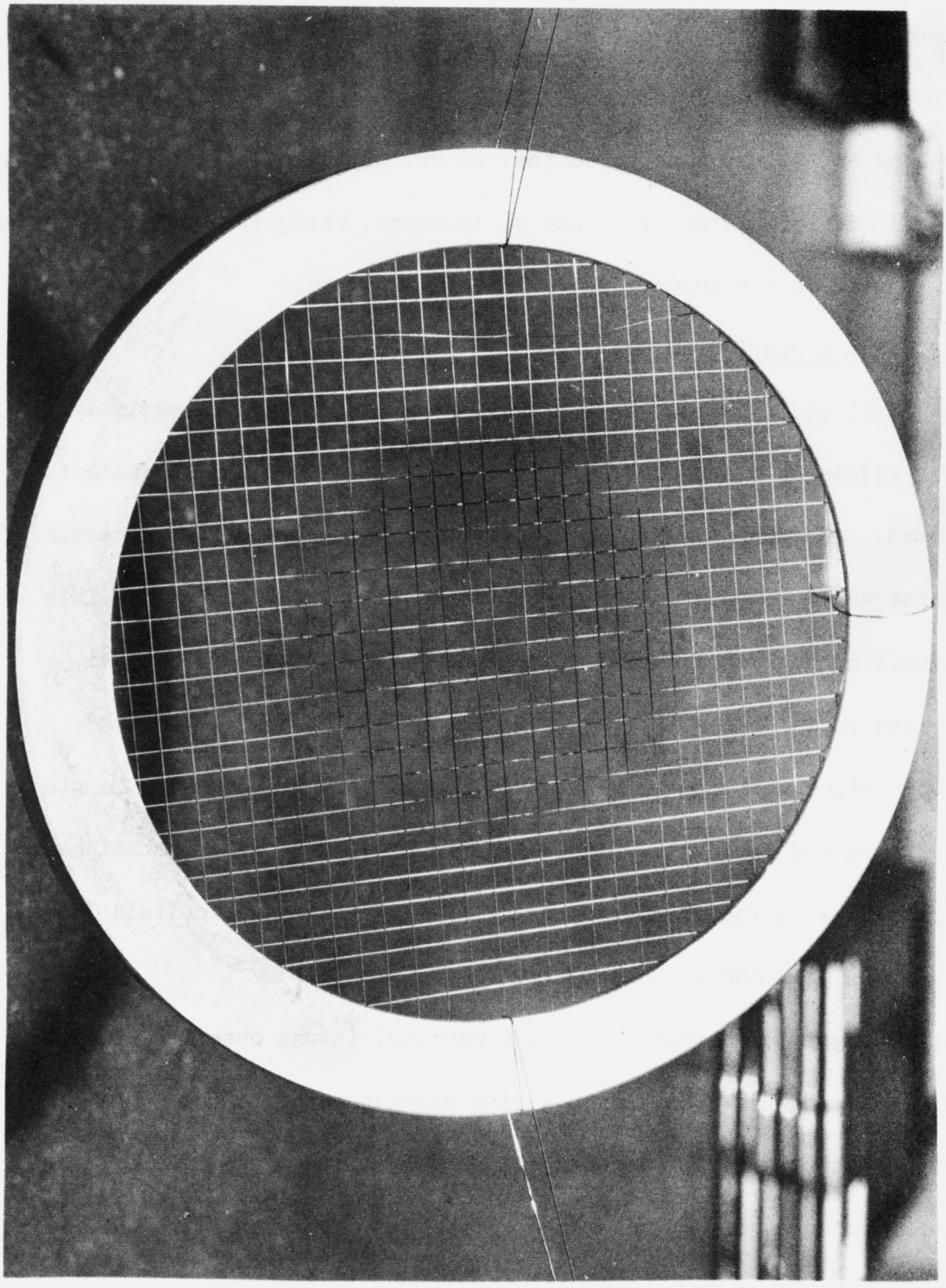

FIG. 3. 1. 12 PHOTOGRAPH OF CATHODE GRID AFTER EXPERIMENT

The major change in configuration was to halve the length of the tube so that the two cathodes were now about 6 feet apart. Once again the discharge was very much like that in the long machine. Within our reproducibility the floating potential and temperature and density distributions were unchanged. The electron density as shown by the microwave system is also the same as before. The discharge characteristic does show a small change in shape, however. This is shown in Figure 3.1.13. The operating voltage at the standard 15 amps current is as before but the curve seems to be somewhat straighter and flatter and also more stable at the low current end than it was for the long machine case. The difference between the long and short machine modes of operation thus is very small implying that the operating characteristics do not scale strongly with length.

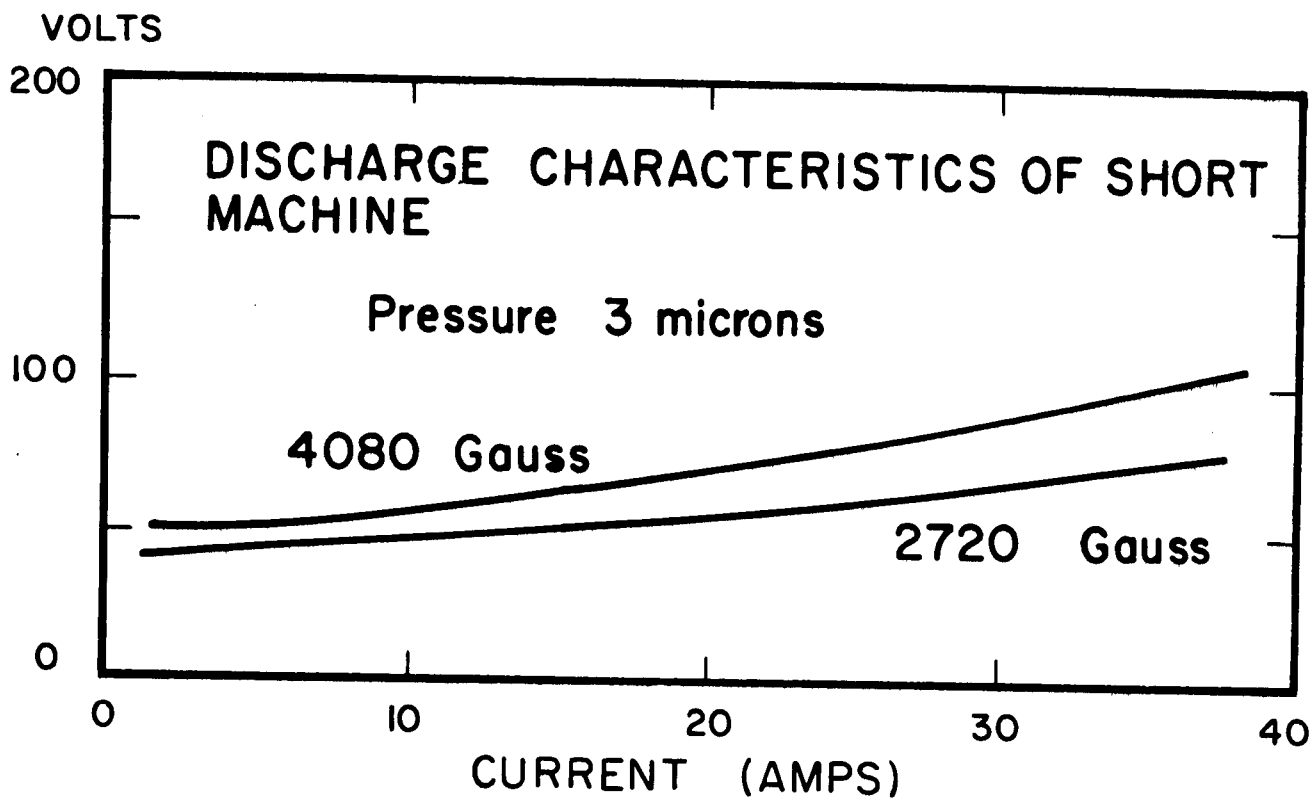

FIG. 3.1.13 CURRENT-VOLTAGE CHARACTERISTIC FOR SHORT MACHINE

3.2 A. C. Measurements

The d. c. measurements above, showing floating potentials as a function of radial distance, indicated that radial fields were occuring in the discharge. If this be so then azimuthal $\underset{\sim}{E} \times \underset{\sim}{B}$ drifts might occur resulting in plasma rotation. Several experiments, both optical and electrical, were carried out to detect and measure such rotation. From these it appeared that the time varying phenomena in the discharge could be divided into two classes:

a) those associated with a collective rotation.

b) random fluctuation phenomena.

3.2.1 Rotation

3.2.1.1 Methods of Measurement

Streak Camera Pictures

Streak camera photographs were taken of the discharge for different currents and confining fields, and various fixed pressures. In the streak camera the 16 mm Tri-X film was placed on a rotating cylinder of 9 cm radius, which could be rotated up to 9000 rpm, checked stroboscopically. The film passed a slit 1 mm across and about 1 cm long. The time scale on the photographs, corresponding to 5900 rpm is therefore about 50 μsec per cm length of film. The camera was placed at the second port from the hot cathode.

Figure 3.2.1 shows clearly that the plasma is rotating, and the frequency is about 35 Kc/s for currents of 7 and 15 amps, with 4000 gauss confining fields, and about twice this at 30 amps. The frequency also depends on the confining magnetic field. It corresponds to drift velocities near the

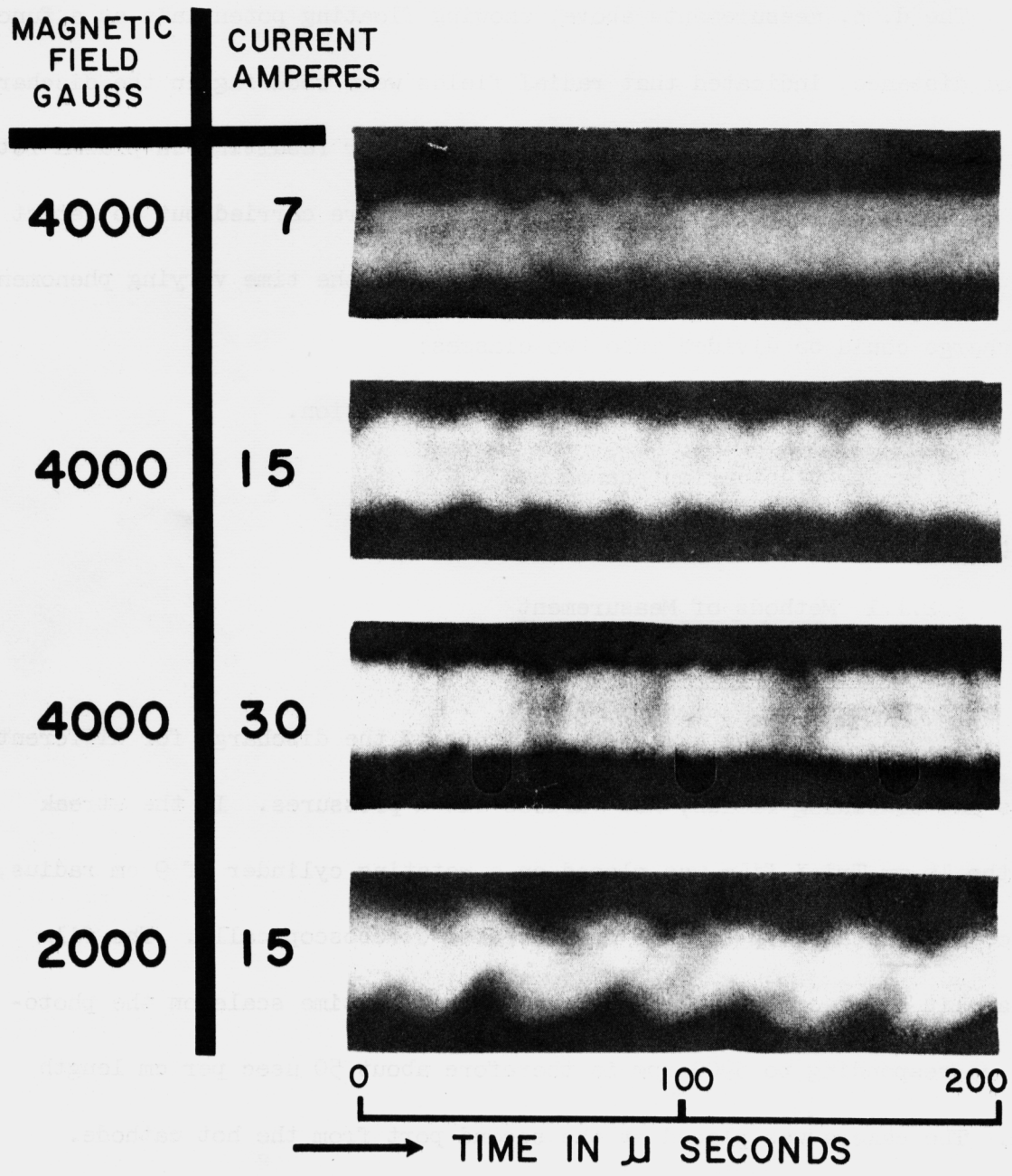

FIG. 3.2.1 STREAK PHOTOGRAPHS OF L-2 DISCHARGE

surface of the plasma of between 10^5 and 10^6 cm/sec.

It would seem that the plasma column, apparently homogeneous to the eye, consists of one or more filaments extending from the hot to the cold cathodes; similar pictures were taken at the port near the cold cathode. Examination of the pictures for 7 and 15 amps at 4000 gauss, and for 15 amps at 2000 gauss, suggest that there is one filament displaced off center; the picture for 30 amps at 4000 gauss suggests two filaments at opposite ends of a diameter, as indicated by the fact that the upper and lower peaks on the picture are opposite.

To answer the question of whether such filaments extend in a straight line down the plasma, first of all the streak camera was turned through 90°, so that the slit was horizontal. The purpose of this was to photograph at one instant of time a length of filament of order 1 cm and look for any curvature. The resulting picture showed a series of bands with straight edges, indicating little susceptible curvature in this short length. Accordingly a photograph was taken as shown in Figure 3.2.2 to find any change in phase in the rotation. The mirror arrangement enabled the images of the discharge at both ends of the machine to be superimposed simultaneously on the film, and thus the relative position of the "peaks" compared. The results were difficult to interpret, due to low light intensity at the end away from the hot cathode, but were not inconsistent with the fact that the filaments were straight or only slightly helical.

It seemed that the frequency of rotation could be accurately estimated at low currents, from the streak photographs, e. g. at 7 amps, f = 34 ± 1 kc/s.

(A) Experimental Arrangement

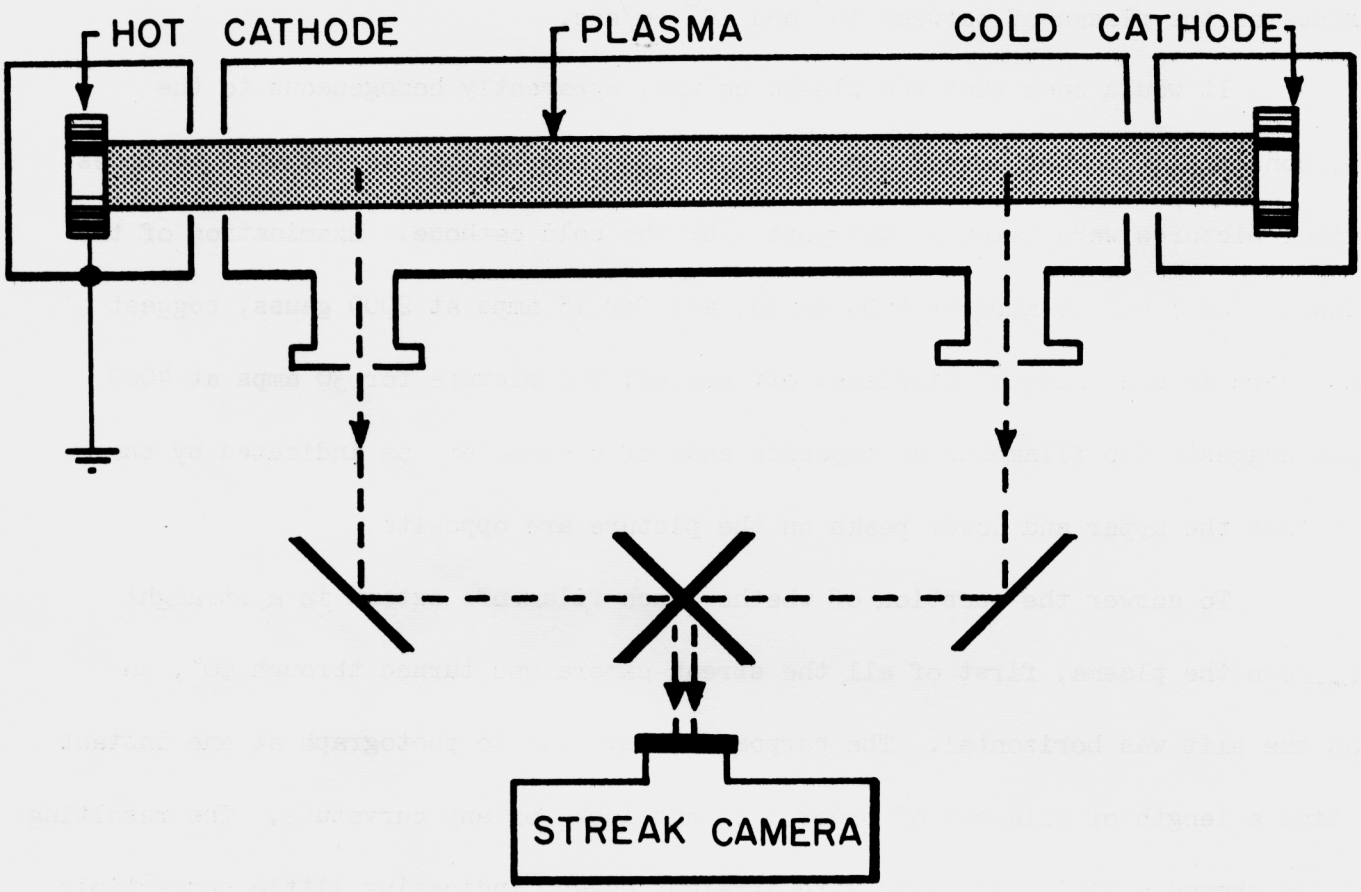

(B) Appearance of film.

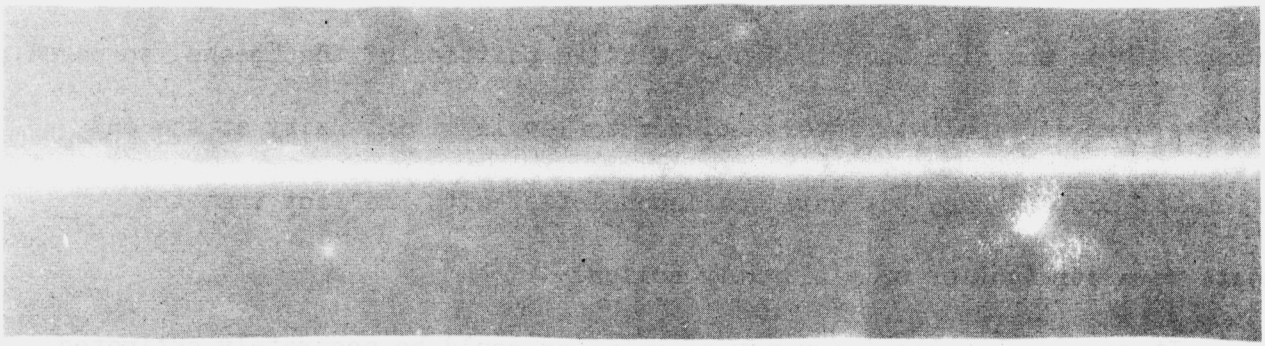

FIG. 3.2.2 SIMULTANEOUS STREAK PHOTOGRAPHS OF TWO ENDS OF THE MACHINE

At higher currents, due to fluctuations, the probable error became greater. A second optical method of estimating the frequency was therefore tried.

Rotation frequency using a photomultiplier

A Du Mont type 6467 photomultiplier was used as shown in Figure 3.2.3 to observe the discharge off the axis through a slit. The frequencies thus measured for different discharge conditions agreed exactly with those from the streak camera within experimental error, and showed the same spread in readings at higher currents.

The values of the rotation frequencies from these optical experiments suggested that the phenomenon might also be detected electrically, by voltage pickup.

Electrostatic probe measurements

The probes here were the same ones used for d. c. measurements. As the signal is alternating, voltage pickup should also occur if the probe wire were completely enclosed in an insulator sleeve, by capacity effects. In practice this gave a considerably reduced signal; hence by exposing the tip we get a measurement corresponding to a small region around it only and in our experiments the wire was always exposed to the plasma. The circuitry is described in the Appendix.

The output was displayed both on an oscilloscope and a spectrum analyser. The oscillographs showed that a strong frequency component existed equal to the

(A) Experimental Arrangement

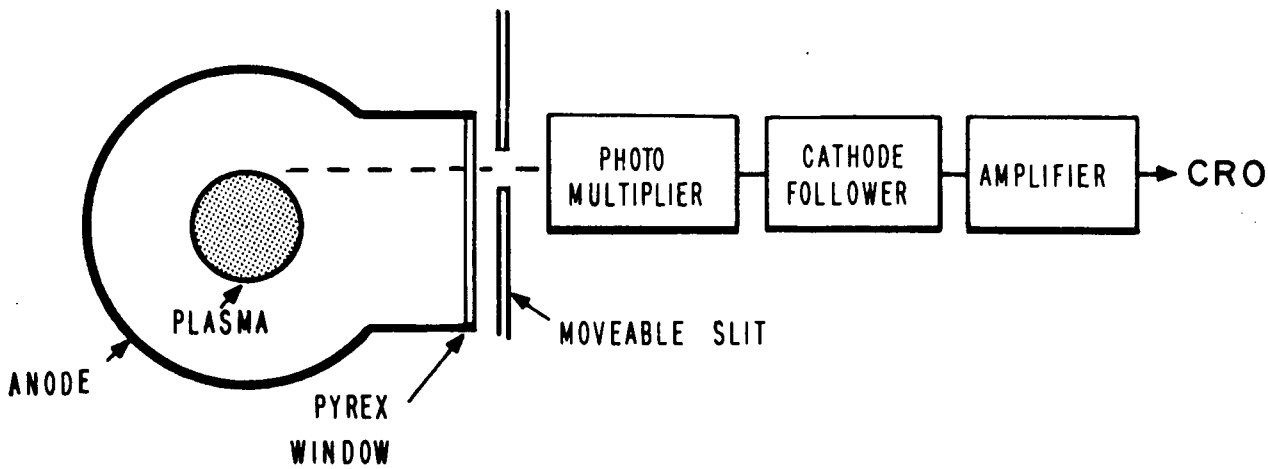

(B) Typical Oscillographs

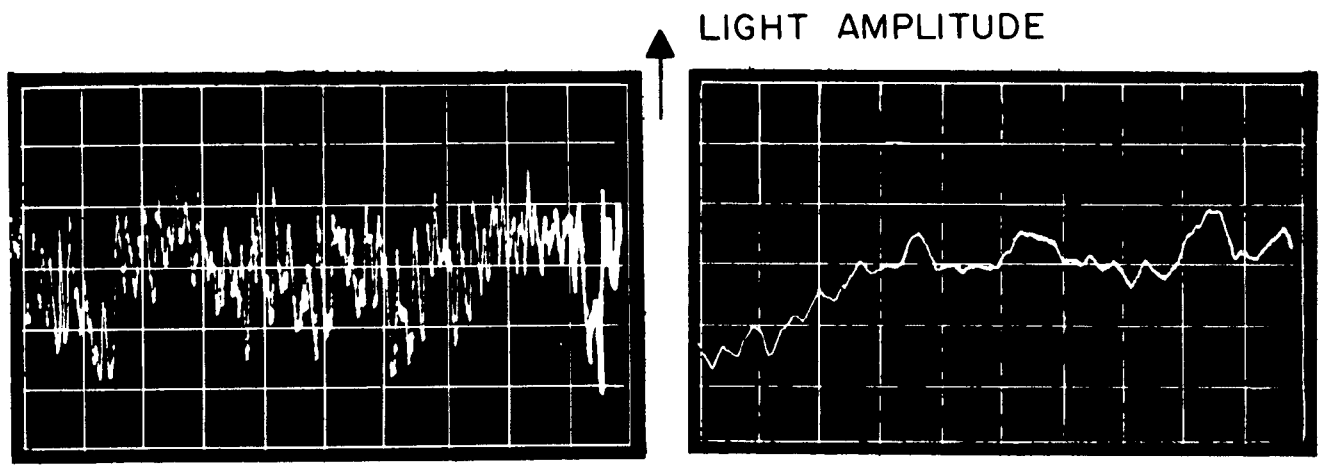

FIG. 3.2.3 ESTIMATION OF ROTATION FREQUENCY BY USE OF PHOTOMULTIPLIER

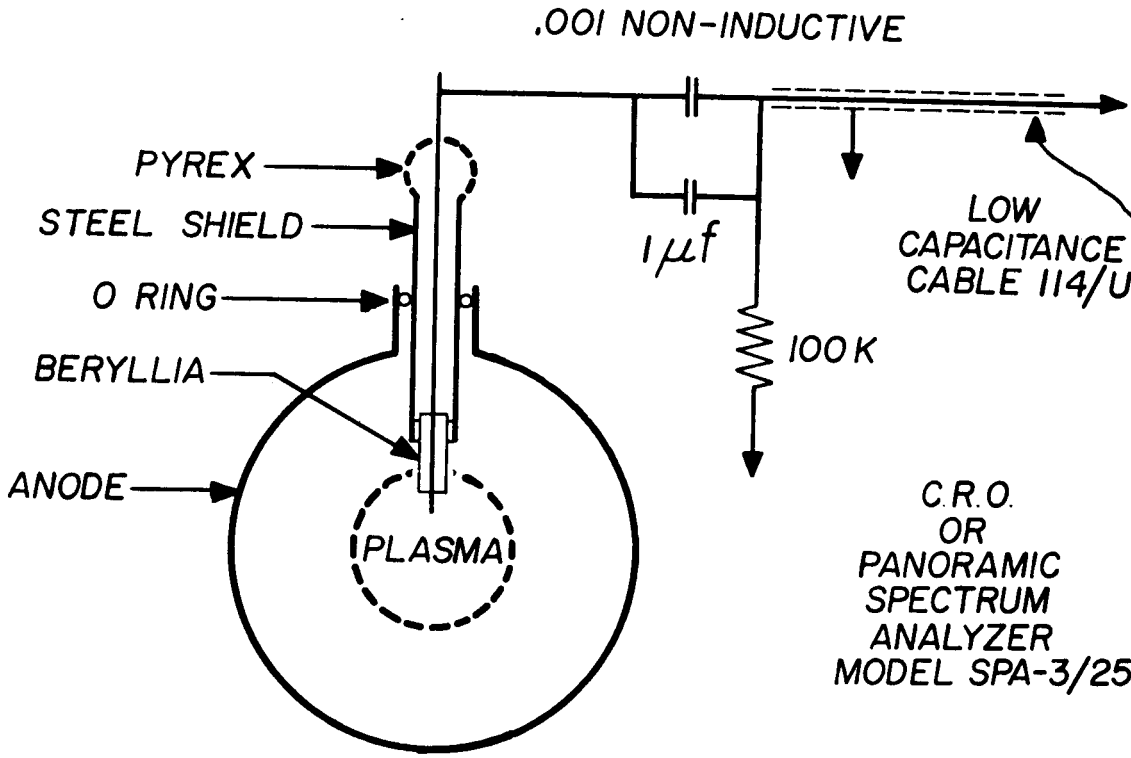

(A) CIRCUIT FOR MEASURING PROBE NOISE

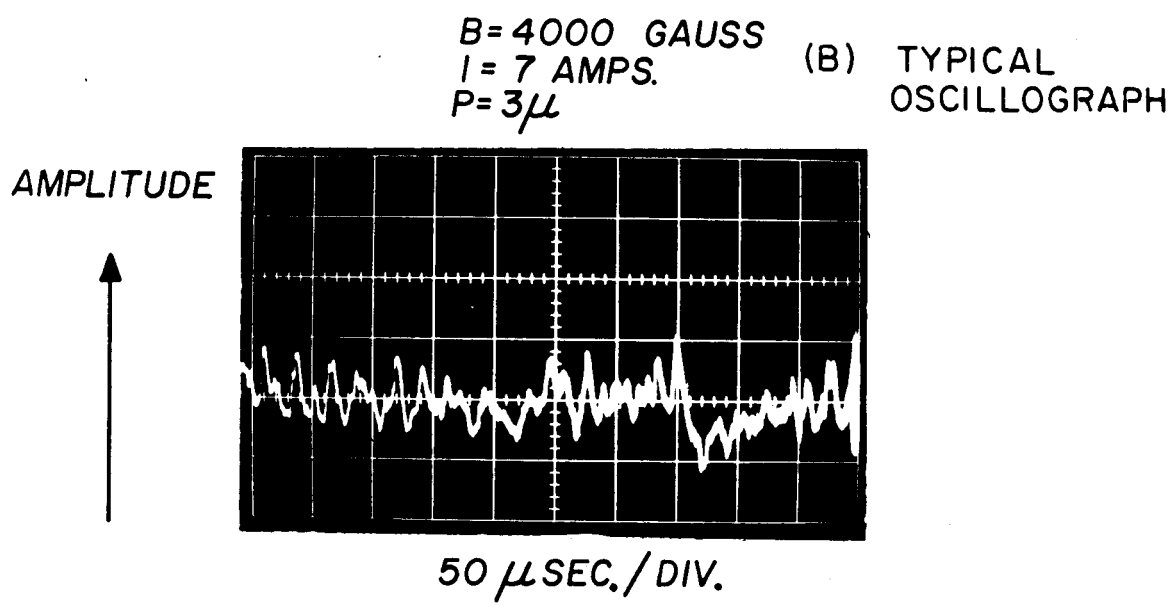

FIG. 3.2.4 MEASUREMENT OF PROBE NOISE

rotation frequency (Figure 3.2.4), but the irregularity of the waveform indicated many other frequencies also. From the known time scale, the main frequency component, measured for the same conditions, agreed within experimental error, with those from the streak photographs.

The spectrum analyser yielded further data. Figure 3.2.5 shows a typical amplitude vs frequency spectrum from 0 to 100 Kc/s. The peaks on the picture correspond within experimental error with the frequencies of rotation measured from the streak photographs. In addition harmonics of these frequencies occur as well as a broad band of noise with higher amplitudes at low frequencies. This will be considered separately later.

A comparison of the rotation frequencies measured by these four methods is shown in Table 1.

Table 1: Comparison of rotation frequencies in kc/s measured by different methods.

Helium discharge, p = 3μ, B = 4000 Gauss

Current amps	Streak Camera	Photomultiplier	Probe noise on oscilloscope	Spectrum Analyser
7	34 ± 1	33 ± 2	34 ± 1	34 ± 1 +Harmonics
15	37 ± 1	39 ± 2	36 ± 1	36 ± 2
30	90 ± 20	82 ± 14	70 ± 5	68 ± 2

3.2.1.2 Effect of Plasma Parameters on Rotation Frequency

The plasma parameters that were varied were the total current, the pressure, and the confining fields. Essentially increasing the current increased

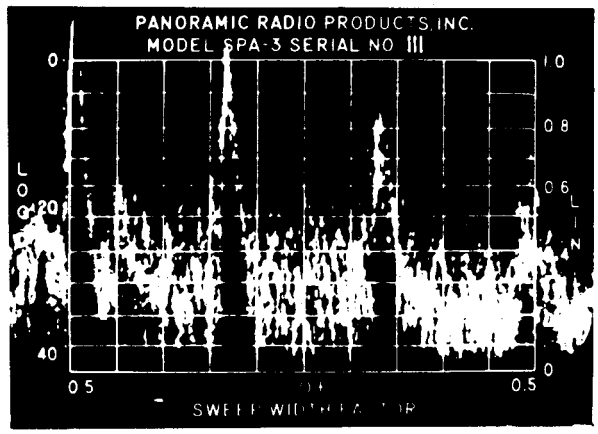

DISCHARGE CURRENT

7 AMPS

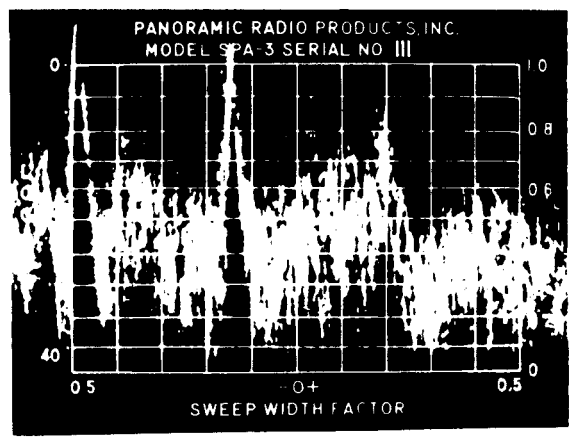

15 AMPS

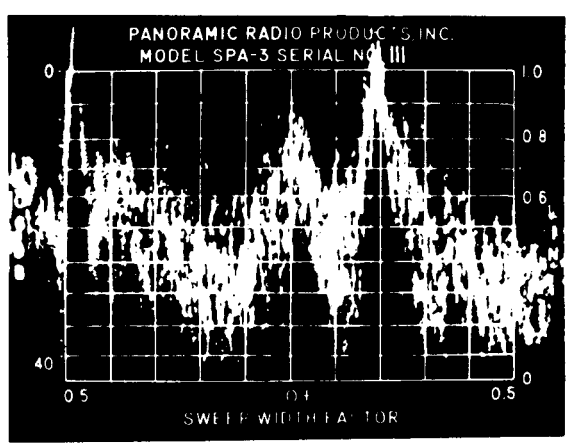

30 AMPS

0 KC/S 100

HELIUM P=3μ B=4000 GAUSS

FIG. 3.2.5 SPECTRUM ANALYSER PICTURES

the density, and also the radial E fields. These were estimated from the d. c. probe measurements. The effect of shortening the inter-cathode distance from 3 m to 1.5 m was also tried.

In general increasing the current increased the rotation frequency if B was kept constant. The rotation frequency was approximately proportional to the radial E field, measured from d. c. probe curves of floating potential vs radial position. Changes in pressure did not greatly alter this result. On keeping the current constant, and reducing B to half value, it was found from the streak camera pictures (Figure 3.2.1) that two effects seemed to occur. For a current of 15 amps with a confining field of 4000 gauss the rotation frequency was about 60 Kc/s. Keeping the current constant, and reducing the B field to 2000 gauss (reducing the radial E field by about 20%), there was a fundamental of about 25 Kc/s. However, there are indications of a higher frequency component at 120 kc in Figure 3.2.1. Thus altering B apparently changed the gross features of the discharge. If the rotation frequency increases as B decreases, the higher frequency component would have been expected.

If we calculate the rotation frequency from an $\underset{\sim}{E} \times \underset{\sim}{B}$ drift, and assume a radius r for the discharge, then

$$f(\sec^{-1}) = \frac{10^8 E}{2\pi r B}$$

where E is in volts/cm, r = 2 cm, B in gauss. On measuring the time-averaged E from radial probe curves we have the comparison of Table 2, where we have

taken the most probable frequency from Table 1.

Table 2: Comparison of measured and calculated frequencies

Helium $p = 3\mu$, $B = 4000$ Gauss

Discharge current amps	Measured value of frequency. Kc/s	Calculated Kc/s
7	34 ± .5	50
15	37 ± 1	68
30	70	81

The calculated frequencies seem to be consistently higher than observed. This point will be discussed in Section 4.

On reducing the length of the machine from 3 m to 1.5 m it was found that at the same current, the rotation frequency was slightly higher. This was not inconsistent with increased radial electric fields caused by small differences in running conditions such as slight pressure drifts.

3.2.1.3 Experiments on phase differences.

By placing two probes at right angles, and displaying simultaneously the pick up voltage on a double beam oscilloscope, a 90° phase difference was shown in the signals as the filament rotated. (Figure 3.2.6) The time scale here is 100 μsec full scale, so this rotation frequency was about 30 Kc/s. The current was 15 amps and this means that the discharge was in the form of one single filament, rotating around the axis, consistent with the streak photographs. Had there been two filaments the phase difference in the

(A) PHASE DIFFERENCE IN VOLTAGE PICK-UP SIGNAL ON TWO PROBES AT RIGHT ANGLES

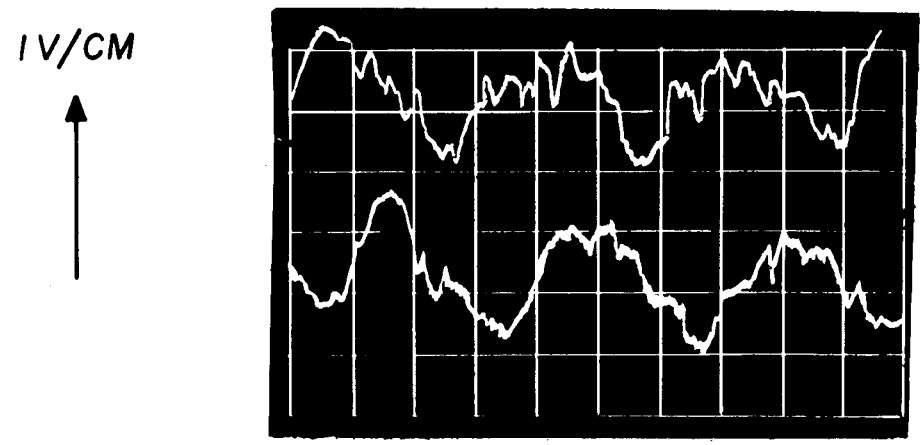

(B) PHASE DIFFERENCE IN CURRENT TO SEGMENTED CATHODE

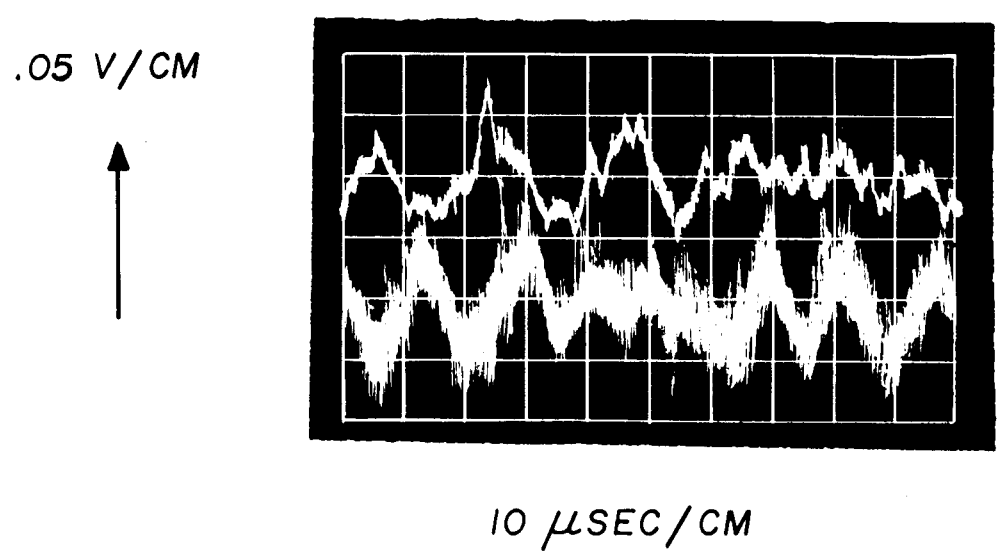

FIG. 3.2.6 PHASE DIFFERENCE EXPERIMENTS WITH THE ROTATING PLASMA

signals would have been 180°.

An attempt to show a 90° phase difference by a Lissajous figure on an x-y oscilloscope (Tektronix 536) was inconclusive, due to the other frequencies present.

3.2.1.4 Rotation measurements on current

In addition to using probes, a segmented cold cathode was also used for rotation experiments to measure current, rather than voltage. All the segments in each half were connected to ground through one ohm resistors as shown in Figure 3.2.6. The low value of the resistors guaranteed that the cathode segments were not varied much above ground potential, as d. c. experiments had indicated the currents to the cold cathode were of order 100 mA. The voltages across the resistors were then amplified and displayed on a double beam oscilloscope against time. (Figure 3.2.6) The result for a discharge current of 15 amps in a confining field of 4000 gauss for the short machine shows a large number of frequency components present. However, if we assume six cycles in a time interval of 100 μsec (60 Kc -a streak camera picture under similar conditions indicated 67 Kc/s), then the two waveforms seem to be 180° out of phase, corresponding to one filament. The different appearance of the two waveforms may be due to misalignment of the tube in the magnetic field.

3.2.1.5 Fluctuations in Electron Temperature and Plasma Density

We have also obtained experimental evidence that there exist different electron temperatures at any instant, in the discharge. This result was deduced

using a time resolved probe technique described elsewhere[8]. Essentially this consists of a probe whose characteristic is displayed on an oscilloscope, the sweep voltage being the noise voltage in the plasma. Photographs of the traces (which gave a time average) showed two distinct characteristics corresponding to electron temperatures of around 4.4 eV, and 3.2 eV, suggesting that the filament was at one temperature, and the rest of the plasma at the other. The photographs also showed two distinct values of ion saturation current, suggesting two different plasma densities, at any instant.

In all of the experiments, in addition to the rotation frequencies, there existed a broad band of noise frequencies. This will now be considered in detail.

3.2.2 Broad Band Electrical Noise

Although several methods had been used to measure rotation, the best way of measuring the broad band noise was undoubtedly to use a probe and a spectrum analyser, as this enabled a separate evaluation of the contribution from rotation and from the broad band noise. The parameters that were varied here were the total discharge current (which meant changing the plasma density and the radial field), the confining magnetic field, the neutral pressure, the radial position of the probe, and the cathode temperature.

3.2.2.1 Effect of varying the discharge current

A probe was connected as shown in Figure 3.2.4, and keeping the pressure (3μ) and the confining field (4000 gauss) fixed, the effect of varying the current

was investigated. The voltage current characteristics on an x-y recorder and the density vs current characteristic from a microwave measurement were monitored continuously. Representative frequency spectra are shown in Figure 3.2.7.

It seems that the electrical noise occurs at all values of the discharge current investigated, together with the rotation frequencies. At any current the noise seems to occur in a broad band from very low frequencies up to several hundred kilocycles, the amplitude being fairly constant at low frequencies, and decreasing at higher frequencies. The pictures were taken by allowing the electron beam on the long persistence screen to sweep across about 8 times, which took about 5 seconds, so a certain amount of time averaging is shown.

The effect of varying current is shown in pictures A and B. A seven-fold current increase has increased the amplitude of the noise by a factor of about 1.3. In addition, the noise bandwidth has increased. Taking the bandwidth to where the amplitude drops to 1/e of the low frequency value we may say that at 5 amps this value is 140 Kc/s, and at 35 amps this is 600 Kc/s. This increasing the current increases the noise in bandwidth, and slightly in amplitude.

A more detailed measurement of the rms noise vs current will be treated in Section 3.2.2.4 where the effect of radial position of the probe is considered.

3.2.2.2 Effect of Varying the Confining Field

In this experiment, the noise voltage from the probe was measured with a Ballantine Type 320 rms voltmeter, which had a frequency response of from d.c. to 300 Kc/s, just sufficient for our needs. Since the measurement is of broad

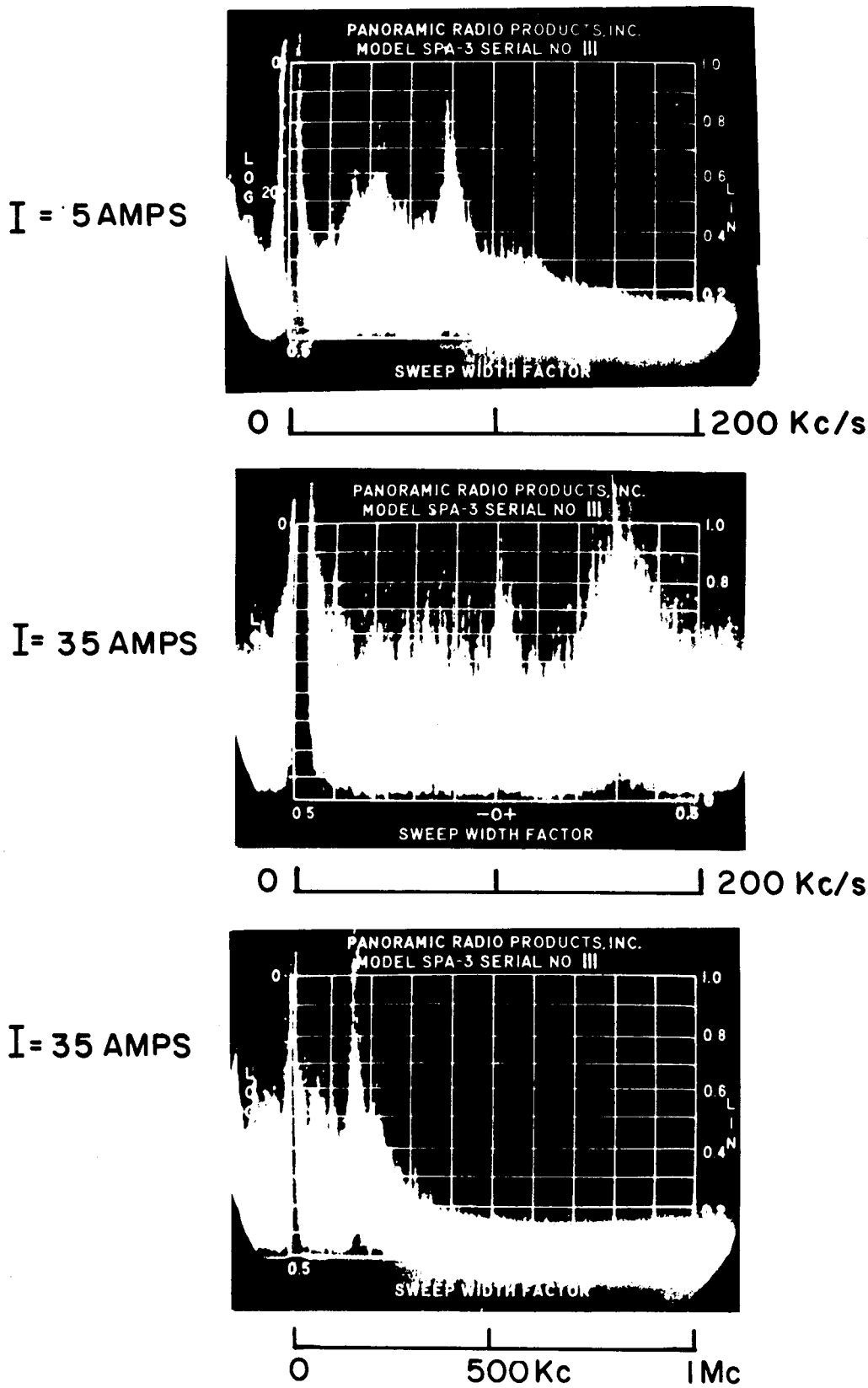

FIG. 3.2.7 EFFECT OF VARYING DISCHARGE CURRENT ON THE NOISE SPECTRUM

band noise, there is some error in also including the coherent rotational frequency. This error is not great, however, as can be seen by integrating the amplitudes in frequency space in the spectrum analyser photographs. The current was kept fixed and the density constantly monitored by our 8 mm μ-wave density apparatus. The pressure was monitored using a Veeco gauge, which was read between each reading with the confining field off, and showed a constant pressure of 4μ. The confining B field was then varied from 2 to 4 kilogauss, the lower limit being dictated by arcing inside the machine, and for each reading the rms voltage was measured. The result is shown in Figure 3.2.8 and indicates that if the discharge current is constant, together with the plasma density, then the root mean square value of the hash voltage is roughly independent of the confining B field.

3.2.2.3 Effect of Radial Position of the Probe on Hash

This experiment was perhaps the most revealing of the nature of the broad band noise. The amplitude of the rms noise voltage was plotted as a function of radial position of the probe tip, for different currents. The circuit is shown in Figure 3.2.9.

The probe tip was moved 1/4" at a time across the discharge, the confining field being fixed at 4000 gauss. The hash voltage was fed through the resistance capacity network into a Ballantine type 320 rms voltmeter. This meter had a mean square output which was displayed as y displacement on an x-y recorder. The voltage difference between the ends of the 20 ohm resistor in

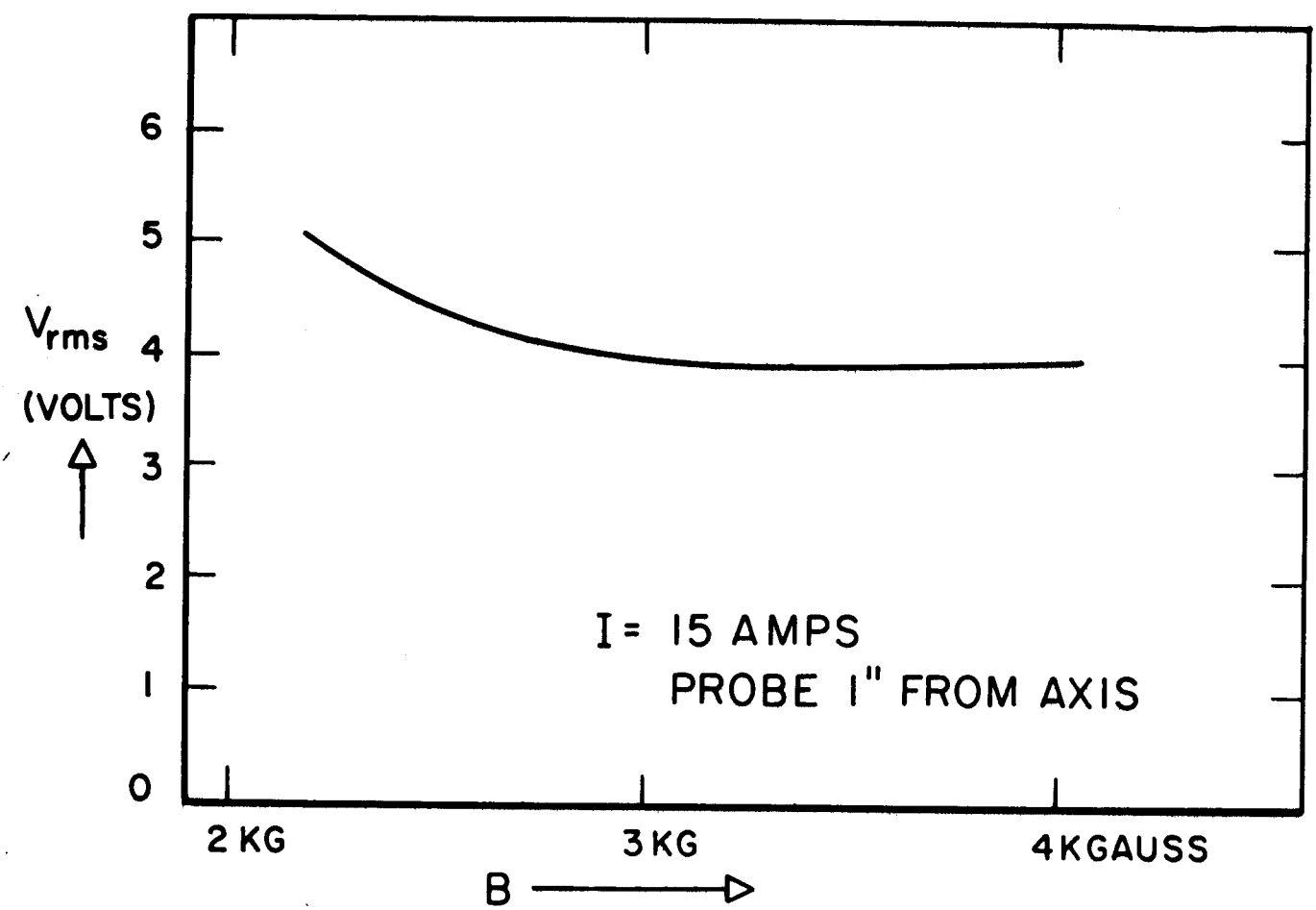

FIG. 3.2.8 EFFECT OF THE CONFINING FIELD ON THE R. M. S. VALUE OF THE NOISE VOLTAGE

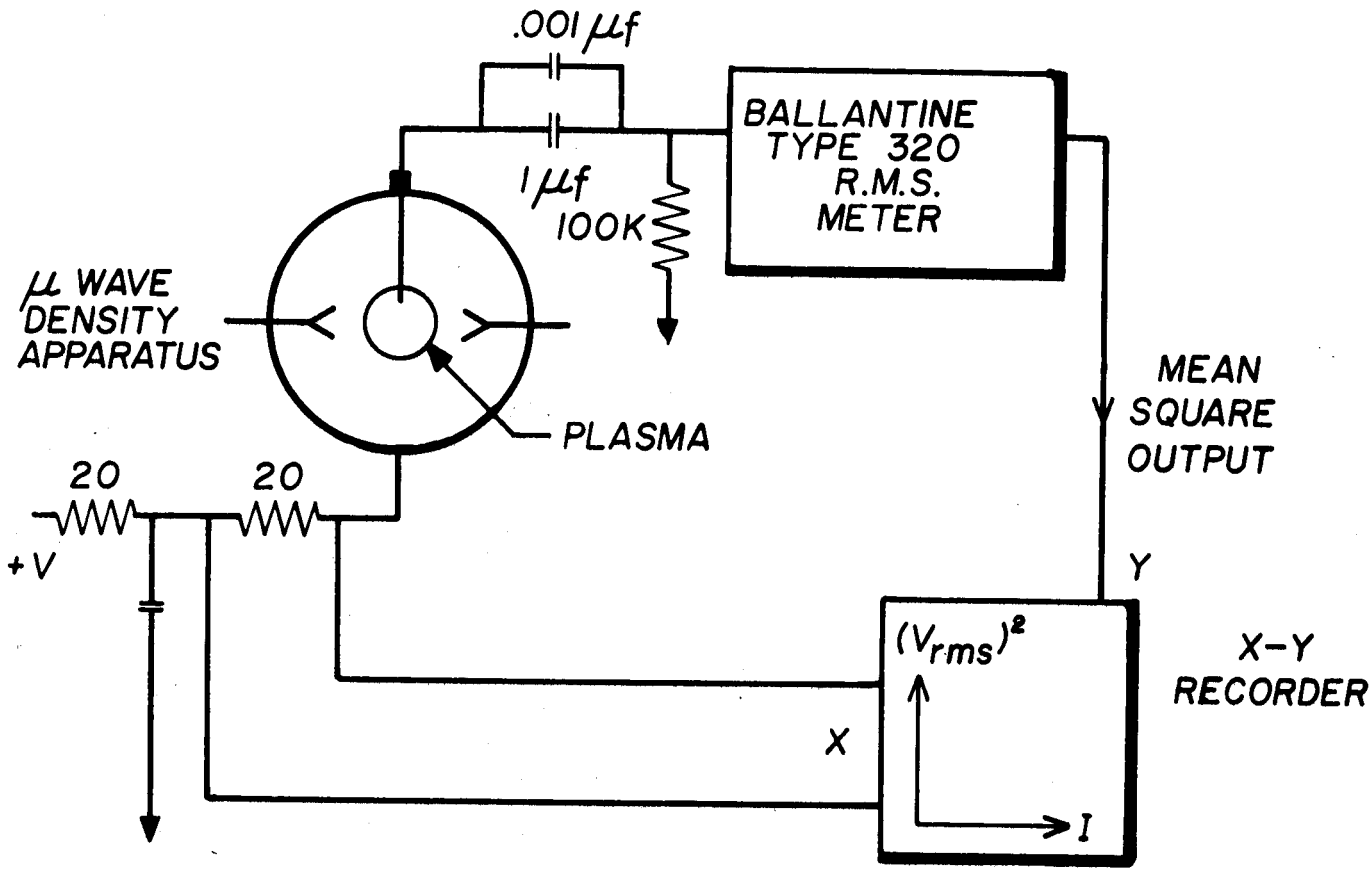

CIRCUIT FOR MEASURING V_{rms} AS A FUNCTION OF r FOR DIFFERENT DISCHARGE CURRENTS

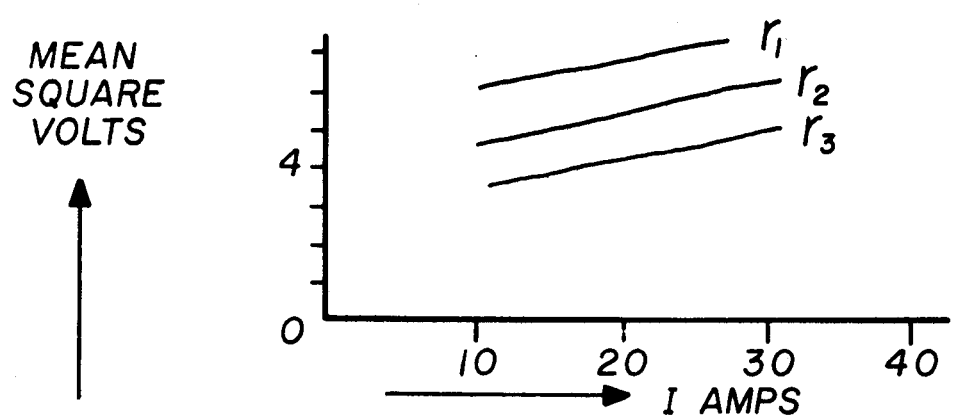

TYPICAL VALUES OF V_{rms} VS CURRENT FOR FIXED PROBE POSITIONS

FIG. 3.2.9 V_{rms} AS A FUNCTION OF RADIUS AND CURRENT

series with the anode, was fed to the differential amplifier controlling the x displacement which thus plotted discharge current. For each probe position an x-y recording of mean square voltage vs current was taken. The plasma density was monitored simultaneously by the 8mm μ wave apparatus.

Some typical mean square noise voltage vs discharge current characteristics are shown, indicating a small increase in noise at higher currents. This result confirms Section 2.1. However, the results show considerable variations with probe position.

If we plot the square root of the mean square voltage vs probe position, for fixed currents we obtain the radial dependence of V_{rms}. (Figure 3.2.10) These values agree both in shape and magnitude with the temperature vs radius characteristics, and suggest the relation $eV_{rms} \cong KT_e$. It must be pointed out that another possibility is $V_{rms} \propto V_{d.c.}$. The former expression suggests that the upper limit of the noise voltage is determined by the electron temperature.

This relation is also consistent with the experimental dependences on varying current, confining field and pressure; the electron temperature shows the same variation as V_{rms}.

3.2.2.4 Effect of Varying Cathode Temperature

The purpose of this experiment was to see if the rotation and the noise spectrum depended on conditions at the cathode, especially in so far as a cathode sheath may be involved. Keeping the confining field, the pressure and the current constant, the emission of the cathode was altered by altering

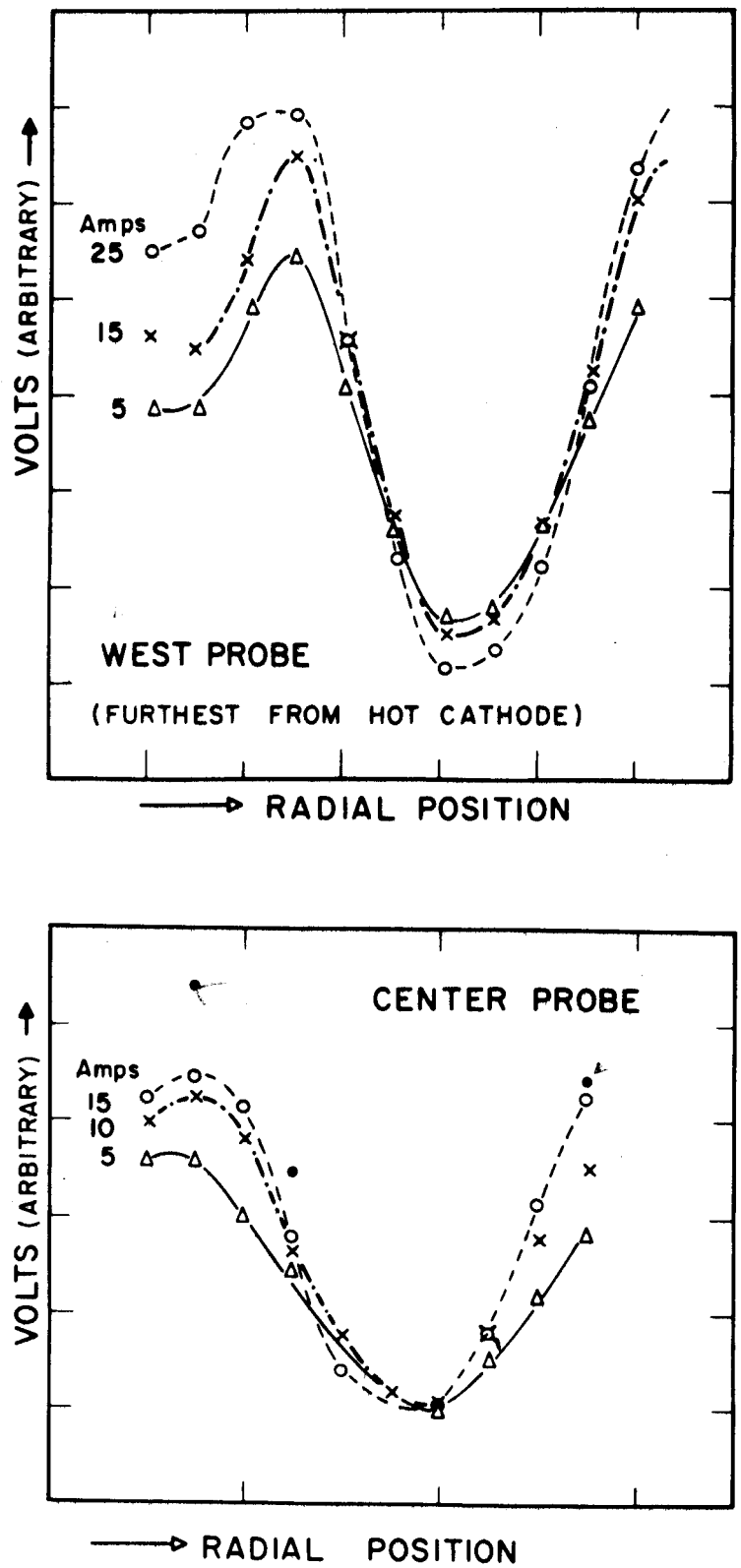

FIG. 3.2.10 V_{rms} AS A FUNCTION OF RADIAL POSITION FOR DIFFERENT CURRENTS

its temperature. The applied voltage across the discharge had to be increased as the temperature was lowered to keep the current constant. The cathode temperature could be varied by altering either the electron bombardment current or the accelerating voltage, and in the experiment the power input was varied from 5.5 to 3.2 kw corresponding to a temperature range of approximately 2700 to 2500°K, and maximum thermionic emission currents of 1.6 amps/cm^2 to o.25 amps/cm^2. For each temperature a spectrum analyser photograph was taken (Figure 3.2.11).

The results show that decreasing the cathode temperature from the normal running value of 2700°K increases the amplitude of the broad band hash, but the rotation peaks do not increase in amplitude. The rotation frequencies are independent of the cathode temperature and the rotation peaks are sharper at high cathode temperature. The first and second harmonics change in relative amplitude and moreover are not exact multiples of each other, for a reason not yet understood.

3.2.2.5. Fluctuations in Probe Current

The circuit of Figure 3.2.12 was constructed, and spectrum analyser photographs taken from connection 1, 2, and 3 over a frequency range of 0 to 200 Kc/s. The power supply was adjusted about 20 v negative of the floating potential of the probe so that saturation ion current flowed. The output from connection (1) then represents the frequency spectrum of the saturation ion current. A second method of measuring the current fluctuations is to use a Tektronix clip-on current probe (2). In contrast, connection (3) represents the voltage fluctuations on the probe. The photographs show that both the rotation frequencies and the broad band noise are fluctuations in density

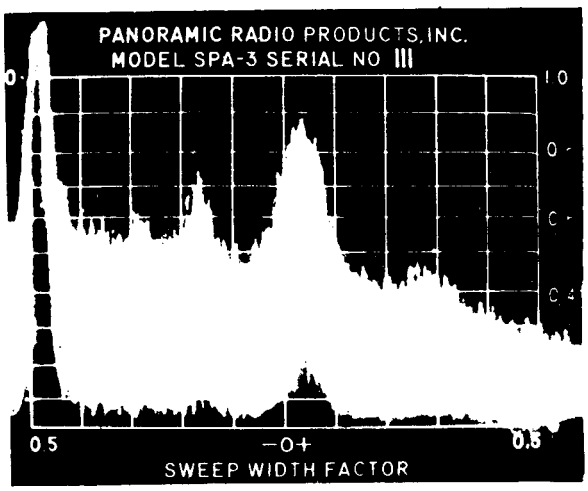

5.7 KW

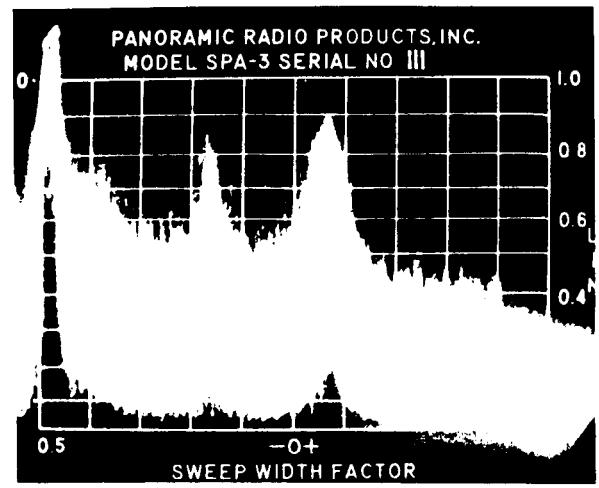

4.7 KW

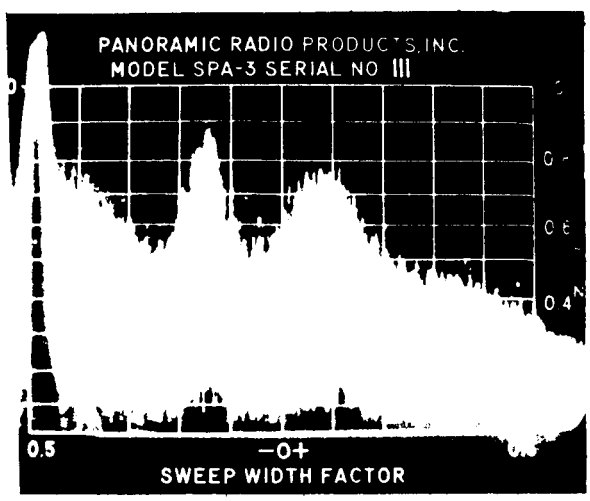

4.1 KW

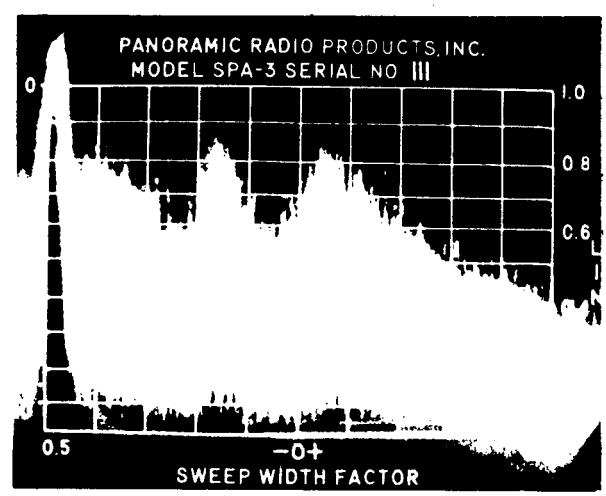

3.8 KW

FIG. 3.2.11 PROBE NOISE AS A FUNCTION OF CATHODE HEATER POWER

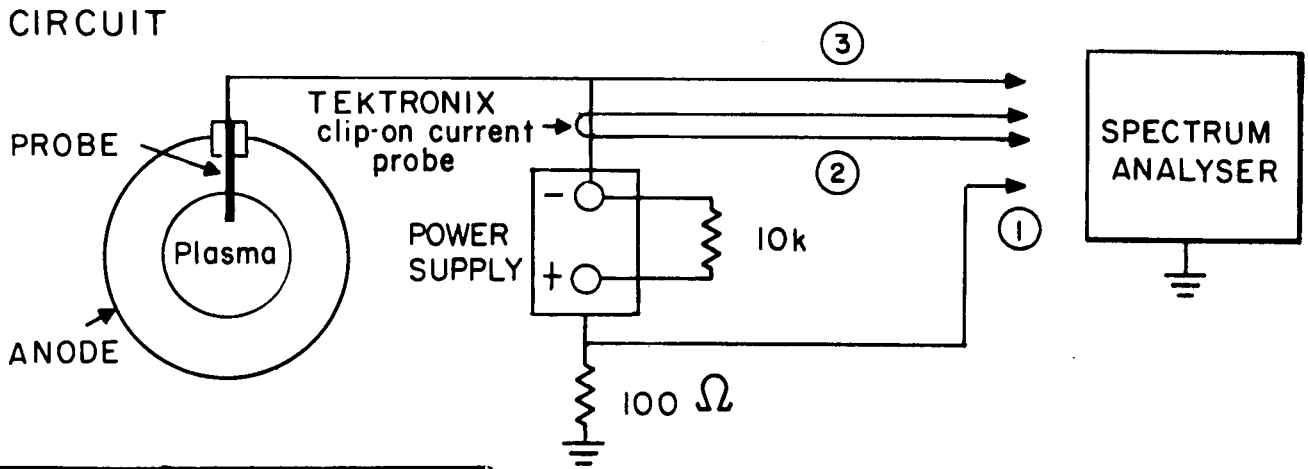

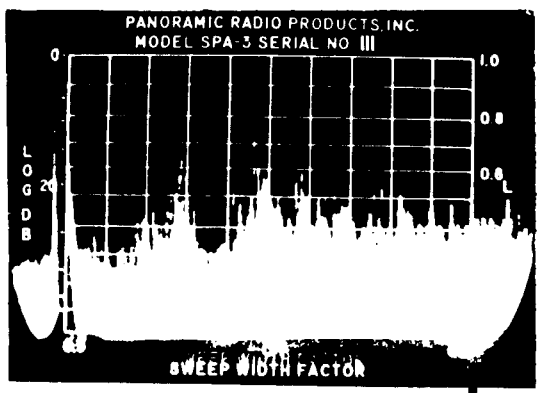

① FREQUENCY SPECTRUM OF VOLTAGE ACROSS 100 Ω. SATURATION ION CURRENT, WITH PROBE AT -20 VOLTS.

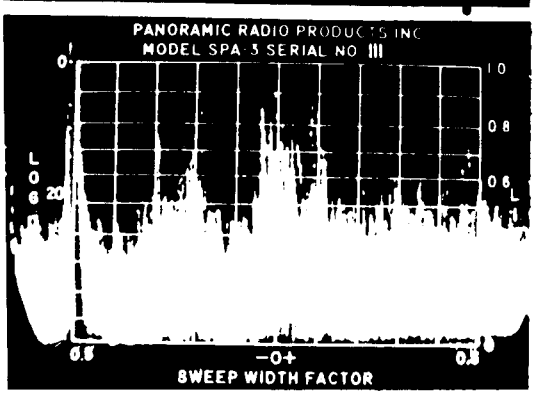

Noise Amplitude

② FREQUENCY SPECTRUM OF SIGNAL FROM TEKTRONIX PROBE.

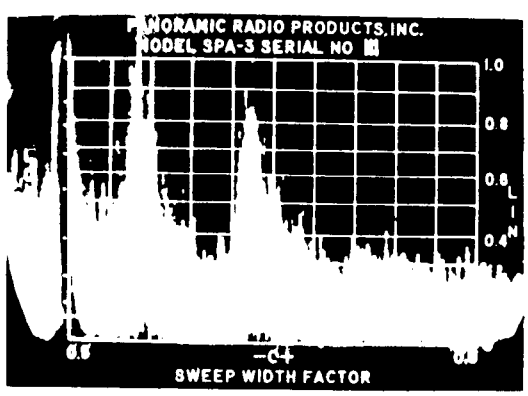

③ FREQUENCY SPECTRUM OF VOLTAGE FLUCTUATIONS OF FLOATING PROBE.

200 Kc/s
f

FIG. 3.2.12 OSCILLOGRAPHS OF CURRENT AND VOLTAGE NOISE

as well as potential.

3.2.2.6 Correlation Distance Measurements

The purpose of this experiment was essentially to find out over what distance in the discharge the noise voltages were in phase. Consider a probe placed in a discharge and picking up a root mean square voltage V_1. Another probe a large distance away would pick up a voltage V_2 and on the average these values would be equal. However, they would be uncorrelated in frequency and phase so the average product $\overline{V_1 V_2}$ would be zero. On the other hand if the probes were infinitely close together the average product would be $\overline{V_1^2}$ or $\overline{V_2^2}$. If the probes are moved slightly apart the product $V_1 V_2$ will become less than $\overline{V_1^2}$, and the separation at which

$$\overline{V_1 V_2} = \frac{1}{e} \overline{V_1^2}$$

is defined as the correlation distance.

In a discharge with a magnetic field we may measure such a distance across or along the field. Here we measured across the B lines only; such a measurement along the B lines would require accurate alignment of the probes which could only be done using an electron beam. The apparatus (Figure 3.2.13) consisted of two probes whose tips could be moved apart known distances, and connected to a wide band differential amplifier. The connections were made through a resistance capacity network giving an output independent of frequency up to 100 kc. The condenser in series with the probe made the d. c. component of the

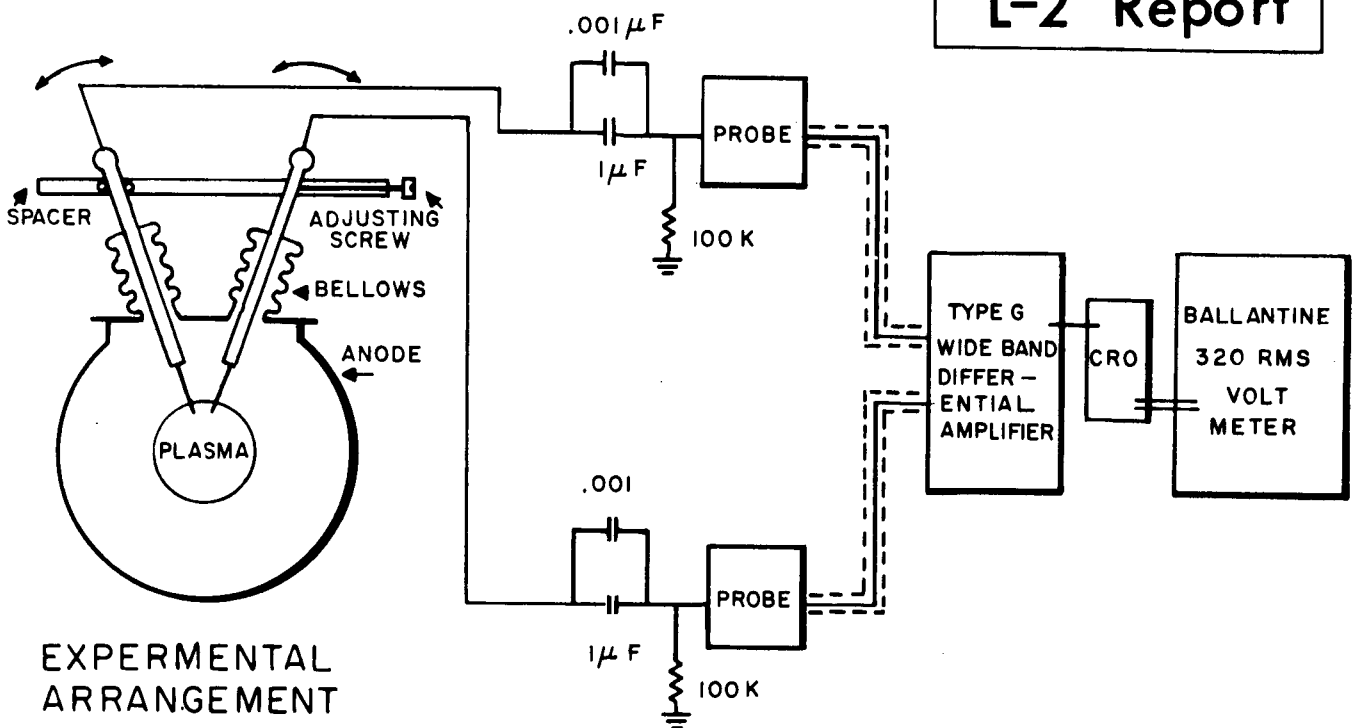

EXPERMENTAL ARRANGEMENT

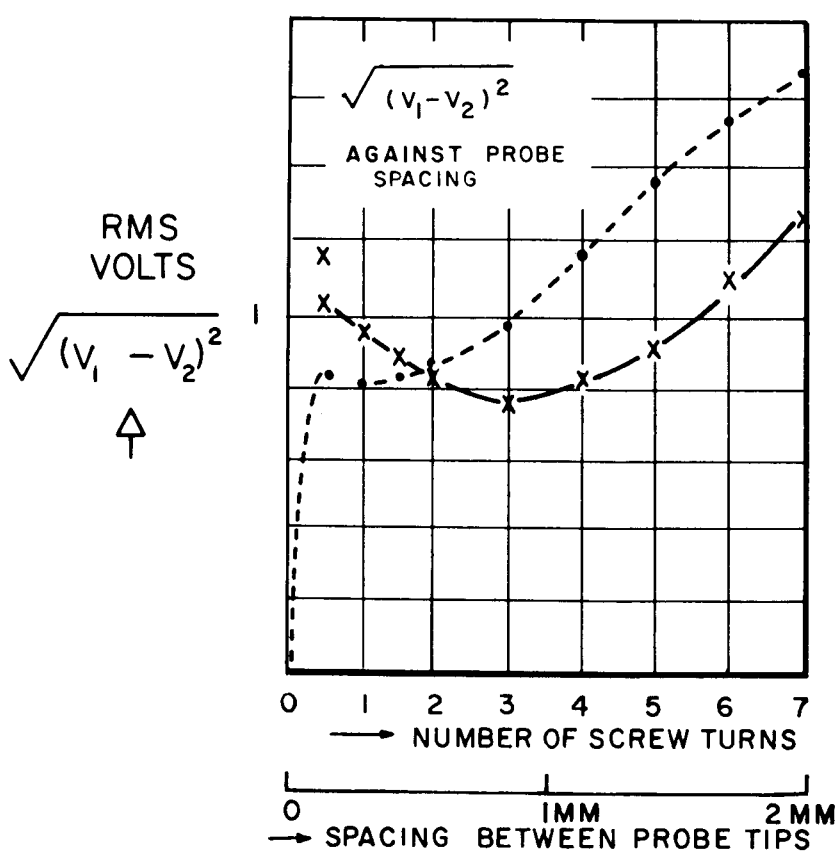

FIG. 3.2.13 CORRELATION DISTANCE MEASUREMENT

current zero. The differential amplifier then gave an output $(V_1 - V_2)$ monitored as a function of time on the oscilloscope. The signal $(V_1 - V_2)$ was then applied to a Ballantine type 320 rms voltmeter. This instrument actually squared the signals using a diode-resistance network, and was accurate to 1%. The scale reading was therefore $\sqrt{\overline{(V_1 - V_2)^2}}$. This quantity can be expressed as $\sqrt{\overline{2V_1^2 - V_1V_2}}$, and from equation (1) we thus see that at the correlation distance

$$\sqrt{\overline{(V_1 - V_2)^2}} \Big/ \sqrt{\overline{V_1^2}} = \sqrt{2(1 - 1/e)} = 1.12,$$

where $\sqrt{\overline{V_1^2}}$ is the rms value of one of the signals. The rms output was plotted against separation of the probes showing a gradual increase in signal as the probes were separated (Fig. 3.2.13.) At small separation, the apparatus did not give zero signal, but over distances of order 1 mm, it behaved reasonably. As $\sqrt{\overline{V_1^2}} = 4$ volts in this case, extrapolation showed that equation (2) was satisfied for distances of 0.3 cm. This result must be considered to give the order of magnitude only.

3.2.2.7 Summary of the A. C. Measurements

Thus we have two main phenomena in the discharge; rotation, and broad band noise. The rotation is probably due to $\underset{\sim}{E} \times \underset{\sim}{B}$ fields, where the E is the steady state averaged radial electric field. The broad band low frequency noise

seems to depend mainly on the electron temperature and has an amplitude of order KT_e. The upper frequency limit, somewhat ill-defined, also increases with current and in a general way increases with electron temperature.

4. THEORY OF THE DISCHARGE I

4.1 Introduction

It is the purpose of this section to gain some insight into the physical processes which are occuring in the discharge and to evaluate them quantitatively whenever possible. As the measurements have shown, there are both steady-state processes and time-varying (oscillatory) phenomena involved. A complete explanation of the discharge is not possible at this time not only because of the number and complexity of the processes involved, but also for the following two reasons. First, the discharge is spatially inhomogeneous, as shown by the streak photographs, so that even axial symmetry cannot be assumed. However, this is believed to be an experimental difficulty which can be overcome by modifying the apparatus. Second, the discharge is essentially a two-dimensional device, in which both radial and axial variations are important. Moreover, the boundary conditions are difficult, since at the outer radius the solution must be matched to the solution in the exterior (anode) region. It is obvious that unless extreme simplifications are made, even a numerical solution of the equations for the discharge would be very difficult. For these reasons, the considerations in this section are to be taken as an indication of our state of thinking about the reflex arc at this time.

Because of experimental difficulties, probably connected with the great length of the arc, a stable discharge could not be obtained over a large variation in magnetic field or pressure. Consequently, the theoretical considerations are primarily aimed at explaining the "standard" discharge at 4000 G., 3μ, He and 15

amperes. Clearly, the theoretical predictions might be severely tested when data at magnetic fields and pressures greatly different from these values are available.

First we shall discuss the time varying phenomena, and examine the physical processes which are occurrring. It will turn out that the nature of the fluctuations in the plasma strongly influences the averaged d. c. characteristics. Then we shall undertake some order of magnitude calculations on various time averaged processes, and based on these make an estimate of the discharge current, to check on the dependencies. Lastly spatial dependencies will be discussed.

4.2 Overall Picture of the Discharge

From the time averaged point of view our probe measurements suggest that the equipotentials as a function of position (Fig. 4.1 (a)) resemble concentric cylinders. In more detail we infer that the lines are approximately cylindrically symmetrical about the Z axis both inside and outside the plasma. Thus in general the electric fields along the B lines in the plasma are small, while there are large radial fields. This picture contrasts to other similar devices*, with lower B fields, which are claimed to have large E fields in the Z direction. Our measurements suggested such fields would be less than $\simeq$ 10 volts/2meters or 0.05 v/cm. As the cathode is at ground potential we must infer a plasma sheath at the cathode whose thickness varies radially, increasing with radius. Thus an electron emitted at the center would see little accelerating field before entering the plasma, and would be of low energy. An electron emitted near the perimeter would be accelerated

* Private discussion with R. G. Meyerand and F. Salz, United Aircraft, Hartford, Conn.

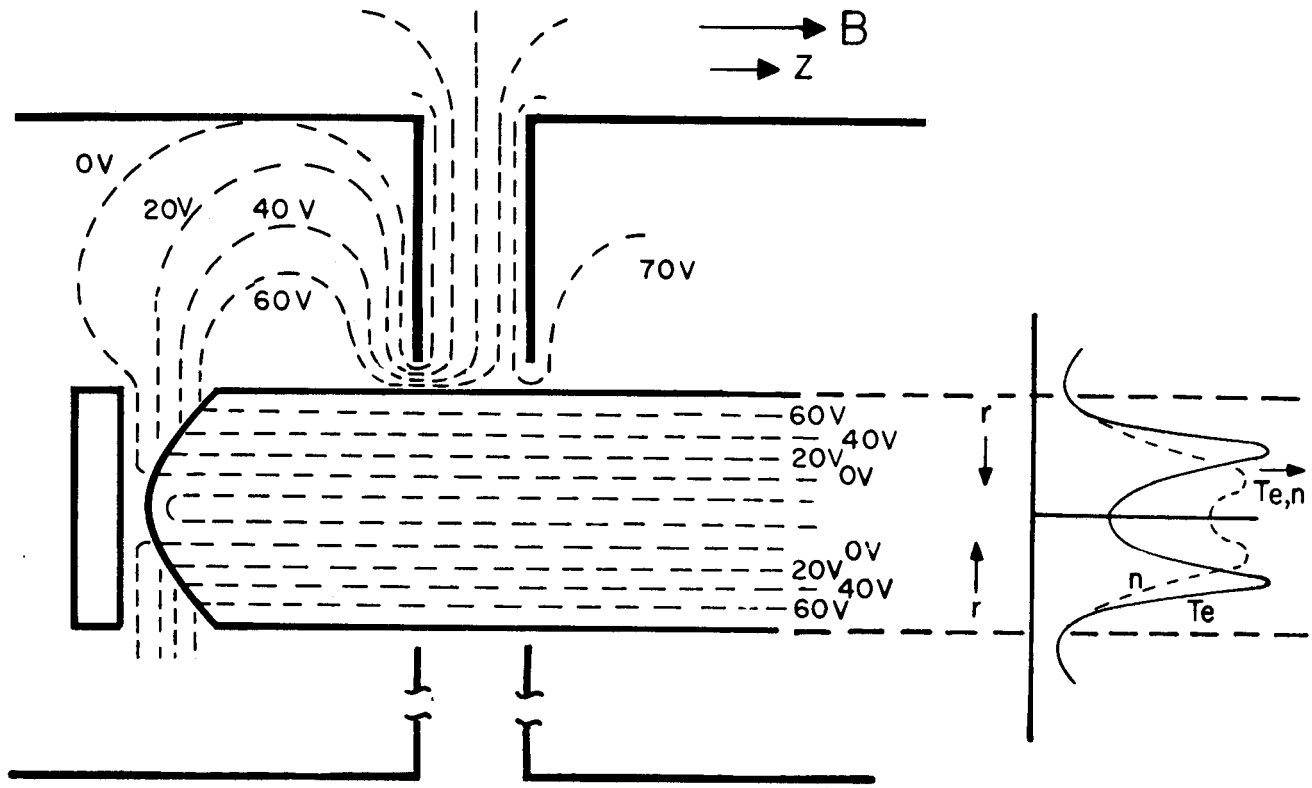

(a) EQUIPOTENTIALS NEAR HOT CATHODE, AND RESULTANT ELECTRON TEMPERATURE AND DENSITY DISTRIBUTION IN PLASMA.

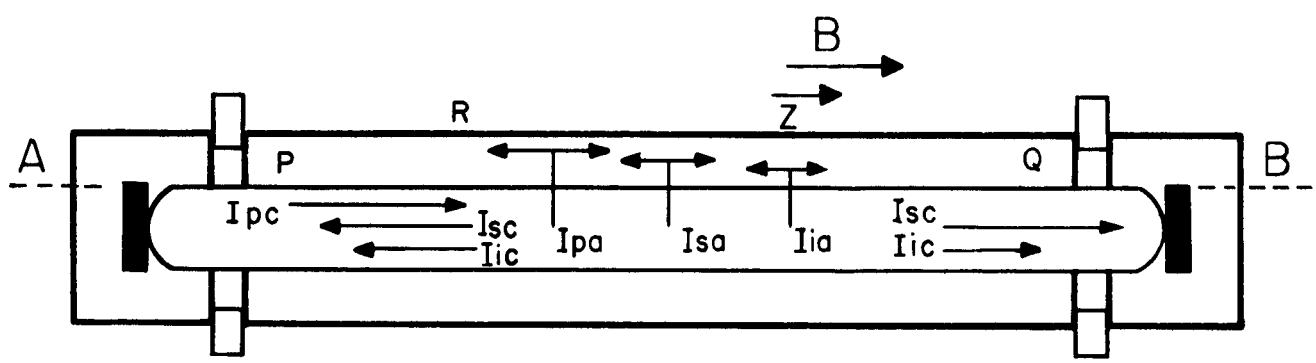

(b) CURRENTS IN THE DISCHARGE.

FIG. 4.1 OVERALL PICTURE OF THE DISCHARGE

say 60 volts in crossing the sheath, but thereafter would acquire negligible energy. Thus the electrons gain all their energy in the sheath only. Outside the plasma column the equipotentials are approximately as shown, as there is still a small density of charged particles there.

This picture is consistent in a qualitative way with the time averaged radial distribution of electron temperature, (Fig. 4.1 (a)) and also with the visible light emitted. Both these quantities show a slight drop the farther they are measured from the hot cathode, as would be expected if all the energy is given to the electrons at the hot cathode.

The cold cathode then mainly acts as a reflector, and on the whole does not impart energy to the electrons. However, it can collect particles. From the equipotentials we must infer a sheath similar to the hot cathode, to a first approximation. Then near the outside edges ions would be attracted from the plasma to the cathode, and this ion current would be limited by the ion diffusion through the plasma up to the sheath. Electrons would be repelled here. Near the center, however, there is little repelling field; and electrons, especially higher energy ones, can now reach the cathode. This picture agrees with measurements with a segmented cathode.

The main current flow then occurs as in Fig. 4.1 (b). The primary electrons enter from the hot cathode. Those near the outer edges have energies of about 60 eV and the main excitation and ionization processes occur here. Secondary electrons, of low energy, and ions are thus produced, in what can be regarded as a hollow cylindrical tube.

The strong confining B field permits the electrons to travel easily along the z axis. But to get to the anode both primary and secondary electrons must cross the line AB. (Fig. 4.1 (b)). Once they are just over, then they can travel along the B lines to the anode plates P and Q, much more easily than to the anode tube R.

The arc current I can be decomposed into the following components:

I_{pc} = primary electron current from the cathode

I_{sc} = secondary electron current to the cathode

I_{ic} = ion current to the cathode

I_{pa} = primary electron current to the anode ($= I_{pc}$)

I_{sa} = secondary electron current to the anode

I_{ia} = ion current to the anode

The arc current is then equal to

$$I = I_{pc} + I_{ic} - I_{sc}$$

In order to preserve charge neutrality, this must also be equal to

$$I = I_{pa} + I_{sa}$$

We neglect I_{ia} since the oscillations do not seem sufficiently large to drive the ions to the anode.

The last equation shows that in order for the discharge current to flow, electrons must cross the magnetic field to the anode in sufficient numbers to account for the entire discharge current.

For given neutral density, plasma density, and electron temperature, one can calculate for any particular geometry and arc current a critical magnetic field above which classical diffusion cannot account for the necessary transverse electron current. For the standard conditions of the L-2 discharge, the magnetic field is 6 or 7 times higher than this critical field. Thus a different diffusion mechanism is necessary for the discharge to operate at all, and an understanding of this discharge may be expected to shed some light on enhanced diffusion across a magnetic field.

4.3 Time varying Phenomena

As shown in the experimental section, these could be divided into phenomena associated with the overall rotation, and those associated with broad band noise.

4.3.1. Rotation

The two questions here are why does the discharge occur in a filament, and secondly what is the velocity of rotation of the filaments?

4.3.1.1. The Cause of the Inhomogeneity

We believe the occurrence of the filaments is based on the formation of a double sheath at the cathode. This will be dealt with later (Section 4.4.6.). It turns out that the current density emitted from the cathode into the sheath when space charge limited is given by

$$j = A\, n\, f(V)$$

where A is a constant, V the cathode-plasma voltage across the sheath, and n the density of the plasma. These emitted electrons, having been accelerated by the

voltage V, cause ionization in the plasma, thus determining n. A small increase in j will increase n, in turn reducing the space charge barrier to increase j still more according to (1). This then is an inherently unstable situation. There is an upper limit to n which may be dictated by temperature limited emission, by depression of V below the ionization potential, by depletion of neutrals, or possibly by recombination. If the current from the cathode were limited by a high impedance, then the emission might tend to concentrate in one spot. The $\underset{\sim}{E} \times \underset{\sim}{B}$ drift would then cause this region of higher density to rotate as observed.

4.3.1.2 Rotation Frequency of Filaments

From Section 3.2.1 we have seen that the rotation velocity of the filaments was given by

$$v_D \lesssim 10^8 E_r/B$$

where E_r was the radial field. Such a velocity was deduced assuming a collisionless plasma. More generally if we take the steady state generalized Ohm's Law, and take the vector product of each term with $\underset{\sim}{B}$. then, with the usual nomenclature, the drift velocity is

$$\underset{\sim}{v}_D = [\underset{\sim}{E} - \eta \underset{\sim}{j} - \frac{c}{en_e} \underset{\sim}{j} \times \underset{\sim}{B}] \times \underset{\sim}{B}/B^2 \qquad (1)$$

neglecting pressure and gravitational effects.

The second term in parenthesis represents the resistive, or energy loss term, due to the radial current density component. Taking the resistivity[9]

$$\eta = m_e c^2 \nu / n_e e^2 \qquad (2)$$

and calculating it both for electron-neutral scattering and for long range coulomb effects, where the collision frequency is essentially the inverse of the deflection time t_D [10], then the values of η are respectively 1.2×10^{-2} and 3.9×10^{-3} Ω cm.

If we include the magnetic field, for the long range coulomb force case, the resistivity across the B lines should be about 4 times higher or 1.5×10^{-2} Ω cm. The radial current density of the machine was $\approx 2.5 \times 10^{-2}$ amps/cm^2, so the ηj term gives fields of 3×10^{-5} and 4×10^{-5} volts/cm. respectively. Clearly this term is negligible compared with the radial E field $\approx$ 50 V/cm.

For the $\underset{\sim}{j} \times \underset{\sim}{B}$ term to have any effect on $\underset{\sim}{E}$ it must be a $j_\theta B_Z$ term. The j_θ arises from the centrifugal force on the ions, and is evaluated in the next section.

Another effect which may decrease v_d is the ion-neutral collisions. Both electrons and ions rotate around the axis, the latter with larger cross sections by a factor of about six. Each time an ion collides with a neutral, it can be considered to be brought almost to rest especially if charge exchange occurs. To continue its E x B drift velocity, the ion has to be accelerated by the E field during the first cyclotron orbit, and the time this takes is of order $1/\nu_{ci}$, where ν_{ci} is the ion cyclotron frequency. This happens once each collision, or in an interval $1/\nu_{i\text{-}n}$, where $\nu_{i\text{-}n}$ is the ion neutral collision frequency. Therefore the effective drift velocity is reduced by a factor

$$F = \frac{1/\nu_{i-n} - 1/\nu_{ci}}{1/\nu_{i-n}} = 1 - \frac{\nu_{i-n}}{\nu_{ci}}$$

For a neutral pressure of 3μ, and an ion velocity of 10^6, $\nu_{i-n} \sim 4 \times 10^5 \text{ sec}^{-1}$, while if B = 4000 gauss, $\nu_{ci} \sim 1.5 \times 10^6 \text{ sec}^{-1}$. Thus F ~ 0.8. In calculating ν_{i-n} we have used the drift velocity V_D, since this is larger than the ion thermal velocity. This can explain the measured discrepancy in rotation frequency.

At times the second, and even the third harmonic of the rotation frequency could be observed in the spectrum. Sometimes, however, there is a peak at approximately, but not exactly, half the rotation frequency. These peaks cannot be connected with standing waves in the longitudinal direction, since the frequencies are more than 10 times too high, and also cannot be standing waves in the radial direction, since the magnetic field is so strong that the group velocity across B must be very small.

NF shown in Figure

4.3.1.3 Azimuthal Current

The balance of forces on an ion is

$$e\left(\underset{\sim}{E} + \frac{1}{c} \underset{\sim}{v}_D \times \underset{\sim}{B}\right) + m_i \underset{\sim}{v}_D^2 \underset{\sim}{R}/R^2 = 0 \qquad (3)$$

where the last term is a centrifugal force term along the radius vector $\underset{\sim}{R}$. This leads to an azimuthal drift velocity of the ions of

$$\underset{\sim}{v}_D = c \frac{\underset{\sim}{E} \times \underset{\sim}{B}}{B^2} - m_i \frac{c}{e} \underset{\sim}{v}_D^2 \frac{\underset{\sim}{B} \times \underset{\sim}{R}}{B^2 R^2}$$

The centrifugal force depends on the particle mass, resulting in different aximuthal velocities for electrons and ions, and a net drift current flow, of

density

$$j_\theta = \frac{n_e}{c} (v_D - v_e)$$

where v_e is obtained from Eq. (4) applied to electrons and neglecting the centrifugal force term; thus

$$j_\theta = - n_e m_i v_D^2 / BR \quad e\ m\ u/\ cm^2$$

Taking the density $n_e = 3 \times 10^{12}$ cm^{-3}, $m_i = 6.4 \times 10^{-24}$ gm, $v_D = 1.25 \times 10^6$ cm/sec, (corresponding to a field of 50 V/cm), B = 4000 gauss, r = 2 cm. This gives

$$j_\theta \simeq 60 \text{ m A/cm}^2$$

This value is to be compared with a radial current density for a column 2 cm radius, 300 cm long carrying 15 amps or

$$j_r \simeq 3 \text{ m A/cm}^2$$

Thus the azimuthal current is about 20 times the radial current. Collisions with neutrals would slow the ions still more, adding to the azimuthal current.

Reverting to Eq. (1) and putting in values we find the $j \times B$ term of order or less than 10% of the E term. This effect is therefore less than that of ion-neutral collisions.

It should be pointed out that the probes actually measured the floating rather than the plasma potential. Using the latter would give still higher

How much is disparity increased by including such effects including radial gradient of temperature?

calculated values, increasing the disparity between theory and measurement. An effect to reduce the disparity would be emission from the probe which is unlikely.

4.3.2 Hash

We shall consider the amplitude and the frequency spectrum of the broad band noise.

4.3.2.1 Amplitude

Our measurements indicate that the amplitude of the noise is given by

$$V_{rms} \simeq kT_e/e$$

and the dependence of V_{rms} on current, B fields, and especially its radial dependence seem to confirm this. This forms a reasonable picture, suggesting the discharge can withstand voltage differences of the order of its electron temperature.

4.3.2.2 Frequency Spectrum of the Noise

The bandwidth of the noise seems to extend from frequencies of a few Kc/s (the lower limit of the spectrum analyzer) up to about 400 Kc/s. The upper end of the spectrum seems to go to higher frequencies for larger plasma currents, which in general correspond to higher electron temperatures. However, the upper end is not too well defined, and it may be that at higher currents, the upper frequencies increase only in amplitude, suggesting a higher cut-off frequency.

The lowest frequencies extended down to about 1 Kc/s. These low frequencies suggest the noise might be due to ion wave instabilities[11], which have a fairly slow propagation velocity, equal to an ion with the mean electron thermal energy or

One might even consider making some additional measurement, using spectrum [illegible] and floating probes at several radial positions, to get Γ as V_{rms} and secondarily.

Question of variation of f with n? Some variation might be explained

Table 3. Comparison of characteristic times for a plasma of density 3×10^{12} cm^{-3} in helium of neutral density 10^{14} cm^{-2}, assuming short range forces and long range coulomb forces.

SHORT RANGE FORCES						LONG RANGE COULOMB FORCES					
Character-istic time	Electrons			Ions		Character-istic time	Electrons			Ions	
	1eV	5eV	100eV	0.1eV	5eV		1eV	5eV	100eV	0.1eV	5eV
Collision time						Collision time					
t_{e-n}	3×10^{-7}	2×10^{-7}	1.5×10^{-7}			t_D	5×10^{-9}	4×10^{-8}	3×10^{-6}		
						Self collision					
t_{i-n}				10^{-5}	2×10^{-6}	$t_{c\ e-e}$	10^{-8}	8×10^{-8}	7×10^{-6}		
						$t_{c\ i-i}$				5×10^{-8}	8×10^{-6}
						Equipartition time					
						$t_{eq\ e-i}$	4×10^{-5}	3×10^{-4}	2×10^{-2}		
						$t_{eq\ e-e}$	5×10^{-9}	4×10^{-8}	4×10^{-6}		

$$V_s = (kT_e/m_i)^{1/2} = 1.5 \times 10^6 \text{ cm/sec}$$

for $T_e = 5$ eV. If the machine length (300 cm) were half a wave-length, the lowest frequency would be 3 KC/s, still slightly higher than observed.

An explanation of the very low frequencies is based on the Doppler effect. The ions entering from the sheath have velocities of the same order as V_s. If ion waves occur in such a fluid, then any waves travelling in the opposite direction to the ions would appear to be of low velocity in the laboratory system, and hence of low frequencies.

4.4 Elementary Processes

4.4.1 The Collision Processes

Our discharge occurs in helium with neutral densities $\cong 10^{14} \text{cm}^{-3}$, and plasma densities $\cong 3 \times 10^{-12} \text{cm}^{-3}$ (3% ionization). The relative importance of long range coulomb forces and short range forces will be considered here.

Table 3 shows a comparison of characteristic times assuming short range forces and long range coulomb forces. The deflection, equipartition, and self collision times are as defined by Spitzer[12], and are calculated on the assumption of a fully ionized plasma which is not the case here. The equipartition times assume the field particles at a much lower temperature than the test particles.

We conclude from comparing these times that at 3% ionization long range coulomb forces are comparable in importance with short range forces.

4.4.1.1 Charge Exchange

When helium ions collide with neutral helium atoms, the predominating

type of collision results in charge exchange. The ion that hands over its charge hands over very little of its kinetic energy, and continues as a fast neutral atom. The newly formed ion starts at almost zero velocity, and then gains energy from the electric field, and travels the next mean free path until charge transfer take place once more, and so on. Thus the process behaves as if a single ion were moving, which at each collision with a neutral, loses all of its kinetic energy.

The probability of collision of helium ions in helium showing charge transfer is given in Fig. 4.2.[13] The values for the probability of charge transfer collisions at energies of a few volts agree roughly with the results of Chanin and Biondi[14] and Hasted.[15]

4.4.2 Energy loss by primary electrons

If we assume that most of the ionization occurs near the edge of the discharge, where a sheath drop of 30-60 volts exists to accelerate the primary electrons, we can estimate the relative rate of loss of energy in ionization and excitation collisions with neutrals, and in elastic collisions with electrons (energy losses in elastic collisions with heavy particles being negligible relative to the latter). The ionization cross section in this energy range is given by Massey and Burhop[16] to be 2×10^{-17} cm^2, and the excitation cross section can be estimated by taking the ratio of exciting to ionizing collisions, from the results of Maier-Leibnitz[17]. The rate of energy loss is then given by $n_o(\overline{\sigma_i v} + \overline{\sigma_e v})\bar{\epsilon}$, where $\bar{\epsilon}$ is the average energy loss in an inelastic collision.

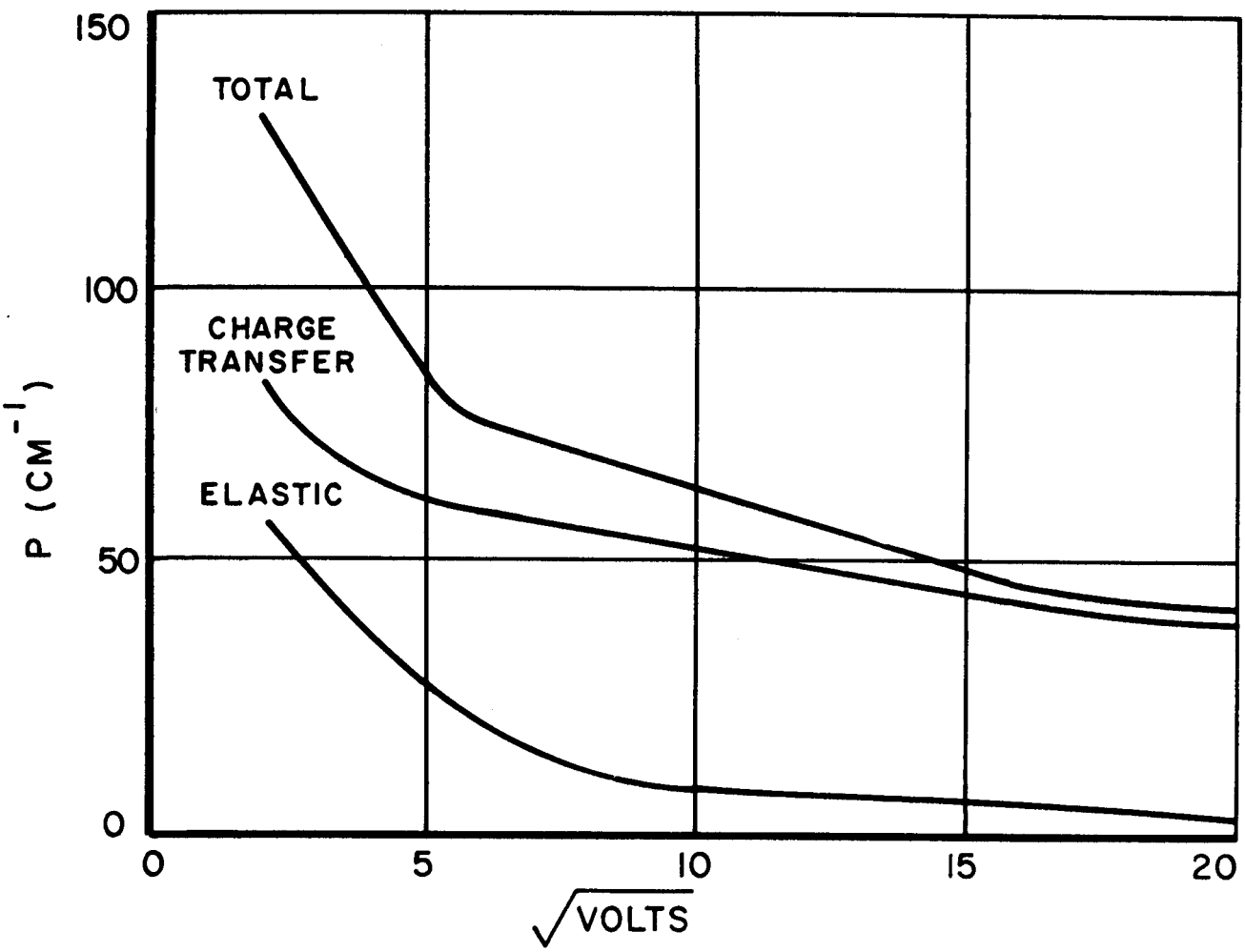

FIG. 4.2 PROBABILITY OF COLLISIONS OF He^+ in He (AFTER CRAMER AND SIMONS)

This is approximately the same for ionizing and exciting collisions, since the first excitation level of He is 19.8 volts, and the ionization potential is only 24.5 volts. This rate is then to be compared with E/t_s, where E is the initial energy of the primary, and t_s is Spitzer's slowing-down time.[12] From this it is seen that the loss in inelastic collisions is 4×10^7 eV/sec, and that in elastic collisions is 8×10^6 eV/sec, so that we may neglect elastic collisions to a first approximation.

The confinement time of the primaries can be estimated by assuming they diffuse across the field with the same coefficient as the plasma electrons (see Sec. 4.6). This yields a confinement time of order 10^{-4} sec. Since the energy loss time is much less than this, the picture is that the primaries are trapped between the cathode sheaths and travel back and forth, losing energy in inelastic collisions, until their energy falls below ϵ_1, the first excitation level of He. After that, they become plasma electrons via elastic collisions with electrons or excitation collisions with impurity atoms. The number of inelastic collisions suffered per primary is then obviously

$$N = (E - \frac{1}{2}\epsilon_{el})/\bar{\epsilon}$$

where $\frac{1}{2}\epsilon_{el}$ is the average remaining energy after the last inelastic collision and $\bar{\epsilon}$ the average energy lost per inelastic collision. If the ratio of ionizing to exciting collisions can be approximated by 1, the number of ion pairs produced per primary is $\frac{1}{2}N$. For the energies E involved, this number is of the order of 1.

Since the mean free path $\lambda = [n_o(\sigma_i + \sigma_e)]^{-1}$ for inelastic collisions is about 250 cm, or slightly less than the length of the machine, the primary beam actually becomes attenuated by the time it reaches the cold cathode. Hence the plasma would not be expected to be uniform axially; this is evident from visual observation.

4.4.3 Calculation of Electron Temperature

The fact that the time the electron takes to lose an appreciable amount of its energy by elastic collisions is several times longer than the time for an inelastic collision, shows that for energies above its ionizing energy not much of the kinetic energy is used for heating the electrons. However, there are two ways in which the plasma can be heated. First, in each ionizing collision, kinetic energy is transferred to the secondary electron. The energy distribution of secondary electrons ejected in ionizing collisions of electrons with helium atoms has been calculated by Massey and Burhop,[18] and it seems that 50 eV primaries yield secondaries in a distribution up to about 30 volts, with a maximum at 6 eV, whereas 25 volt primaries yield a distribution up to about 9 volts with a peak at 4 volts. These values, based on Born's approximation are too high, as can be seen by the fact that a 25 eV electron could at most hand over 0.5 eV to the ejected electron if the ionization energy is 24.5 eV. For simplicity we shall take them to be correct in order. Second, the primary electrons lose increments ϵ_i or ϵ_{ex} volts each inelastic collision plus the imparted kinetic energy to the secondaries until eventually their energy is below ϵ_{el}. As the inelastic collisions resulted

in losses of large increments of energy the final energy now can be anything from zero to ϵ_{el}. This remaining energy, on the average $\epsilon_{el}/2$, is dissipated by elastic collisions in heating the plasma and in inelastic collisions with impurity atoms, which have lower excitation levels. A rough estimate of the plasma temperature can be made if we assume that primaries enter from the sheath each producing n_i secondaries with a kinetic energy ϵ_K, and finally giving to the plasma an average $\epsilon_{el}/2$ surplus energy. The electrons in the plasma share this energy but remain in the plasma only for a time τ, (see Sec. 4.6). Thus consider a tube of cross-section 1 cm^2, and length L, the machine length. Then if the primary flux entering the tube is j_p, balancing the energies we have

$$j_p(\epsilon_{el}/2 + n_i\epsilon_K) = n\ L\ \epsilon_{th}/\tau \qquad (1)$$

where n_i is the number of secondaries per primary, and ϵ_{th} is the average energy of the plasma. This employs the basic assumption that the diffusion process is energy independent. Putting in values:

$j_p \sim 10^{19}$ electrons/sec cm^2, $\epsilon_{el} \sim 20$ eV, $n_i(V) \sim 0.6$ for $V = 50$,

$\epsilon_K \sim 5$ eV, $n = 3 \times 10^{12}$, $L = 300$, $\tau = 9 \times 10^{-5}$ sec, then

$$\epsilon_{th} \approx 10 \text{ eV}$$

This is somewhat higher than observed, probably due to the neglect of impurities and energy loss to He ions via oscillations. The first term in parenthesis is independent of the energy V of electrons from the sheath, but both n_i and ϵ_K

are functions of V. In the above example, for 50 eV electrons the contribution from the $\epsilon_{el}/2$ is about twice that from the secondaries. If V were 100 volts then $n_i \sim 1.7$, $\epsilon_K \sim 5$ eV and the two contributions would be comparable.

Variations in T_e along the Z axis can also be deduced from (1). The ionizing mean free paths for primaries were of order the machine length for primaries of 70 eV, so that most of the ionization collisions occurred near the hot cathode. Hence the contribution $(j_p)n_i\epsilon_K$ from the secondaries was greater near the hot cathode and the temperature a few electron volts higher there than at the cold cathode end, as measured. The $\epsilon_{el}/2$ term resulted from electrons which had completed inelastic collisions, and would be expected to be fairly constant along the Z axis.

4.4.4 Ion Velocity Distribution

At first sight it was thought that the ion temperature T_i in the discharge was much lower that the electron temperature T_e, and of order 0.1 eV. This value was estimated by assuming that the primary and secondary electrons handed over energy by elastic collisions to both ions and electrons so that the ratio of energy handed to the ions, to that handed over to electrons by either short or long range collisions was of order $m/M_i = 1/8000$. However, a consideration of the oscillations in the plasma has led us to the view that this picture is incorrect.

We have measured oscillations in the plasma of voltage

$$V_{rms} \approx KT_e/e$$

These voltages are random in frequency, and the electric fields random in direction. The fields extend over distances of order a few mm, where this distance is the correlation distance a. We shall show later that

$$a = r_{Li}$$

the Larmor radius of the ion. Now if this be so it follows that the ions can move this distance taking energy from the E field even across the B lines, or the kinetic energy of the ions at their maximum velocity in their orbits is

$$\epsilon_i = kKT_e$$

where k is a constant less than, but of order of, 1. Hence the ions have an average energy comparable with that of the electrons. Thus the concept of ion temperature is inapplicable here, although we shall use a quantity T_i, as a measure of ion energy.

It follows if $T_i \approx 5$ eV that the Larmor radius of the ions is about 2mm, and the path traced out per revolution is about 1.2 cm. For ions of energy 5 ev, the ion neutral mean free path ≈ 3 cm at p = 3μ, so the ions hit a neutral helium atom about once every 3 revolutions. At 4000 gauss the ion cyclotron frequency = 1.5 Mc/s, so that the collision rate is 5 x 10^5 sec^{-1}. If charge exchange occurs this means that the random fields can hand over energy to the ions which in turn is handed to the neutrals, and this should damp the oscillations. Charge exchange collisions reduce the ion energy, probably to about 2/3 kKT_e on

I believe this computation neglects the fact that ω_{ci} > freq. of oscillation. The ions will move along the instantaneous equipotentials with the E × B velocity, & they may gain a K.E. comparable to what you have computed. But the random energy will be much less.

You do not mention acceleration along the lines of force. For these the [illegible] Energy = kT_e + kT_i + eV_{rms} (Macroscopic Mean Energy)

the average as one neutral collision occurs per 3 oscillations.

The ion velocity can therefore reach a sizable fraction of the sound velocity $v_s \equiv (KT_e/M_i)^{1/2}$. Superimposed on this would be an E x B drift velocity v_D, and the resultant path is a random walk, the length of a step being comparable with r_{Li}. During each step then

$$v_D \simeq cE/B \simeq c\ KT_e/e\ Br_{Li} \simeq (KT_e/M_i)^{1/2}$$

So

$$v_{i\perp} = v_s \approx v_D$$

4.4.5 Diffusion by Oscillation

Calculations of current based on classical diffusion will be given later, and show that classical diffusion is not the main process in our discharge. We shall assume that the diffusion process is enhanced or oscillatory diffusion due to plasma instabilities. This mechanism was first suggested by Bohm et al,[19] on the assumption that such large amplitude oscillations did exist, and Bernstein et al[11] have investigated the origin of such instabilities, which they ascribe to ion waves.

The following picture is helpful in understanding the diffusion process. Assume that voltage differences can exist between different points in a plasma a distance a apart of value

$$V_{rms} = kKT_e/e$$

where k is a constant less than 1. This means the random electric field E is V_{rms}/a. Now assume the perpendicular component of these fields to be in random directions thus giving rise to E x B drifts. Thus imagine a number of tubes of cross-section a and length a side by side and parallel to the B lines. Then due to the randomness of direction of the E fields, the E x B drifts will cause the particles to random walk. Since the observed oscillation periods are longer than the time to cross a correlation length a, the E field is essentially constant during each random walk, and the number of such tubes crossed per sec.is

$$N \cong \frac{v_D}{a} \cong \frac{ck\, KT_e}{Ba^2 e}$$

Thus the diffusion coefficient is

$$D = Na^2 \cong \frac{ck\, KT_e}{B\, e}$$

This diffusion is across the B lines; and if $KT_e/e = 6$ volts, B = 4000 gauss, k = 1, then $D = 1.5 \times 10^5$ cm^2 sec^{-1} for electrons, compared to a value of 8 cm^2 sec^{-1} for classical diffusion. D is independent of the assumed value of a and proportional to 1/B.

This coefficient is the same for electrons and ions, as it is based on E x B drifts which are independent of charge, particle mass, and energy so both electrons and ions would move together. Note that ions do not undergo a real E x B drift motion, since the correlation distance is the same as their gyroradius. However, their velocity perpendicular to B is in any case approximately v_s. As

A

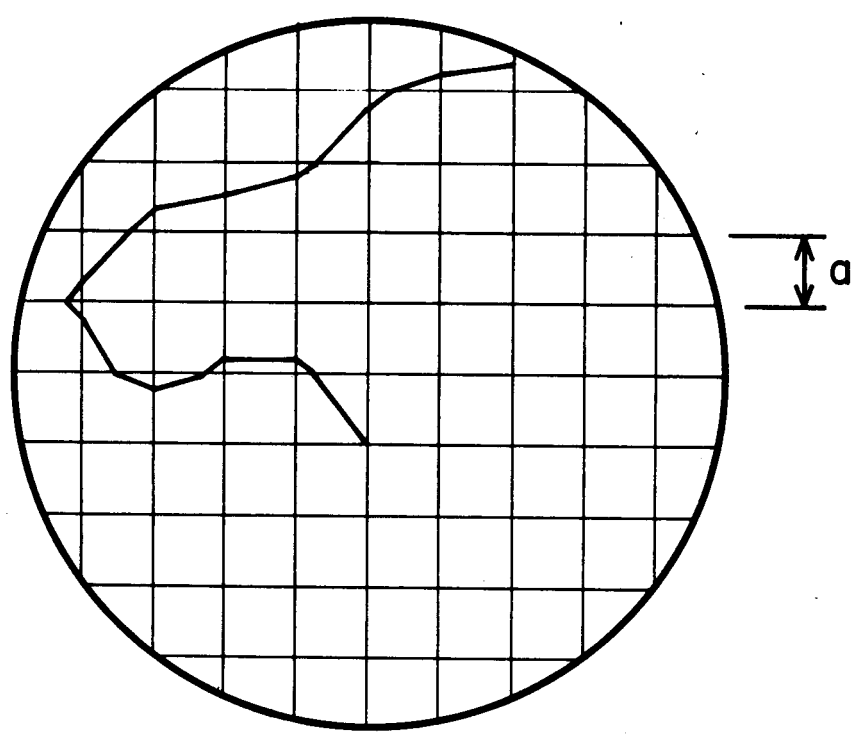

B

"Drain" diffusion of an electron along an equipotential line (A) and an equivalent representation (B) in terms of a random walk with step length equal to the correlation distance a. The transverse electric fields are assumed to vary slowly with respect to the time of a step. The magnetic field is perpendicular to the plane of the drawing.

the E fields are created by instabilities they vary in space and time. The distance a is the correlation distance across the B lines, while b is along them; we expect b to be much greater than a.

4.4.5.1 The Correlation Distance

This has been defined already in Section 3.2.2.6. and measured using two probes giving a value of about 0.3 cm. This is in reasonable agreement with the value expected for ion waves, i.e., the ion Larmor radius at the electron temperature which in this case is about 0.2 cm.

We are unsure of how to evaluate b, the correlation distance along the B lines, and did not measure it experimentally.

4.4.5.2. Oscillatory Diffusion for Low B Fields, or for Electrons with High $v_{\parallel}$

As the correlation distance is of order the ion Larmor radius an interesting speculation arises on the effect of low B fields, or alternatively for particles with high velocities $v_{\parallel}$, parallel to the B lines. In this case an electron will leave a region of coherence by traveling a distance b along the field before it drifts a distance a across the field. The length of a random walk will therefore be shortened by the parallel motion of the electron and will be equal to

$$\Delta x = cE/B.t$$

where $t = b/v_{\parallel}$. The number of such displacements per second will be

$$N = 1/t$$

and if these displacements are random in direction because E is random in direction in successive tubes along the Z axis, the total displacement perpendicular to Z in one second can be calculated, giving rise to the diffusion coefficient

$$D' = (ck \frac{KT_e}{eBa})^2 \frac{b}{v_{ll}}$$

However, if a is the Larmor radius, then D becomes independent of B and

$$D' = \frac{k^2 v_s^2}{v_{ll}} b.$$

D' is less than D. The dependence of D on B might look like the curve shown in Fig. 4.3.

4.4.5.3 Oscillatory Diffusion as a Function of Hash Frequency

A similar effect occurs if the hash frequencies are so high that the correlation time is shorter than a/v_d. We now have a displacement $\Delta x'$ similar to Δx above except that now

$$t \sim \tau$$

where τ is the correlation time. Then continuing as above we find now

$$D'' = kv_s^2 \tau,$$

again a value less than D, and independent of B. This shows that low frequency oscillations cause the greatest diffusion.

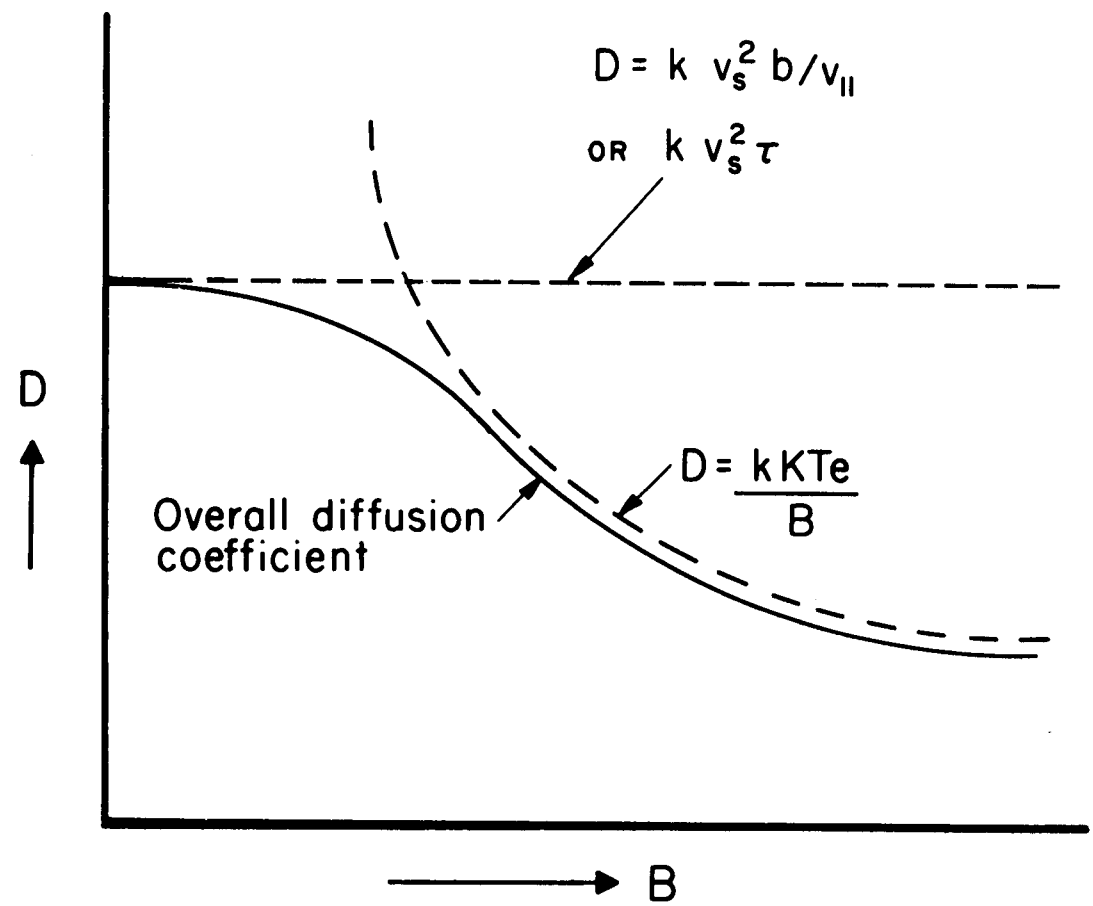

FIG. 4.3 DEPENDENCE OF OSCILLATORY DIFFUSION COEFFICIENT ON CONFINING FIELD B

4.4.5.4 Resultant value of D

An overall expression for D including all of these effects can be obtained if we rewrite, for high B,

$$D = \frac{ckKT_e}{eB} = k\frac{KT_e}{M_i} \cdot \frac{1}{\omega_c} = kv_s^2 t_c$$

where $t_c = 1/\omega_c$.

For fast electrons and low B,

$$D' = kv_s^2 t_f$$

where $t_f = b/v_{ll}$; and for very high frequency hash

$$D'' = kv_s^2 \tau$$

Thus the effective diffusion coefficient is

$$D_{eff} = kv_s^2 t$$

where

$$\frac{1}{t} = \frac{1}{t_c} + \frac{1}{t_f} + \frac{1}{\tau}$$

In our discharge the first term is dominant.

4.4.6 Cathode Mechanism

The first question to be examined is whether the emission for the cathode is temperature or space charge limited.

The cathode was usually run at a temperature of approximately 2700°K. As it was tungsten, the saturation electron-emission current density would be 1.6 amps/cm^2.[20] With an area of 20 cm^2, the maximum emission current would be 32 amps. However, our discharge current under standard conditions was 15 amps, and this included both the electron-emission, and any positive ions arriving at the cathode.

Experiments were run with the cathode at approx 2500°K, when the saturation emission current would be about 0.25 amps/cm^2. Thus now the primary electron current would be at the most 5 amps, yet the discharge at 15 amps was not markedly different in appearance, although it was considerably noisier.

We conclude that the emission could be both temperature or space charge limited, depending on experimental conditions, and is probably both at once, being emission limited in the hot rotating column of plasma, and space charge limited elsewhere. Curves of I vs V as a function of T_c, the cathode temperature, indicate that with greater than 5.6 KW input power into the cathode, the current is independent of cathode temperature, suggesting space charge limitation.

We have undertaken an analysis of a space charge limited emitting cathode placed near a plasma, somewhat similar to that of Langmuir.[21] The treatment is involved and will be given elsewhere.[22] The solution is given by

$$j = An(kT_e)^{1/2} f(V)$$

where A is a constant, n is the plasma density, and f(V) is shown in Fig. 4.4.

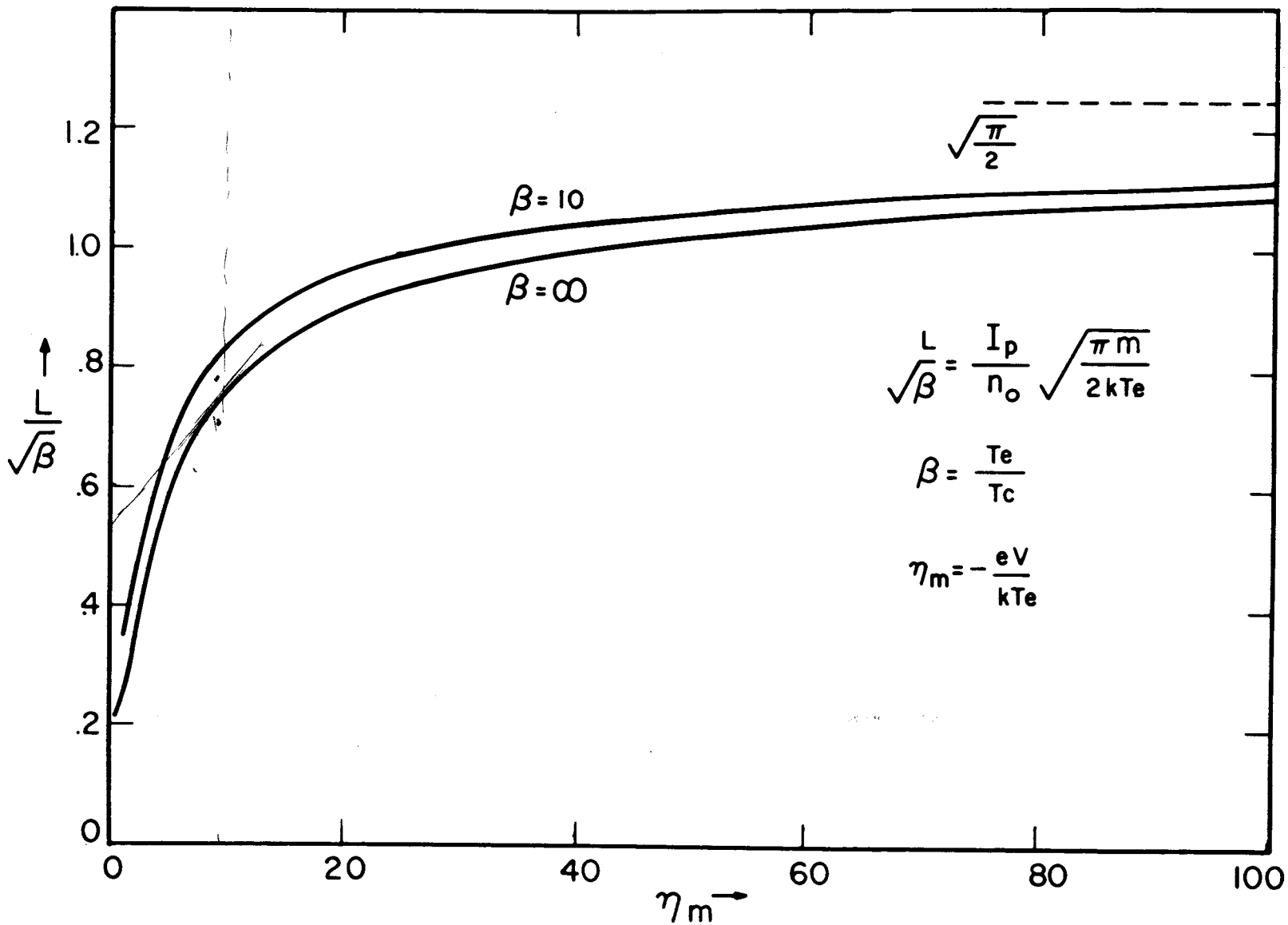

620092

FIG. 4.4 SPACE CHARGE LIMITED ELECTRON EMISSION INTO A PLASMA

which essentially shows this relation in dimensionless variables. The dependence on n is reasonable physically - a greater plasma density would provide more ions to be accelerated to the region of negative space charge reducing the height of the hill, and enabling more electrons to cross.

The upper limit of emission at a given temperature on the other hand is then given by the Richardson-Dushman equation.

4.5 The Current Flow Mechanism

In this section we estimate the magnitudes of the different current components by neglecting radial variations of density and assuming the measured value of the dc radial electric field.

4.5.1 The Electron Current Flow Mechanism

We have a plasma in helium at $p \cong 3\mu$, of density $n \cong 3 \times 10^{12} cm^{3}$, and electron temperature $Te \cong 5$ eV. The plasma is in a cylinder of length $L = 300$ cm, radius $r = 2.5$ cm, and the confining magnetic field is 4000 gauss. The percentage ionization is around 3%, where long range coulomb forces become comparable to electron-neutral collisions in importance for scattering. With neutral collisions, the classical diffusion coefficient along the B lines is

$$D_{lle} = 9 \times 10^{8} \ cm^{2} sec^{-1}$$

Then assuming ∇n of order $n\pi/L$ the electron current to the cold cathode by diffusion would be about 5 amps per sq. cm, or for a cathode of 20 cm^{2} of order 100 amps. There may also be electric fields along the B lines which are discussed

below in relation to ion flow. These fields would cause still larger electron flow. This does not include the primary electrons which travel down the B lines with velocities around 5×10^8 cm/sec.

However across the B lines

$$D_{\perp e} = D_{\perp\perp e}/(\omega_{ce}\tau)^2 = 8 \text{ cm}^2\text{sec}^{-1}$$

where ω_{ce} is the electron cyclotron resonance frequency (7×10^{10} rad sec^{-1}) and τ the electron-neutral collision time (1.5×10^{-7} sec). Then the electron current in the device of length L and plasma radius r is

$$I_e \cong 2\pi r L e D_{\perp e} \frac{2.4n}{r} = 17 \text{ mA}$$

where e is the charge of an electron, and we have taken the gradient to be of order $\frac{2.4n}{r}$, 2.4 being the first zero of J_0. This value is about 3 orders of magnitude too small compared with the discharge current.

However, there are radial electric fields in the discharge ~ 50 v/cm. Assuming that across the B field the electron mobility is

$$\mu_{\perp e} = \frac{-eD_{\perp e}}{KT_e}$$

the value for the discharge current for the standard operating conditions, is of order 220 mA, still two orders too small.

In contrast if we assume oscillatory diffusion, then

$$I_e \cong e(2\pi rL)\left(\frac{ckKT_e}{Be}\right)\ \frac{2.4n}{r}$$

and with the same conditions as above, and k = 1, we find $I_e \cong 100$ amps, to be compared with the measured current of 15 amps. This value is high but not too far out in order, remembering n and T_e are not constant down the Z axis, and that the gradient is approximated by 2.4n/r. Moreover k could be less than 1, and a value of 0.2 does not seem too unlikely.

4.5.2 The Ion Current Flow Mechanism

Consider next the ion current flow. The ions can diffuse along the B lines with a diffusion coefficient of $D_{lli} = 1.4 \times 10^5$ cm^{2}sec^{-1} for 0.1 eV ions at p ~ 3μ. This value is 4 orders of magnitude below D_{lle}. For ions of 5 eV, $D_{lli} = 1.3 \times 10^6$ cm^{2}sec^{-1}. Using these values for D_{lli}, and again assuming $\nabla n = \frac{n\pi}{L}$, the ion current to each cathode is between 14 and 40 ma/cm^2 or a total current of between 280 mA and 3 amps, compared to the discharge current of 15 amps.

In addition to diffusion flow along the B lines, mobility flow can also occur. There may be dc potentials along B of the order of KT_e, or even greater when volume ionization is present, although very large potentials have not been observed. Moreover the discharge has voltages $\approx KT_e$ in it due to oscillations. The fields along the B lines would then be $E \approx 2\ KT_e/el \sim 0.03$ V/cm. Although these fields are small the mobility term will be larger than the diffusion term. Taking the ratio we find

$$\frac{\mu_{lli} nE}{D_{lli} \nabla n} \gtrsim T_e/T_i$$

Remembering that $\mu_{lli}/D_{lli} = e/KT_i$, and taking $\nabla n = 2n\pi/L$ we find that the mobility current to the two cathodes is of order 12 amps for $T_i = 5$ eV.

Across the B lines the classical diffusion coefficient of the ions depends on the value assumed for their energy. Thus assuming $T_i = 0.1$ eV, $D_{\perp i}$ is 14 $cm^2 sec^{-1}$; but if we assume $T_i = 5$ eV then $D_{\perp i}$ becomes 3.3×10^3 cm^2 sec^{-1}. The radial ion current then becomes 32 mA for the former value, and 7.5 amps for the latter. It is probable that the value of 5 eV is too high for an assumed ion temperature as the ion velocities correspond to this only during a part of their gyration.

Assuming oscillatory diffusion we shall have ion currents of order 100 amps, equal to the electron currents, but the direction of the density gradient is such as to drive the ions in the direction of the anode, and not many ions have enough energy to actually reach the anode.

The radial ion current due to dc electric fields, however, is greater than that due to classical diffusion, by the ratio $\frac{eV}{KT_i}$, where V is now the radial potention drop. Since the latter is of the order of 50 V, the mobility term gives a radial ion current of between 16 and 75 amps (assuming $T_i = 0.1$ and 5 eV respectively). These values are larger than the discharge current. This current goes radially inwards and must either go to the cathode or be lost through recombintion. It will be shown that recombination is negligible. Most likely, the discrepancy in the value of the ion current is due to our neglect of the radial variation of n and E.

4.6 Recombination

First, to get an idea of what order we require for the recombination coefficient in order for recombination to be of importance, we estimate the time the electrons spend on the average in the discharge. The number of electrons reaching the anode per second is of the order of the discharge current, and this is equal to the total number of electrons in the discharge divided by the average confinement time τ. Thus

$$I/e = 2\pi rLn/\tau$$

For I = 15 amps, $n = 2 \times 10^{12}$, L = 300 cm, r = 2.5 cm, τ is approximately 10^{-4} sec. The minimum value of α, the recombination coefficient, which would make the recombination time this small is

$$\alpha = 1/n\tau = 5 \times 10^{-9} \text{cm}^3 \text{ sec}^{-1}$$

We shall now consider several possible recombination processes to see if we get α of this value. The recombination process depends on the purity of the gas, and we consider first pure helium, then impure helium.

For pure helium a recombination process is dissociative recombination

$$He_2^+ + e \longrightarrow He^* + He$$

forming two He atoms. Rough theoretical estimates put the recombination coefficient of this process as high as 10^{-7} cm^3 sec^{-1} although this value ought to be accepted

with caution.[23]

The process is unlikely to occur in our discharge as He_2^+ is only formed at higher pressures, because it is formed from a three-body process

$$He + He + He^+ = He_2^+ + He$$

the third body being necessary to balance energy and momentum.

If we assume radiative recombination, then the recombination coefficient will be very low, of order 10^{-13}[24]. Recombination based on double excitation gives values probably around $10^{-12} cm^3 sec^{-1}$[25]. In this process the electron is captured into one of the upper levels, and the surplus energy excites a second electron to a higher level. It can either lose part of its energy by radiation of a quantum thereby forming a singly excited atom, or lose all the excitation energy and become an ion again. Thus the recombination coefficient depends on the speed with which the first process takes place. Recombination of an ion involving two electrons as proposed by N. D'Angelo[6] at electron temperatures as high as 5 eV gives values of the recombination coefficient of order 10^{-13}.

For impure helium, electronegative impurities could attach electrons, and then instead of electron-helium ion recombination, a slow process, the dominating process would be impurity negative ion-helium ion recombination. From spectra of the discharge, it is known that such impurities exist. We also know that at certain times when the helium was impure, estimated by the color of the discharge to the eye, that the density was lower than normal.

For recombination via impurities, for instance O_2, first electron

attachment occurs according to:

$$e + O_2 + K \rightarrow O_2^- + (E_a + K)$$

where K is the kinetic energy, and E_a the affinity energy. The energy liberated appears as radiation so this process would be independent of three-body collisions and hence neutral pressure, and its rate would be proportional to the electron density and the impurity density. The probability of attachment increases as the electron energy decreases, because the electron remains longer within the range of the atomic field.

For this process to be effective, the slower of the attachment rate and the recombination rate must be larger than τ^{-1}. We estimate the probability that an electron will be attached to an impurity atom as follows.

First we estimate the probability of attachment by the ratio of the time an electron spends near an atom, $t = r_A/v_{re}$, where r_A is the atomic radius $\sim 10^{-8}$ cm, and v_{re} the electron random velocity, say 10^8 cm/sec, to the time for spontanteous emission of a quantum or 10^{-8} sec. This probability per collision is small, between 10^{-8} to 10^{-7}, say. Now at $p = 3\mu$ an electron of energy 5 eV has a collision frequency of 6×10^6 sec^{-1}, and if it stays in the discharge 10^{-4} sec it collides 5×10^2 times. If the percentage impurity is 10%, say, it hits 50 impurities in this time. The probability it will attach is $\sim 5 \times 10^{-6}$, a value much too low.

Alternatively, taking the measured attachment coefficient a for air expressed as $a/p \cong 10^{-2}$ with p in mmHg pressure for values of E/p from 20 to 60, which might hold near the axis, we find $a \sim 3 \times 10^{-5}$. Unlike the above probability this quantity represents the number of attachments per cm path the electron travels in the field direction. Then in helium with say 10% impurity of air, $a \sim 3 \times 10^{-6}$. Assuming the velocity of the electron 10^{8} cm/sec, then during its time in the discharge it travels about 10^{4} cm, so the number of attachments it makes are 3×10^{-3}, or one electron in 300 attaches to an impurity.

This estimate differs from the above, but both are so low as to suggest that recombination via electronegative impurities is not a dominant process, because the attachment rate is too slow.

Thus we do not believe that recombination is a dominant process in our discharge.

5. THEORY OF THE DISCHARGE II

5.1 Derivation of The Discharge Equations

With the insight gained in the previous section into the relative importance of the various physical processes, it is possible to write down heuristic equations to describe the discharge. These equations are in general too complicated to be solved exactly, even by numerical computation. Consequently, a number of simplifying assumptions will be made, particularly in regard to the geometry. Assumptions regarding relative magnitudes of terms will be based on the "standard conditions" of our discharge (R = 2.5 cm, L = 300 cm, p = 3μ He, B = 4 kg, I = 15 amps, V = 70 v, $T_c > 2700^\circ K$); the theory must be modified to describe discharges with greatly differing parameters.

The first assumption is that the discharge can be divided into the main plasma and the cathode sheath. In the main plasma, it is assumed that $n_e = n_i$, and therefore Maxwell's equations do not have to be used. The sheath region will be taken into account by assuming it has only three effects: 1) it absorbs all ions incident upon it, 2) it governs the emission of primary electrons, and 3) it reflects plasma electrons according to an exponential law.

In the plasma region, the equation of motion of each species of charged particle can be written, in Gaussian units, as

$$nm\left(\frac{\partial \underline{v}}{\partial t} + \underline{v}\cdot\nabla\underline{v}\right) = qn\underline{E} + \frac{nq}{c}\underline{v}\times\underline{B} - \nabla\cdot\underline{\underline{P}} - \frac{mn\underline{v}}{\tau}, \qquad (5.1)$$

where $\underline{v}$ is the macroscopic velocity and n, m, and q the particle density, mass, and algebraic charge. The collision time τ will be assumed to be due entirely to collisions with neutrals. In steady state, the first term vanishes, $\underline{E}$ is the dc electric field in the plasma, and $\underline{B}$ is the applied magnetic field. The off-diagonal elements in the stress tensor $\underline{\underline{P}}$, which give rise to viscosity effects and like-particle diffusion, have been evaluated with reference to the experimental data and the theoretical results of Robinson and Bernstein* and found to be entirely negligible; hence $\nabla \cdot \underline{\underline{P}}$ will be replaced by $\nabla (nkT)$.

Similarly, the $\underline{v} \cdot \nabla \underline{v}$ term has been evaluated for the present experimental situation, and the only significant component is the term $nm\, v_\theta^2/r$, arising from the differentiation of the unit vector in cylindrical coordinates. This is the centrifugal force and gives rise to an azimuthal current, as noted in a previous section. With a parabolic potential profile of the observed magnitude and 4000 gauss, this term is 6% of the dominant term, and since its primary effect is to produce a rotation rather than diffusion, it will be neglected. However, it should be noted that the relative magnitude of the centrifugal force term goes as B^{-2}, so that at 1000 gauss this term would be very large, and this theory probably would not be accurate. It is conceivable that large transverse currents could cause an instability of the discharge column; this would explain the difficulty of obtaining a stable discharge below 1 or 2 kg.

---

* B. R. Robinson and I.B. Bernstein, Annals of Physics (to be published).

With these two simplifications, Eq. 1 can readily be separated into components in Cartesian coordinates and solved for $\underline{v}$. The result can be written

$$-\underline{v} = (\underline{\underline{\mu}} \cdot \underline{\nabla})V + \frac{1}{n}\underline{\nabla} \cdot (\underline{\underline{\tilde{D}}} n), \tag{5.2}$$

in which $\underline{\nabla}V = -\underline{E}$, $\underline{\underline{D}} = \underline{\underline{\mu}} kT/q$, $\underline{\underline{\tilde{D}}} = \underline{\underline{D}}^{\text{transpose}}$, and the mobility matrix is

$$\underline{\underline{\mu}} = \begin{pmatrix} \mu_\perp & \omega\tau\mu_\perp & 0 \\ -\omega\tau\mu_\perp & \mu_\perp & 0 \\ 0 & 0 & \mu \end{pmatrix}, \tag{5.3}$$

where $\omega = qB/mc$, $\mu = q\tau/m$, $\mu_\perp = \mu/(1 + \omega^2\tau^2)$, and $\underline{B} = B\hat{z}$. The diagonal terms are merely classical mobility and diffusion in a magnetic field, and the off-diagonal terms the $\underline{E}$ x $\underline{B}$ and $\underline{\nabla}$ p x $\underline{B}$ drifts. In addition to (2) there is for each species an equation of continuity:

$$Q = \underline{\nabla} \cdot (n\underline{v}), \tag{5.4}$$

where Q is the rate of production of particles per cm^3. In order to write down a simple expression for Q, we must now assume that the primary electrons produce ion pairs uniformly along the length of the machine. This would be true if the length, L, were so short that the primaries oscillated many times between cathodes before losing their energy and that the neutral pressure is uniform along the vacuum chamber. In our discharge L was so long that neither of these conditions obtained; however, it is felt that the assumption of axial uniformity of ionization will not introduce any error that cannot

be corrected by using an "effective length" somewhat less than the true length of the machine. With this assumption, the number of primary electrons injected per cm^3 is j_p/L, where j_p is the number of primaries emitted per cm^2 from the hot cathode (s) and is a function of position in the cross-sectional plane. For electrons, we can write

$$Q_e = \frac{j_p}{L}(1+M) + nn_n\overline{\sigma v} - \alpha n^2, \tag{5.5}$$

where M is the average number of ion pairs created per primary, $nn_n\overline{\sigma v}$ the rate of ionization by the plasma electrons, and α the recombination coefficient. For ions, the corresponding expression is the same, except for the absence of the first term. The multiplication factor M is given by the total energy available divided by the energy required for each ionization:

$$M = \begin{cases} \dfrac{eV - E_i}{E_i + gE_x}, & eV > E_i \\ 0, & eV < E_i \end{cases} \tag{5.6}$$

where E_i and E_x are the ionization and average excitation energies, and g the ratio of excitation to ionization cross sections. Eq. (6) assumes that the potential difference V between the plasma and the cathode is concentrated in the cathode sheath, in which the primaries are accelerated, and that the primaries lose all their energy excess over E_i before they diffuse out or recombine. Both these assumptions are comparatively good.

The term involving ionization by the plasma electrons is not negligible even though only the extreme tail of the distribution can ionize. This is

because the density of primaries is relatively small. At large radii, where e $V > E_i$, the ionization rates of primaries and of plasma electrons are comparable. At small radii, where e $V < E_i$, the plasma electrons will be less efficient in ionizing, not only because kTe is smaller there, but also because the electrons capable of ionizing are not reflected by the cathode sheath and the mean free path for ionization is greater than the mean distance to the cathodes. (The spiralling motion of the electrons can change the effective mean free path by only $\sqrt{2}$. The thermalization time t_c is shorter than or comparable to the time of flight of a fast electron to the cathode.) However, if e $V < E_i$, the primaries cannot ionize at all. Hence for the time being, we must keep the $nn_n \overline{\sigma v}$ term, realizing that $\overline{\sigma v}$ may be a very complicated function of V. On the other hand, we may safely neglect the recombination term αn^2, which was evaluated in a previous section. It will do no harm to leave it in, however, for the sake of completeness.

The expression for j_p will depend on whether the emission is temperature or space-charge limited. In general, it is possible for both mechanisms to occur simultaneously in different parts of the cathode. For temperature limited emission, the emitted current depends only on the cathode temperature:

$$j_p = j_p(T_c), \tag{5.7}$$

For space charge limitation, the emitted current is given by

$$j_p = n\left(\frac{2\kappa T_e}{m}\right)^{\frac{1}{2}} \cdot \left(\frac{eV}{kT_e}\right), \tag{5.8}$$

where $\iota(\frac{eV}{kTe})$ is a function previously computed by one of the authors,* and n_s is the plasma density at the edge of the sheath (to be defined better later).

The substitution of (2) and (5) into (4) now gives, for the electrons,

$$\frac{j_p}{L}(1+M) + nn_n\bar{\sigma v} - \alpha n^2 = -\underline{\nabla}\cdot(n\underline{\underline{\mu}}\cdot\underline{\nabla})V - \underline{\nabla}\underline{\nabla} : (\underline{\underline{\tilde{D}}}n). \qquad (5.9)$$

A similar equation (minus the first term) obtains for the ions. If the temperatures, and hence the transport coefficients, are known, these are two simultaneous second-order differential equations in 3 dimensions for n and V. Actually, the temperatures are related to V in a manner described previously; for simplicity we shall assume they are given. At the boundary r = R the solution of these equations has to be matched to the solution in the external region, where $j_p = 0$. This would be extremely difficult, and for simplicity we shall assume that at r = R, n = 0 and $V = V_o$, the anode voltage. In other words, the transit time of particles moving along B to the anode after they have diffused out of the discharge has been neglected; i.e., the anode has been assumed to be a conducting cylinder of radius R and length L, and any anode sheath has been neglected.

Since rotation of the plasma does not produce a divergence of current, one would expect that the off-diagonal elements of $\underline{\underline{D}}$ and $\underline{\underline{\mu}}$ do not contribute to Eq. (9). Consideration of the last term of (9) in Cartesian coordinates shows that this is indeed true for $\underline{\underline{D}}$; for the operator $\underline{\nabla}$ commutes with itself, and the double scalar product $\underline{\nabla}\underline{\nabla} : \underline{\underline{\tilde{D}}}\, n$ is then a product of a symmetric matrix with a skew-symmetric one. The same is not

---

* This is the same as the function $\iota/\sqrt{\beta}$ shown in Fig. 4.4, evaluated for $\beta = 20$.

true of the term containing $\underline{\underline{\mu}}$ since a space-dependent quantity n $\underline{\underline{\mu}}$ occurs between the two $\underline{\nabla}$'s. To make further progress we must assume cylindrical symmetry. With this assumption, the two ∇'s in the $\underline{\underline{\mu}}$ terms can be commuted, and again the terms containing off-diagonal elements cancel, as can be verified by writing $\underline{\nabla}\cdot(n\,\underline{\underline{\mu}}\cdot\underline{\nabla})\,V$ out in cylindrical coordinates and setting $\frac{\partial}{\partial\theta}$ to 0. Since the matrices $\underline{\underline{\mu}}$ and $\underline{\underline{\mathbb{D}}}$ have the same form in cylindrical coordinates as they do in rectangular coordinates, we may henceforth work in cylindrical coordinates and retain only the diagonal elements of $\underline{\underline{\mu}}$ and $\underline{\underline{\mathbb{D}}}$.

The assumption of cylindrical symmetry is probably not a good one in view of the rotating filaments that have been observed. If, as has been hypothesized, the emission of primaries is temperature limited inside the filament but space-charge limited outside, the cross-sectional area of the filament seems to be indeterminate. For this reason, and for mathematical simplicity, we have had to assume cylindrical symmetry. It seems not unreasonable, however, that the macroscopic behavior of the discharge should be predictable by a theory which averages all quantities over θ. Eq. (9) now becomes

$$-Q = \nabla_r\cdot(D_\perp n) + \mu_\perp n\nabla_r V + \frac{\partial(\mu_\perp n)}{\partial r}\frac{\partial V}{\partial r} + \frac{\partial^2(Dn)}{\partial z^2} + \mu n\frac{\partial^2 V}{\partial z^2} + \frac{\partial(\mu n)}{\partial z}\frac{\partial V}{\partial z}, \qquad (5.10)$$

where

$$\nabla_r \equiv \frac{1}{r}\frac{\partial}{\partial r}\left(r\frac{\partial}{\partial r}\right).$$

This has been derived for classical mobility and diffusion. We now make the basic assumption that in the case of enhanced diffusion, the form of Eq. (10) remains the same but that $D_\perp$ and perhaps also $\mu_\perp$ take on values

different from the classical ones. Specializing to the case of space-charge limited emission, we have

$$Q_e = \frac{N n_s}{L}\left(\frac{2kT_e}{\pi m}\right)^{\frac{1}{2}} L\left(\frac{eV}{kT_e}\right)\left[1+M(V)\right] + n n_n \overline{\sigma v}\,(V) - \alpha n^2, \qquad (5.11)$$

and a similar equation for ions. N is the number of emitting cathodes, either one or two, and L the total length of the discharge.

Up to now we have let μ and D be functions of position. This is true because they depend on kT, which is a function of radius, owing to the difference in energy of the primary electrons (and hence to a lesser extent of the secondary electrons) at different radii. Thus there is a relation $kT_e = f(V)$. To simplify the problem, we must now assume that kT_e is a constant, and therefore that the transport coefficients μ and D are constant in space. This is not as poor an assumption, as far as the radial potential distribution is concerned, as one may infer from the fact that kT_e varies experimentally more than a factor of 2. It will become apparent that what really matters here is the ratio eV/kT_e, and if we compare the theoretical results for eV/kT_e with the experimental values of eV/kT_e, computed with measured temperatures, the effects of assuming constant kT_e largely disappear.

With the abbreviations

$$\begin{aligned} \varphi &\equiv eV/kT_e \\ \mu^* &\equiv |\mu| \frac{kT_e}{e} \\ \mu_\perp^* &\equiv |\mu_\perp| \frac{kT_e}{e} \\ v_e &\equiv (2kT_e/\pi m)^{\frac{1}{2}}, \end{aligned} \qquad (5.12)$$

and with the assumption of constant μ and D, Eqs.(5.10) and(5.11) become, for electrons and ions separately:

$$Q_e(\varphi) + D_{\perp e}\nabla_r n - \mu^*_{\perp e} n \nabla_r \varphi - \mu^*_{\perp e} \frac{\partial n}{\partial r}\frac{\partial \varphi}{\partial r} + D_e \frac{\partial^2 n}{\partial z^2} - \mu_e^* n \frac{\partial^2 \varphi}{\partial z^2} - \mu_e^* \frac{\partial n}{\partial z}\frac{\partial \varphi}{\partial z} = 0 \quad (5.13)$$

$$Q_i(\varphi) + D_{\perp i}\nabla_r n + \mu^*_{\perp i} n \nabla_r \varphi + \mu^*_{\perp i} \frac{\partial n}{\partial r}\frac{\partial \varphi}{\partial r} + D_i \frac{\partial^2 n}{\partial z^2} + \mu_i^* n \frac{\partial^2 \varphi}{\partial z^2} + \mu_i^* \frac{\partial n}{\partial z}\frac{\partial \varphi}{\partial z} = 0,$$

where

$$Q_e(\varphi) = \frac{N n_s}{L} \nu_{eL}(\varphi)[1 + M(\varphi)] + n n_n \bar{\sigma v}(\varphi) - \alpha n^2$$

$$Q_i(\varphi) = \frac{N n_s}{L} \nu_{eL}(\varphi) M(\varphi) + n n_n \bar{\sigma v}(\varphi) - \alpha n^2. \quad (5.14)$$

These equations, together with the proper boundary conditions, prescribe the density and potential everywhere in the plasma of a hot-cathode reflex arc. These equations are difficult to solve not only because the parameters in them are inaccurately known, but also because the equations are non-linear and two-dimensional.

It should be pointed out that μ_e^*, defined in Eq. 5.12, is just the diffusion coefficient D in the case of ordinary collisions. However, since anomalous diffusion is present in the discharge, we shall allow for the possibility that the Einstein relation, $\mu_e = eD/kT_e$, is not satisfied, at least for the transverse coefficients.

5.2 Separation of the Equations

Equations 5.13 and 5.14 are difficult to solve even numerically because they are two-dimensional, in r and z. They cannot be separated by ordinary methods because they are not homogeneous in the unknowns n or ϕ.

The fact that they are non-linear is of little consequence once one is resigned to a numerical solution.

To reduce the equations to a single dimension, the radius, we must now make use of the experimental fact that the potential and density do not vary greatly in the z-direction except near the cathodes. This will allow us to eliminate the z-dependence in terms of the boundary conditions on the currents in the z-direction. Actually, this procedure does not really separate the problem, which is intrinsically two-dimensional, but it does reduce the problem of separation to the adjustment of a single parameter.

Formally, we may expand n and Φ on each line of force in a series in even powers of z (by symmetry), retaining only the first two terms*:

$$n(r) = n_0(r)\left[1 - \tfrac{1}{2}\nu_1(r)\frac{4z^2}{L^2} + \dots\right]$$

$$\varphi(r) = \varphi_0(r) - \tfrac{1}{2}\varphi_1(r)\frac{4z^2}{L^2} + \dots, \qquad (5.15)$$

where ν_1 and φ_1 are much less than 1, and n_0 and Φ_0 are the radial profiles at the mid-plane. This represents a profile in the z-direction resembling both the parabolic and cosine distributions usually encountered in one-dimensional diffusion problems. Since electrons can be expected to be in thermal equilibrium along a line of force, we note that there is a relation between ν_1 and φ_1:

$$n(r,z) = n_0(r)\,e^{-(\varphi_0-\varphi)} \approx n_0(r)(1-\varphi_0+\varphi)$$
$$\approx n_0(r)\left[1 - \tfrac{1}{2}\varphi_1(r)\frac{4z^2}{L^2}\right] \qquad (5.16)$$
$$\therefore\ \nu_1 = \varphi_1$$

to this order of approximation.

---

* The formality of writing out this expansion is not necessary but may make the analysis clearer.

We now integrate Eqs. 5.13 with respect to z from o to $\frac{L}{2}$, assuming that n and Φ are constant as far as $Q(\Phi)$ and the radial terms are concerned. These terms then are merely multiplied by $\frac{L}{2}$. This is justified by the assumption that in almost the entire range of integration n and Φ differ trivially (by 5.15) from their values at the mid-plane. The z-terms in (5.13), upon integration, become:

$$\int_0^{\frac{L}{2}} dz \left[D_i \frac{\partial^2 n}{\partial z^2} + \mu_i^* n \frac{\partial^2 \varphi}{\partial z^2} + \mu_i^* \frac{\partial n}{\partial z} \frac{\partial \varphi}{\partial z} \right] = \left[D_i \frac{\partial n}{\partial z} + \mu_i^* n \frac{\partial \varphi}{\partial z} \right]_{\frac{L}{2}} \equiv -j_i(r), \quad (5.17)$$

where $j_i(r)$ is just the ion flux to the cathode. A similar equation obtains for the electrons. By the expansion (5.15), we have

$$j_i(r) = \frac{2n_0}{L} (D_i \nu_1 + \mu_i^* \varphi_1)$$
$$j_e(r) = \frac{2n_0}{L} (D_e \nu_1 - \mu_e^* \varphi_1). \quad (5.18)$$

The boundary consitions at the cathodes are known in terms of these currents. For the ions, the sheath criterion[22] tells us that the mean ion velocity is $v_s = (kT_e/M)^{\frac{1}{2}}$, and hence that

$$j_i = n_s(r) v_s, \quad (5.19)$$

where n_s is the density at the "sheath edge" and will be discussed later. For the electrons, which are in equilibrium in a potential well, the current to the cathodes is just the random current at the mid-plane times the exponential factor:

$$j_e = \tfrac{1}{4} n_0 v_e e^{-\varphi_0(r)}, \quad (5.20)$$

the potential of the cathodes being defined as 0.

Since $\underline{n}$ is supposed to be fairly constant along z, one is tempted to substitute n_o for n_s in (5.19). Unfortunately, if one does this, the value of ν_1 computed from (5.18), (5.19), and (5.16) becomes comparable to n_o, in contradiction to both (5.15) and experiment. The difficulty lies in the transition region between the domains in which (5.18) and (5.19) are valid. This situation is illustrated in Fig. 5.1. The concept of mobility is valid in the collision-dominated region, which is assumed to extend up to a point t, where the density is n_t. To the right of this point the ions have a fairly isotopic distribution, with a slow drift toward the cathode caused by the longitudinal electric field in the plasma (the diffusion current is relatively small). In the transition region, which may extend several mean free paths away from the cathode, the ion motion becomes more and more directed as the ions are accelerated in an increasing electric field and at the same time suffer less and less back-scattering off the neutrals. By the time the ions reach the sheath edge s, they suffer no more collisions and form a directed stream with density n_s and average velocity v_s directed toward the cathode. This transition region, or region of plural collisions, would be expected to be several mean free paths long. Since the ion-neutral mean free path is of the order of 1 cm, this region is still small compared with the length of the discharge column; and one can safely neglect both ionization and radial diffusion in this region. Moreover, quasineutrality must hold in this region, since deviation from quasineutrality brings one by definition into the sheath. None the less, computation of the ion density variation in the

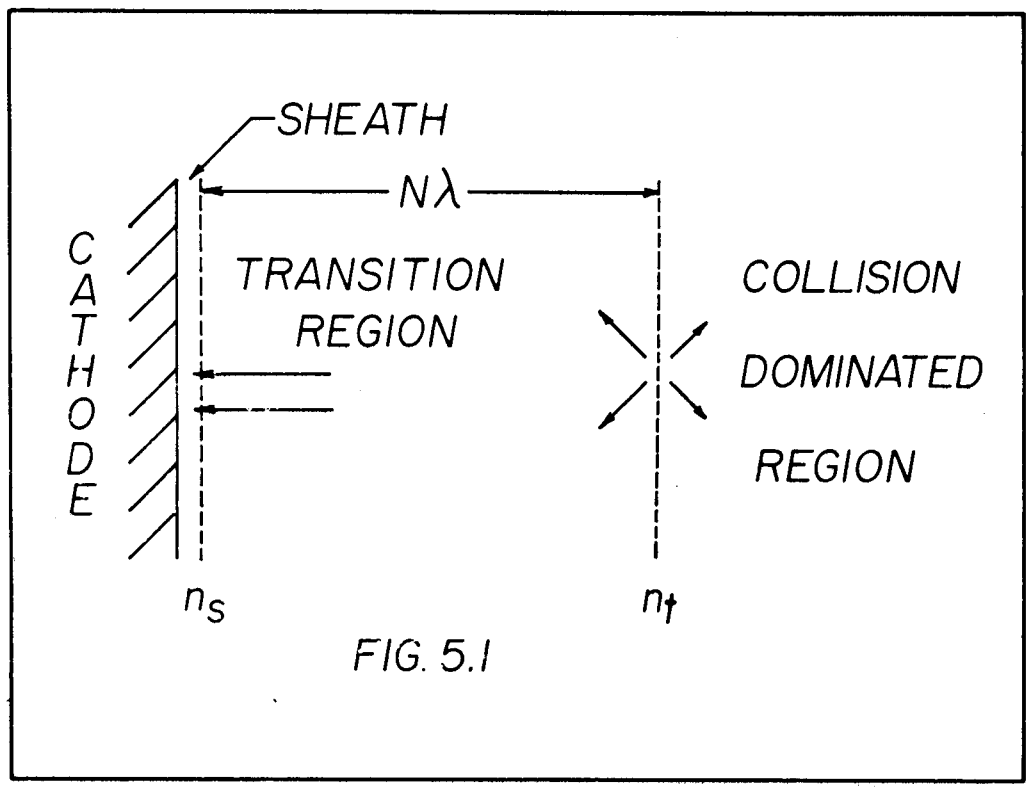
SHEATH
Nλ
CATHODE
TRANSITION REGION
COLLISION DOMINATED REGION
n_s
n_t

FIG. 5.1

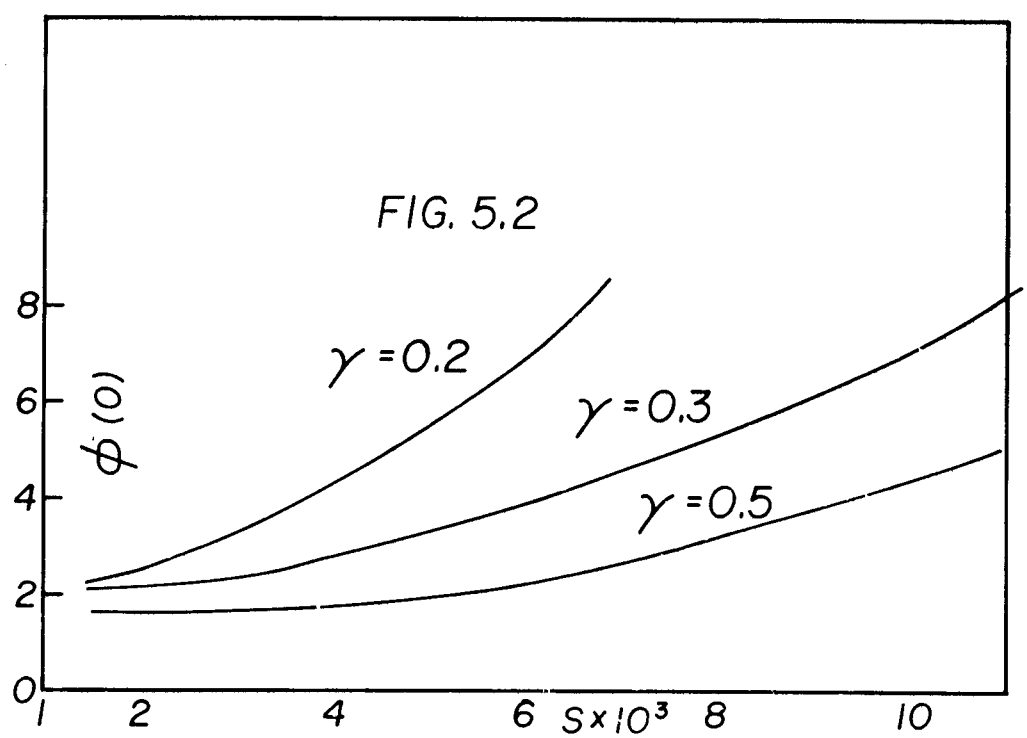
FIG. 5.2
$\phi(0)$
$\gamma = 0.2$
$\gamma = 0.3$
$\gamma = 0.5$
0
2
4
6
8
1
2
4
6
$s \times 10^3$
8
10

transition region would be very difficult, since collisions would have to be taken into account in an accurate way.

Instead of attempting to calculate this, we shall introduce a parameter γ:

$$\gamma \equiv \frac{n_s}{n_t} \approx \frac{n_s}{n_o} . \tag{5.21}$$

Since we do not know γ, we shall let it be an adjustable parameter. A knowledge of γ is equivalent to knowing the ion current, from (5.19). In a plane-parallel discharge, the ion current is easily computed: it is merely the total number of ions created in the discharge per second. Our inability to calculate j_i stems from the fact that the ions have another escape route—namely, by radial motions. Hence the need for leaving γ unspecified is a manifestation of the fact that we have not really suceeded in separating the discharge equations into the r and z components but have merely lumped the difficulties of separation into a single parameter γ.

In order that we may later evaluate our theoretical results, it would be helpful to obtain an estimate here of the magnitude of γ. The concept of mobility is valid when $\mu^* \frac{\partial \varphi}{\partial z}$, the drift velocity, is small compared to the ion thermal velocities. The boundary t of the transition region is therefore the point where the mobility concept begins to break down, or where

$$\mu^* \frac{\partial \varphi}{\partial z} = \frac{1}{2} \left(\frac{2kT_i}{\pi M} \right)^{\frac{1}{2}} . \tag{5.22}$$

In (5.17), we may evaluate the bracket at z = t and set the resulting current equal to $n_s v_s$, since ionization and radial diffusion are negligible between s and t. We may also neglect the $D_i \frac{\partial n}{\partial z}$ term, since it is a factor $e(V_o - V_t)/kT_i$ less than the mobility term. Thus we have, from (5.17), (5.19), and (5.22) that

$$\tfrac{1}{2} n_t \left(\frac{2kT_i}{\pi M}\right)^{\frac{1}{2}} \approx n_s v_s = n_s \left(\frac{kT_e}{M}\right)^{\frac{1}{2}},$$

or

$$\gamma = \frac{n_s}{n_t} \approx \left(\frac{kT_i}{2\pi kT_e}\right)^{\frac{1}{2}} \approx 0.2 \qquad (5.23)$$

for kT_i = 1 eV and kT_e = 4 eV.

With such a value of γ, (5.19) and (5.18) are no longer inconsistent with the requirement $\nu_1 \ll 1$. We note that if γ is a constant, as in the approximation (5.23), then by (5.18), (5.16), and (5.19) ν_1 and ϕ_1 are independent of r, and j_i has the same r-dependence as n_o.

Returning now to the boundary condition for electrons (5.20), we note first that je can be a strong function or r, whereas j_i is not, and second that this current does not depend on any argument about collisions or transition regions, since the electrons are in thermal equilibrium. This current is the flow of electrons leaking through the potential barrier to the cathodes.

At first glance, one might have thought that n_s, and hence γ, could be computed in terms of n_o and ϕ_o, since (5.16), (5.18), (5.19), and (5.20) are five equations in the five unknowns j_i, j_e, ν_1, ϕ_1, and n_s. However, the equation (5.18) for j_e turns out to be trivial, since $\nu_1 = \phi_1$, and D_e

almost certainly equals μ_e^* or $\mu_e \frac{kT_e}{e}$, since motion along the field is probably classical. Therefore, to this approximation, $j_e = 0$. Physically, j_e is the small difference between a large diffusion current going toward the cathodes and a large mobility current going away from the cathodes, and it is reasonable that an expansion to first order in z^2 cannot give a value for this difference. We cannot neglect j_e, however, since it is comparable to other terms in the discharge equations.

After integrating with respect to z and using (5.17), (5.19), (5.20), and (5.21), we obtain from (5.13) the following equations for the radial dependence of n and ϕ:

$$\frac{L}{2}\left[Q_e(\varphi) + D_{\perp e}\nabla_r n - \mu_{\perp e}^* n \nabla_r \varphi - \mu_{\perp e}^* \frac{\partial n}{\partial r}\frac{\partial \varphi}{\partial r}\right] - \frac{1}{2} n v_e e^{-\varphi} = 0 \qquad (5.24a)$$

$$\frac{L}{2}\left[Q_i(\varphi) + D_{\perp i}\nabla_r n + \mu_{\perp i}^* n \nabla_r \varphi + \mu_{\perp i}^* \frac{\partial n}{\partial r}\frac{\partial \varphi}{\partial r}\right] - \gamma n v_s = 0 \qquad (5.24b)$$

where Q_e and Q_i are defined by (5.14). These equations describe the balance of particle flows between two coaxial cylindrical surfaces in the discharge. The Q's describe the creation and annihilation of ion pairs and the injection of primary electrons. The other terms in the brackets describe the radial fluxes of particles, and the last terms account for the loss of particles by motion along the magnetic field to the cathodes. These are two coupled non-linear second-order differential equations in one dimension for $n_o(r)$ and $\phi_o(r)$, (the subscript o has been suppressed). If the cross sections and transport coefficients are known sufficiently accurately, the density

and potential profiles can in principle be found numerically. Because of the approximations we have had to make, we did not feel that such a long calculation was justified.

5.3 Calculation of the Radial Potential Profile

To calculate the function $\Phi(r)$ alone is comparatively simple. One merely substracts (5.24b) from (5.24a). Since all the terms in the expressions (5.14) for Q_e and Q_i correspond to production in pairs except one, upon substraction we have only the term $\frac{N}{2}\gamma n \nu_{ei}(\varphi)$ corresponding to the injection of primaries. As for the radial mobility terms, we can neglect $\mu_{\perp e}^*$ relative to $\mu_{\perp d}^*$ in our strong magnetic field. According to the mechanism of anomalous diffusion discussed in Section 4, we can expect $D_{\perp e}$ to be almost equal to $D_{\perp i}$; and these terms will cancel upon subtraction. Expressing v_s in terms of v_e, we have finally

$$\frac{N}{2}\gamma n \nu_{ei}(\varphi) - \frac{1}{2}\mu_{\perp i}^* \left(n \nabla_r \varphi + \frac{\partial n}{\partial r}\frac{\partial \varphi}{\partial r}\right) - \frac{1}{4} n v_e \left(e^{-\varphi} - \gamma\sqrt{\frac{2\pi m}{M}}\right) = 0 \quad (5.25)$$

The physical meaning of this equation is that the negative charge injected into each tube of force by the primaries (first term) and by the loss of ions to the cathode (last term) is balanced by the positive charge accumulated by radial mobility (second and third terms) and by loss of electrons to the cathode (fourth term). Note that the assumption of equal $D_\perp$'s for ions and electrons has eliminated this coefficient from the equation: radial diffusion can cause no charge accumulation by this assumption. Regarding the ions alone, we note that although their radial diffusion and their

radial mobility are separately large, they are almost equal and oppositely directed; and the difference is the small ion current flowing to the cathodes. By subtraction we have eliminated all the uncertain cross sections in the pair production processes.

One remaining loose thread is the use of $\iota(\phi)$ in (5.25). Q here is the potential difference between the cathode and the plasma region, beyond the transition layer. However, ι was computed for the potential between the cathode and the sheath edge. The difference however, is slight. Since $n_s = n_t e^{-(\varphi_t - \varphi_s)}$, $\phi_t - \phi_s = -\ln \gamma \approx 1.6$. The potential is much larger than this except near the axis, so this is a small correction. Here, where ϕ is of the order of 1 or less, the theoretical calculation for $\iota(\phi)$ breaks down anyway. Also, near the axis the electron flux to the cathode is somewhat smaller than given in the fourth term in (5.25), since the deviation from a Maxwell distribution due to the loss to the cathodes was not taken into account. This effect is in a direction to counteract the effect of using too large a φ in the first term of (5.25).

For the purposes of computation we shall now put r into dimensionless units:

$$\rho = \frac{r}{R}, \quad R = \text{radius of discharge},$$

and divide (5.25) by $-\frac{1}{2} n v_e$. Using the definitions of ∇_r, μ^*_{1i}, and v_e (5.10, 5.12), we obtain

$$S\left[\frac{1}{\rho}\frac{\partial}{\partial\rho}\left(\rho\frac{\partial\varphi}{\partial\rho}\right) + \frac{1}{n}\frac{\partial n}{\partial\rho}\frac{\partial\varphi}{\partial\rho}\right] + e^{-\varphi} - \gamma\left[N_-(\varphi) + \sqrt{\frac{2\pi m}{M}}\right] = 0, \quad (5.26)$$

where the dimensionless parameter S is defined as

$$S \equiv \frac{L \mu_{\perp i}}{e R^2} \left(\tfrac{1}{2} m \pi k T_e\right)^{\frac{1}{2}}. \tag{5.27}$$

Equation (5.26) is to be solved with the boundary conditions

$$\begin{aligned} \varphi &= \varphi_d \quad \text{at} \quad \rho = 1 \\ \frac{\partial \varphi}{\partial \rho} &= 0 \quad \text{at} \quad \rho = 0, \end{aligned} \tag{5.28}$$

where Φ_d is the applied potential between the anode and the cathode.

Since $\iota(\Phi)$ is a known function, S and γ are the only two adjustable parameters left in the problem, and of these γ probably does not vary much with anything. Thus equation (5.27) provides a scaling law for reflex discharges of the type we have been considering. We see that the potential profile scales with the length of the discharge and inversely with the square of the radius and the magnetic field (appearing in $\mu_{\perp i}$). The dependence on kT_e is weak. The only transport coefficient appearing is $\mu_{\perp i}$, a consequence of the assumption $D_{\perp i} = D_{\perp e}$.

Equation (5.26) has been numerically solved on an IBM 650 computer by assuming a $\Phi(o)$, integrating to $\rho = 1$, and iterating until $\Phi(1) = \Phi_d$*. For this computation the experimentally measured density profile was used, since a solution for both n and Φ would have been immensely more complicated. The effect of the term containing $\frac{1}{n}\frac{\partial n}{\partial \rho}$ was evaluated by omitting it in one run (Fig. 5.7b); it was not great. The computation was performed with the following values of the parameters:

$$kTe = 4.5 \text{ ev}$$

$$\Phi d = 15$$

---

* The authors are indebted to Dr. I. Rabinowitz and Mrs. H. Selberg for carrying out this computation.

$(2\pi m/M)^{\frac{1}{2}} = .0294$ (He)

N = 1, L = 300 cm, R = 2.5 cm

B = 4000 g

The values of S used and the corresponding assumptions for kT_i (if μ_{1i} is classical) are as follows:

S	kT_i
1.9×10^{-3}	0.1 eV
3.4×10^{-3}	0.3 eV
6.2×10^{-3}	1.0 eV
1.1×10^{-2}	3 eV

For each S, γ was varied to find the best fit with experiment.

The experimental points for the potential profile are shown in Fig. 5.3-5.5 for different runs on different occasions, at different axial positions, and with two different L's and B's. These curves were obtained by dividing the measured floating potentials on probes by the measured kT_e at each radius after correcting the floating potential V_f to the space potential V_s by the following formula:

$$V_s = V_f + \frac{kT_e}{e} \ln \frac{2}{\pi}\sqrt{\frac{M}{2\pi m}} = V_f + \frac{3kT_e}{e}. \qquad (5.29)$$

The very smooth measured curves for V (r) become less smooth when converted to $\Phi(\rho)$, since the probe measurements of kT_e did not always give a smooth curve. The assumptions used in the theory require that $\Phi(\rho)$ be independent of axial position, and we see from Fig. 5.3 that this is quite true.

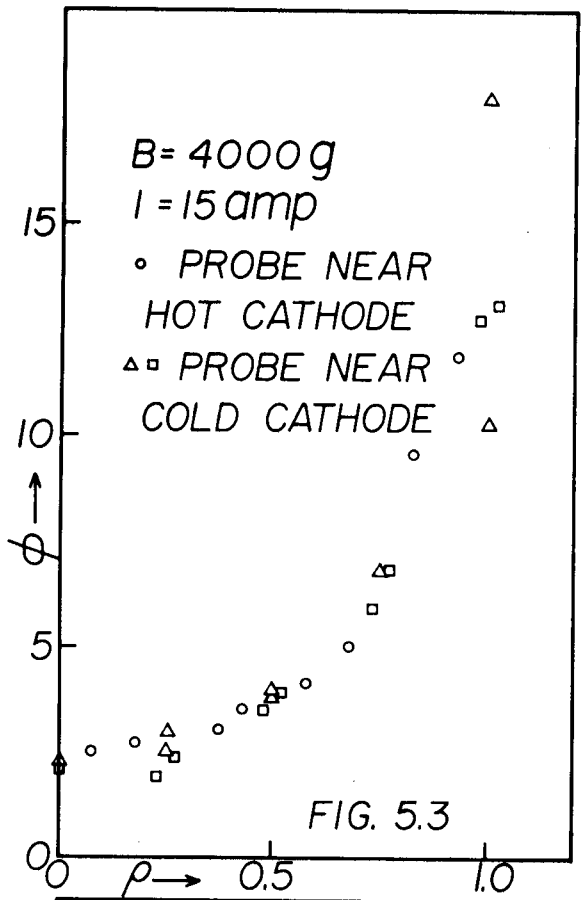

FIG. 5.3

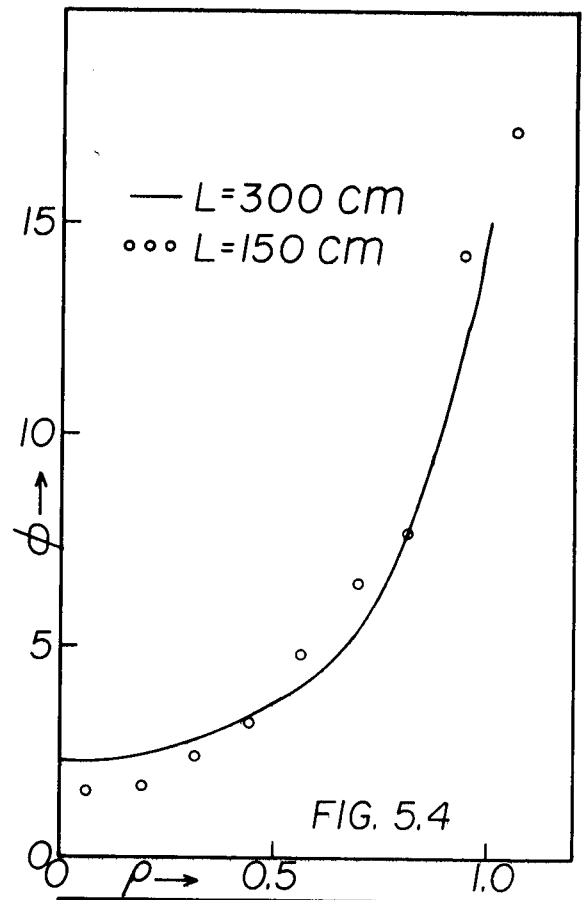

FIG. 5.4

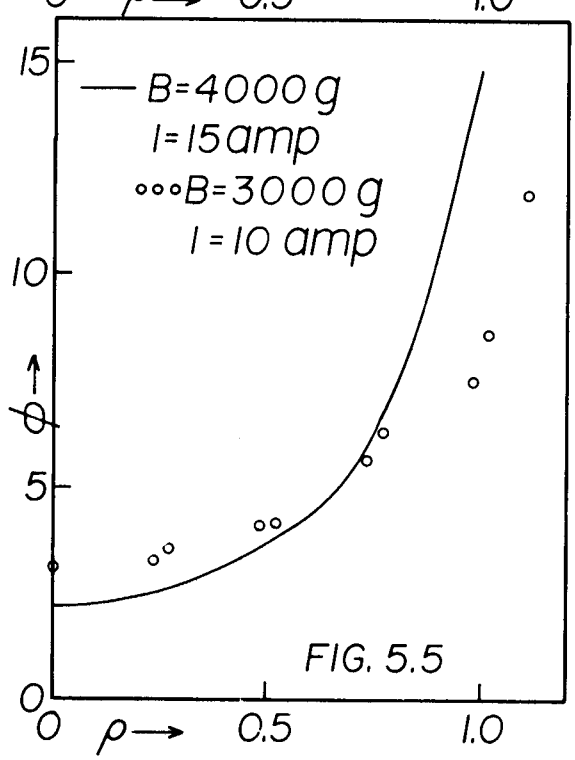

FIG. 5.5

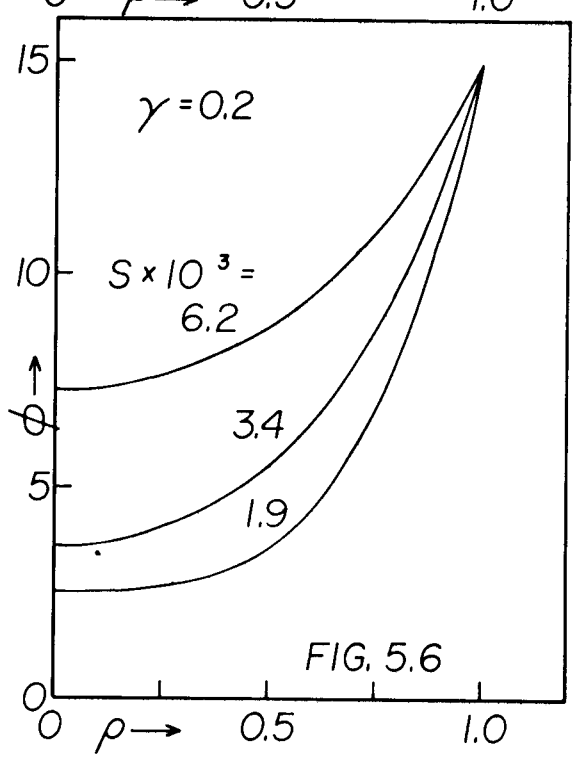

FIG. 5.6

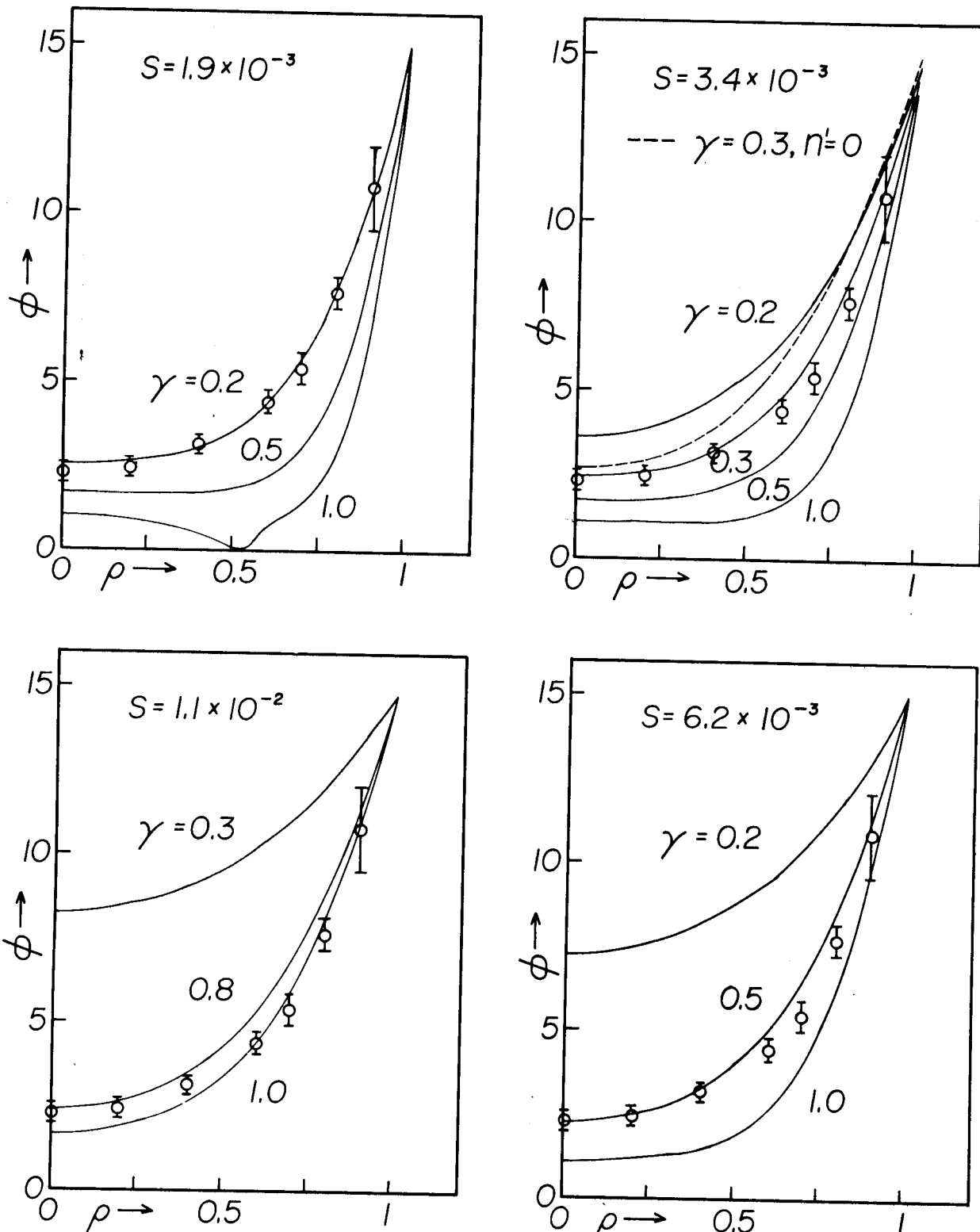
S = 1.9 × 10⁻³
γ = 0.2
0.5
1.0
S = 3.4 × 10⁻³
--- γ = 0.3, n' = 0
γ = 0.2
0.3
0.5
1.0
S = 1.1 × 10⁻²
γ = 0.3
0.8
1.0
S = 6.2 × 10⁻³
γ = 0.2
0.5
1.0
φ
ρ →
0
0.5
1
5
10
15

FIG. 5.7

The theoretical curves for $\phi(\rho)$ are shown in Figs. 5.6-5.7. The experimental points shown are averages taken from Fig. 5.3, and the error bars indicate the amount of scatter from run to run at standard conditions. The error due to uncertainty in the temperature measurements is of the same order of magnitude. In Fig. 5.6 is shown the variation of the radial potential profile with S, at constant γ; one notes that large values of S give rise to shallower potential wells. Since $S \sim B^{-2}$, this explains why a radial potential depression is not noticeable in reflex discharges in weak magnetic fields[26]. The variation of the potential on the axis $\phi(0)$ with S is shown in Fig. 5.2 for different γ; this graph is a very approximate one. In Fig. 5.7 are shown the potential curves for different S as γ is varied. For the lowest value of S, corresponding to an ion temperature of 0.1 eV, there is good agreement for $\gamma = 0.2$. This is exactly the value of γ found in Eq. (5.23); however, the latter was computed for $kT_i = 1$eV. At higher S, corresponding to $kT_i = 0.3$ and 1.0 eV, there is a fit, but not quite as good, for higher values of γ. For the highest S computed, corresponding to $kT_i = 3$ eV, the fit is poor and an unreasonably large γ is necessary to match the magnitude of the potential minimum. In view of the uncertainty in γ and in effective L, one can say that a reasonably good fit with experiment can be obtained for assumed ion temperatures from 0.1 to 1.0 eV. This assumes that the ion mobility is classical. On the other hand, one might expect the ion mobility to be enhanced, since the diffusion coefficients are assumed to

be enhanced. In this case, writing $\mu_{\perp i} = e D_{\perp i}/kT_i$ and $D_{\perp i} = \alpha ckT_e/eB$, we find that for $\alpha = 1/16$ (the Bohm value) and $T_e/T_i = 4$, $S = 1.9 \times 10^{-2}$, which is too large to be consistent with experiment. If $\alpha = 0.2$, the value found in stellarators, the value of S is so large that no solution is possible for any γ. Thus there is some evidence, in view of the theory, that the ion mobility is classical, while the ion diffusion is enhanced. This statement, however, depends on the assumption than $D_{\perp i} = D_{\perp e}$. If, in particular, $D_{\perp i} > D_{\perp e}$, as would be the case if streaming along lines of force increased the oscillation frequency seen by the electrons and hence diminished $D_{\perp e}$, then the fit of the potential profiles would be consistent with a somewhat higher $\mu_{\perp i}$.

If L is decreased, the theory predicts that the radial potential well would be deepened, since S would be decreased. Fig. 5.4 compares the experimental profiles with L = 150 cm and L=300 cm. The latter data were taken from Fig. 5.3. One sees that indeed the profile for the short machine is steeper. The difference is slight, however, since the "effective length" of the long machine is less than 300 cm (cf. Sec. 5.1). If the magnetic field is decreased, one would expect the potential well to be shallower, since S is increased. Fig. 5.5 shows this. Again the solid curve represents the data of Fig. 5.3. Unfortunately, the discharge current was also changed in this run, but according to the theory there should be no dependence on I except for the corresponding change in ϕ_d, the boundary condition at the anode.

5.4 The Voltage-Current Characteristic

A consequence of the assumption of space-charge-limited emission by the cathode is that all the terms (except the small recombination term) in the discharge equations are linear in n. Hence Eqs. (5.24) give the absolute value of Φ for any given value of Φ_d, the discharge voltage, but they can yield only the shape of the density profile. The absolute value of the density, and hence of the discharge current, is indeterminate.

This would not be true if temperature-limited emission occurred, since then the first term of Eq. (5.14) would not contain n, and hence n could no longer be multiplied by an arbitrary constant. However, temperature limitation is inconsistent with the experimental results when the cathode temperature is varied. The situation is not improved by assuming a cathode spot in which there is temperature limitation, with space-charge limitation elsewhere, since then the diameter of the spot would be indeterminate. If recombination were the limiting factor, the observed density would not have been so small that the recombination term is negligible. The density dependence of γ or M (through depletion of neutrals) must also by very small.

To understand what it is that determines the density, we must consider the expression for the discharge current I and the equation for the external circuit. Consider Eq. (5.25):

$$\frac{L}{2}\mu_{\perp i}^{*}\left(n\nabla_r\varphi+\frac{\partial n}{\partial r}\frac{\partial\varphi}{\partial r}\right)=\frac{N}{2}\gamma n v_e\iota(\varphi)+\gamma n v_e\sqrt{\frac{\pi}{2}\frac{m}{M}}-\frac{1}{2}n v_e e^{-\varphi}. \tag{5.25'}$$

This can be integrated over the cross section of the discharge to obtain

$$\frac{1}{2}L\mu_{\perp i}^{*}\,2\pi R\left[n\frac{\partial\varphi}{\partial r}\right]_R = \pi N\gamma v_e\int_0^R n\iota(\varphi)r\,dr + 2\pi\gamma v_e\sqrt{\frac{\pi m}{2M}}\int_0^R nr\,dr - \pi v_e\int_0^R nre^{-\varphi(r)}dr$$

$$\frac{1}{2}J_p \qquad\qquad \frac{1}{2}J_i \qquad\qquad \frac{1}{2}J_e \qquad (5.30)$$

The terms marked J_p, J_i, and J_e represent respectively the current of fast electrons leaving the cathodes, the ion current to the cathodes, and the electron current flowing into the cathodes. Thus the sum $J_p + J_i - J_e$ is just $\frac{1}{2}I/e$.

To clarify the role of the total density, we may write

$$n(r) = \bar{n}\,\nu(r), \qquad (5.31)$$

Where $\bar{n} = \int_0^R n(r)\,rdr$ and $\int_0^R \nu(r)\,rdr = 1$, so that $\bar{n}$ represents the absolute magnitude of the density, and $\nu(r)$ the density profile, which is determined by Eqs. (5.24) once Φ_d is given. Dividing by $\bar{n}$, we have for Eq. (5.30)

$$\frac{I}{2e\bar{n}} = L\mu_{\perp i}^{*}\pi R\left[\nu\frac{\partial\varphi}{\partial r}\right]_R$$

$$= N\pi\gamma v_e\int_0^R \nu(r)\iota(\varphi)r\,dr + 2\pi\gamma v_e\sqrt{\frac{\pi m}{2M}}\int_0^R \nu(r)r\,dr - \pi v_e\int_0^R \nu(r)\,e^{-\varphi(r)}r\,dr \qquad (5.32)$$

The circuit containing the discharge follows the equation

$$E = IR^{*} + \frac{kT_e}{e}\varphi_d + V_a, \qquad (5.33)$$

where Φ_d is the normalized plasma potential at r = R, R^{*} the total effective

resistance in series with the discharge, E the power supply voltage, and Va the voltage drop between the anode and the surface of the plasma. As before, we neglect Va.

For each Φ_d, Eqs. (5.24) give Φ (r) and ν (r), and therefore $I/\bar{n}$ as some function h of Φ_d. Eq. (5.33) then becomes

$$E = R^* \bar{n}\, h(\varphi_d) + \frac{kT_e}{e}\varphi_d . \qquad (5.34)$$

As the discharge builds up, I, and therefore $\bar{n}$, increases, and Φ_d must decrease, according to (5.34). However, Φ_d cannot decrease indefinitely. In ordinary arcs, the lower limit to the arc voltage is the ionization potential of the gas. In our case the observed Φ_d is several times the ionization potential. This is because there is another lower limit on Φ_d imposed by (5.32). This can be illustrated by assuming ν (r) to be constant; then (5.32) takes the form

$$A\left[\frac{\partial \varphi}{\partial r}\right]_R = B\int_0^R \iota(\varphi) r\,dr + C - D\int_0^R e^{-\varphi(r)} r\,dr , \qquad (5.35)$$

where A, B, C, and D are constants. Evidently, the l. h. s. is positive, but the r. h. s. can become negative if Φ is two small and the last term too large. Thus there is a lower limit $\Phi_{d\ min}$. Physically, this merely means that the potential barrier at the cathodes must be sufficient, when averaged over the radius, to prevent the plasma electrons from flowing into the cathodes in such numbers that the discharge current becomes negative.

If the discharge settles on the voltage $\phi_{d\ min}$, then Eqs. (5.32) and (5.33) determine I and $\bar{n}$ uniquely. Thus this theory predicts a constant-voltage discharge (with a horizontal V-I characteristic), in which the current, and therefore plasma density, is determined only by the external circuit. This is in general agreement with the observed characteristic (Fig. 3.1.1), which is nearly horizontal. The deviation from constant voltage is due to effects not included in the theory. Examination of Eq. (5.32) shows that $I/\bar{n}$ is an increasing function of ϕ_d. Actually, $I/\bar{n}$ must also depend on the efficiency of ionization. At high currents, this efficiency might be expected to decrease, say due to depletion of neutrals or increased diffusion losses, so that $I/\bar{n}$ would increase. Thus it is not unreasonable that ϕ_d should be higher than $\phi_{d\ min}$, at high currents. In other words, the slope of the V-I curve is due to any non-linearity in the dependence of (5.14) on $\underline{n}$.

The change of the I-V characteristic with pressure and magnetic field can also be explained qualitatively. Consider the curves of Fig. (5.6). As p increases or B decreases, $\mu_{\perp i}$ increases, and therefore S increases. As S increases, the potential well becomes shallower, and it is possible to sustain a sufficient cathode barrier with a smaller ϕ_d. Thus $\phi_{d\ min}$ would be expected to decrease as p increases or B decreases. This is in agreement with the experimental results shown in Figs. (3.1.1) and (3.1.2).

A remark should be made regarding an apparent contradiction in Eq. (5.32). If R is taken not to be the discharge radius but some interior

radius, the observations show that $\frac{\partial \varphi}{\partial r}$ is positive for all R, and therefore I (R) must be positive for all R. The measurements with a segmented cathode (Sec. 3.1.3), however, showed a negative current for small R. The reason is that the term containing $\iota(\phi)$ is missing for the cold cathode. When currents from both cathodes are added together, I (R) must always be positive. This means that there must be considerable emission from the center of the hot cathode, although the emitted electrons cannot gain enough energy to produce ionization.

5.5 Conclusion

By making a number of simplifying assumptions, it has been possible to derive equations for the radial distribution of density and potential in a reflex arc. By further assuming that $D_{\perp i} = D_{\perp e}$, one can obtain a simple equation for the radial potential distribution which contains a parameter S, which gives the scaling law of such discharges with changes in length, radius, pressure, and magnetic field. The potential profiles computed theoretically are in good agreement with experiment. The theory also predicts a constant-voltage discharge, in approximate agreement with experiment. The variation of the discharge voltage with pressure and magnetic field can also be qualitatively explained.

These results refer to the time-averaged characteristics of the discharge. The detailed mechanism of enhanced diffusion and its cause are left for further study.

APPENDIX

Probe Circuits and Techniques

This section deals with some developments in probes and probe techniques, both for d.c. and a.c. type measurements.

Our standard probe (Figure A.1) is encased in $\frac{1}{4}$" o.d. type 305 stainless steel seamless tubing. The probe itself is a tungsten wire with a tip diameter of approximately .015" and an exposed length of .060" to .070". A ceramic tube fits between the outer shaft and the tungsten core, extending some 2" beyond the shaft. The entire assembly is sealed on the top by a kovar-glass seal.

The ceramic used in the probe must satisfy the following criteria: it must withstand high temperature, provide good insulation and not outgas under bombardment in the discharge. The two best materials seemed to be BeO and Al_2O_3. It was found that the Al_2O_3 developed a conductive coating after exposure to the discharge, which did not occur on the BeO. Also tests were made with "blind" probes in which the ceramic extended 1/16" or more beyond the tungsten probe tip. The BeO covered probes showed less noise pick up than the others and less tendency to become coated with a conductive layer. This was therefore chosen as the standard ceramic for use in our probes.

Our standard probe circuit (Figure A.2) was used in obtaining characteristic curves as in Figure 3.1.4. The 4K resistors across the power supply

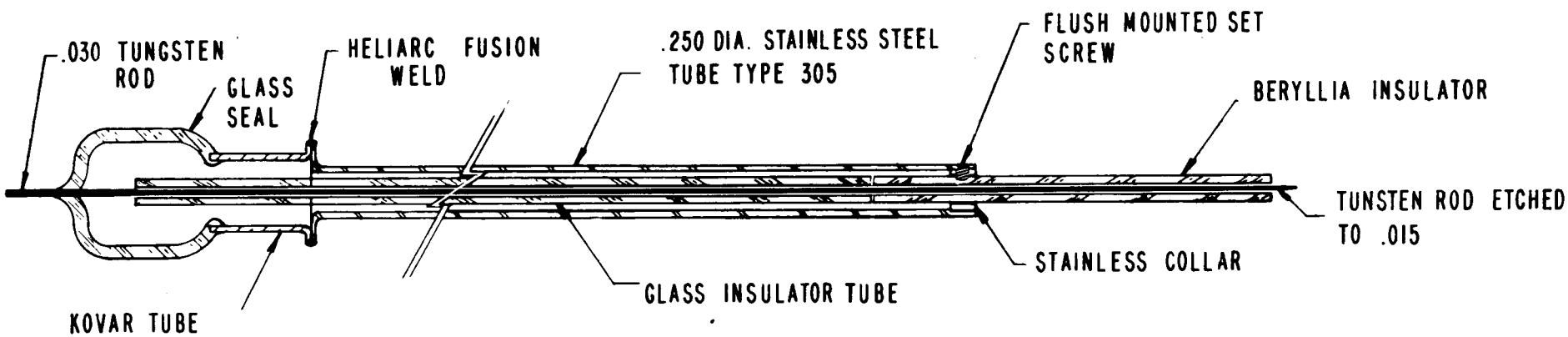

TYPICAL PROBE USED IN L-2 MACHINE

FIG. A. 1 DIAGRAM OF STANDARD PROBE

outputs are necessary to permit reverse currents through the supply. The two power supplies permit tracing the entire probe curve and centering it conveniently on the graph for any plasma floating potential. The probe current is measured by the voltage across the resistor R.

For measurements of the plasma noise, a different technique was used. The probe is terminated at the top of its shaft and connected by low capacitance cable to the appropriate analyzer (Figure A.3). The 100 K terminating resistor is chosen to have an impedance which is low compared to the input impendance (including cable capacitance) of the analyser in order to obtain an output independent of frequency up to hundreds of kc. The condenser in the terminating network is required to anchor the resistor load line at the floating potential of the probe. This is illustrated schematically in Figure A.4. In Figure A.4a are shown two probe traces differing only in their floating potential, and the resistor load line is given by the dashed line, no condenser being used in the terminating network. It is clear from the diagram that as the floating potential of curve (a) oscillates (i.e. the curve moves right and left between the dotted curves), a large voltage signal will be generated -- corresponding to the intersection points of the two lines. For probe curve (b), however, it will be seen that the generated signal will be very small. In Figure A.4b the condenser has been used and the load line goes through the $i = 0$ point of the d.c. curve, and hence the measured voltage depends only on the probe characteristic and not its floating potential.

By changing the 100 K termination resistor it was possible to find the value which cut the voltage signal to one half of its open circuit value, thus giving a measure of the source impedance of the oscillations. For most of our probe work this was found to be of order 5K. For the "blind probe" the source impedance was probably much higher, since the pickup voltage was lower by at least a factor of 10. This higher impendance is due to the necessity of coupling to the probe through the ceramic instead of by the exposed tip. This means that the exposed tip probe effectively indicates conditions at its tip rather than along its entire length.

The source impendance of the anode noise has been measured in a similar manner. Insertion of a 15μf condenser between the machine anode and ground did not reduce the amplitude of the anode noise signal, showing a source impendance of less than $\frac{1}{2}\ \Omega$ for frequencies $\gtrsim$ 30 kc, where the noise had its lowest frequency peak. When a large condenser ($\sim$ 1000μf) is used as a short across the discharge, it is found that the anode can be held at constant potential and that the current fluctuations are increased by an order of magnitude in the wire between the condenser and the P.I.G. anode. This suggests that the anode noise may be due to fluctuations in the discharge current, the condenser supplying current as necessary to hold the anode voltage constant. Under normal operating conditions, the current fluctuations are kept low by the constant current supply. It is interesting to note that while this large condenser essentially eliminates the voltage fluctuations on the anode, no

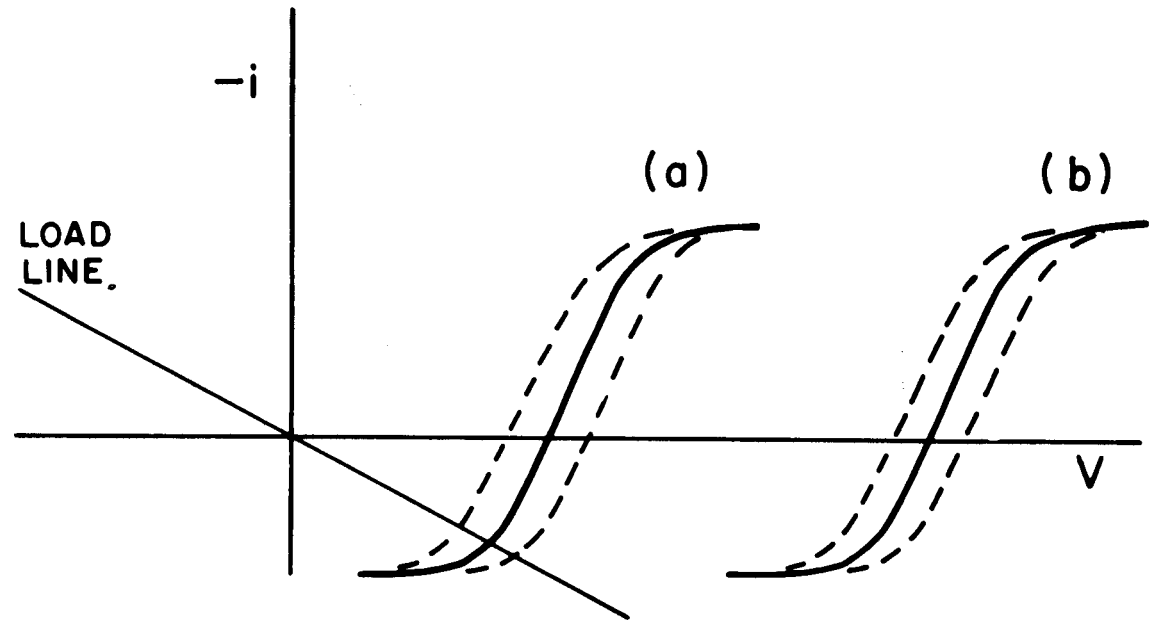

A. 4a

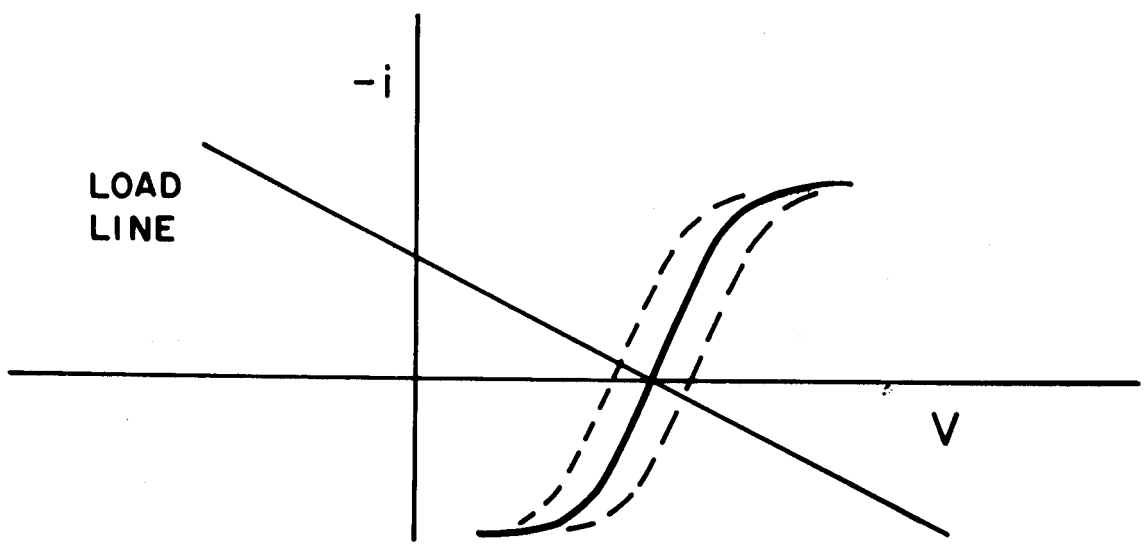

A. 4b

FIG. A.4 EFFECT OF CONDENSER TO MAKE PROBE SIGNAL INDEPENDENT OF FLOATING POTENTIAL

effect is observed on the noise signal of a floating probe inserted in the plasma, indicating that the oscillations in the body of the plasma are indeed independent of the anode fluctuations.

Frequently it was observed (Figure A.5) that the density profiles given by the probe were not symmetrical about the center of the discharge but gave a lower value when the probe was inserted beyond the axis. Inserting a probe from the opposite direction gives just the complementary effect so that the sum of the two curves is symmetric (Figure A.6). That this is due to local phenomena has been shown by experiments on the effect of the probes on the discharge. In particular there is no change in the probe characteristic of a fixed probe as another probe is moved in front of it through the nearest upstream port available. Also when a probe is inserted beyond the center of the discharge no effect can be seen on the microwave density monitor as the probe characteristic is swept out. If the probe did in fact cause a 10% reduction in plasma density, this should have been observable in such a test.

In operation the probes were outgassed before use. This procedure consisted of drawing electron current to heat the probe until it was white hot. Only after outgassing were reproducible characteristics obtained. This was not sufficient, however, to eliminate the effects discussed in the preceding paragraph, and which are probably connected with the heating of the ceramic insulator by the discharge.

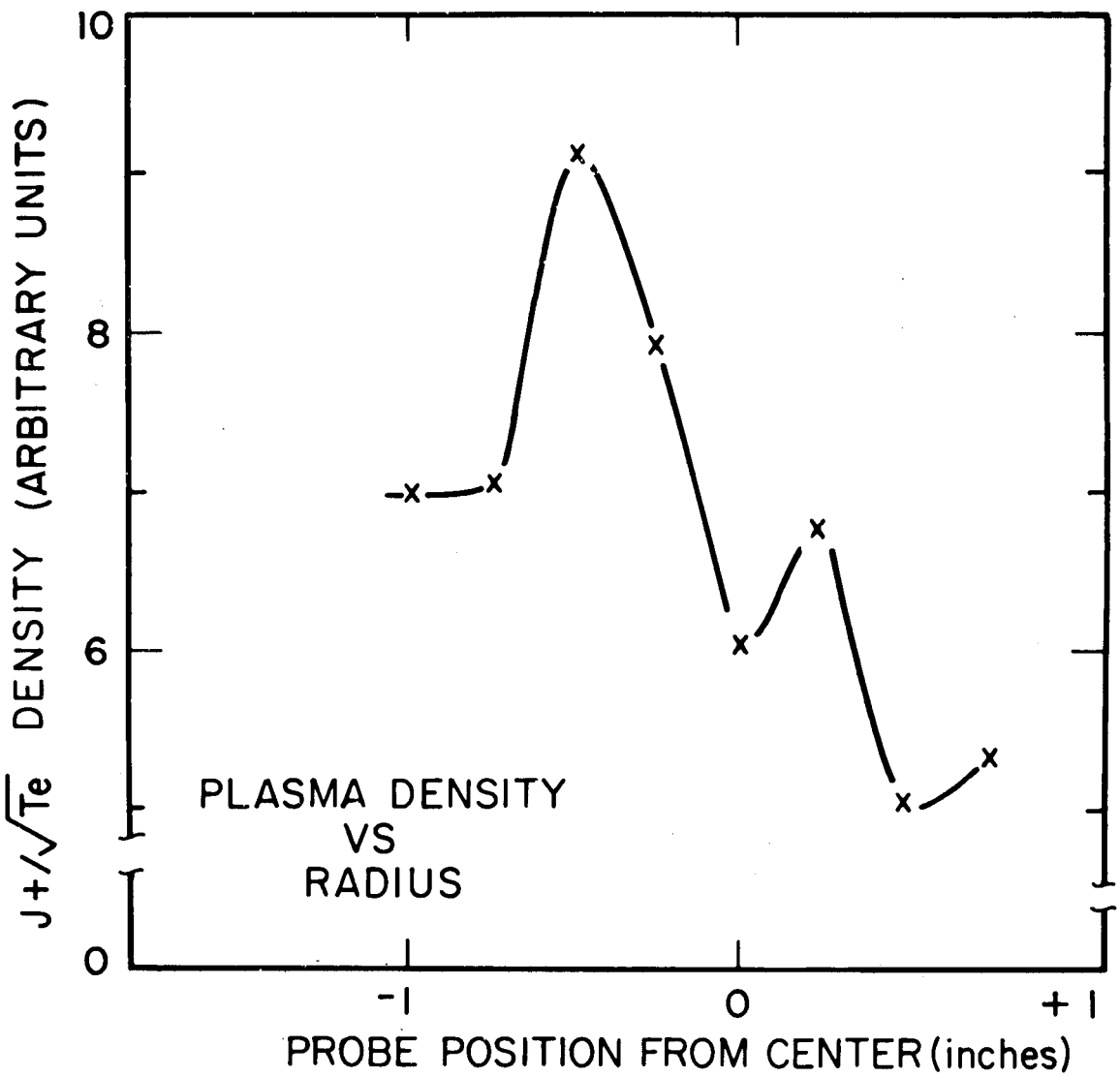

FIG. A.5 EFFECT OF INSERTING PROBE BEYOND DISCHARGE AXIS

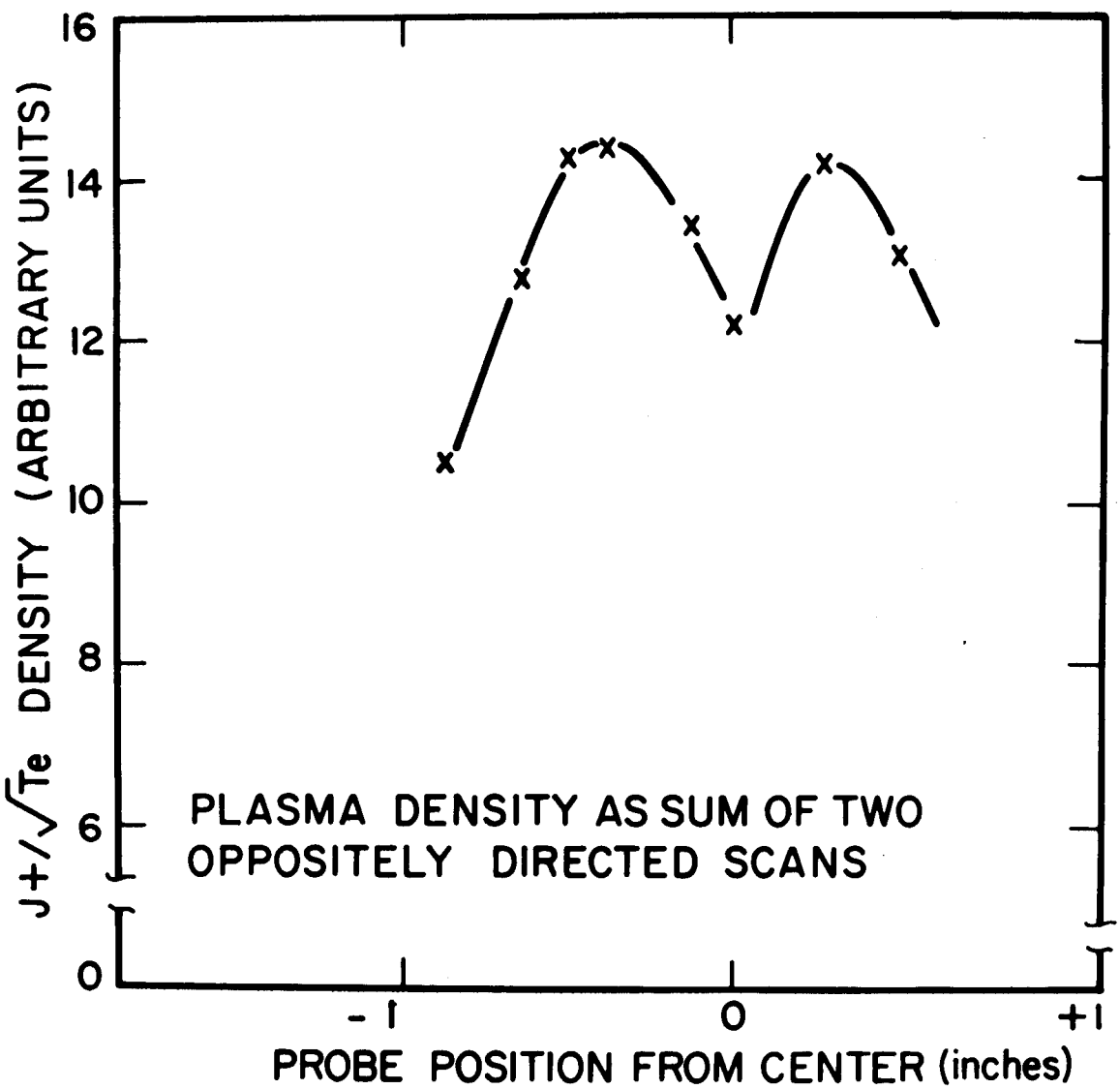

FIG. A.6 SUM OF TWO PROBE CURVES TAKEN FROM OPPOSITE SIDES OF DISCHARGE

A technique for following fast variations in the probe characteristic due to changes in the plasma has been devised by F. F. Chen. This is essentially a double probe technique and is described fully in MATT-62.

Some of the probe and cable capacitances of interest are:

BeO probe	7-8μμf
Al_2O probe	10-15μμf
Coaxial shielded probe	25μμf
10 feet RG 114/u cable	75μμf

The shielded probe (Figure A.7) cited above is similar to the standard probe except that the inner conductor is surrounded by a thinner ceramic enclosed in a thin molybdenum tube, which is in turn covered with another layer of ceramic. In spite of its more complete shielding, this probe was very much like the others in its operation, since pickup through the ceramic was negligible even in the unshielded probe. With about 100μμf of stray capacity on the probe, and a source impedance of about 1K for the probe hash, it is evident that good frequency response cannot be obtained beyond 1 or 2 mc.

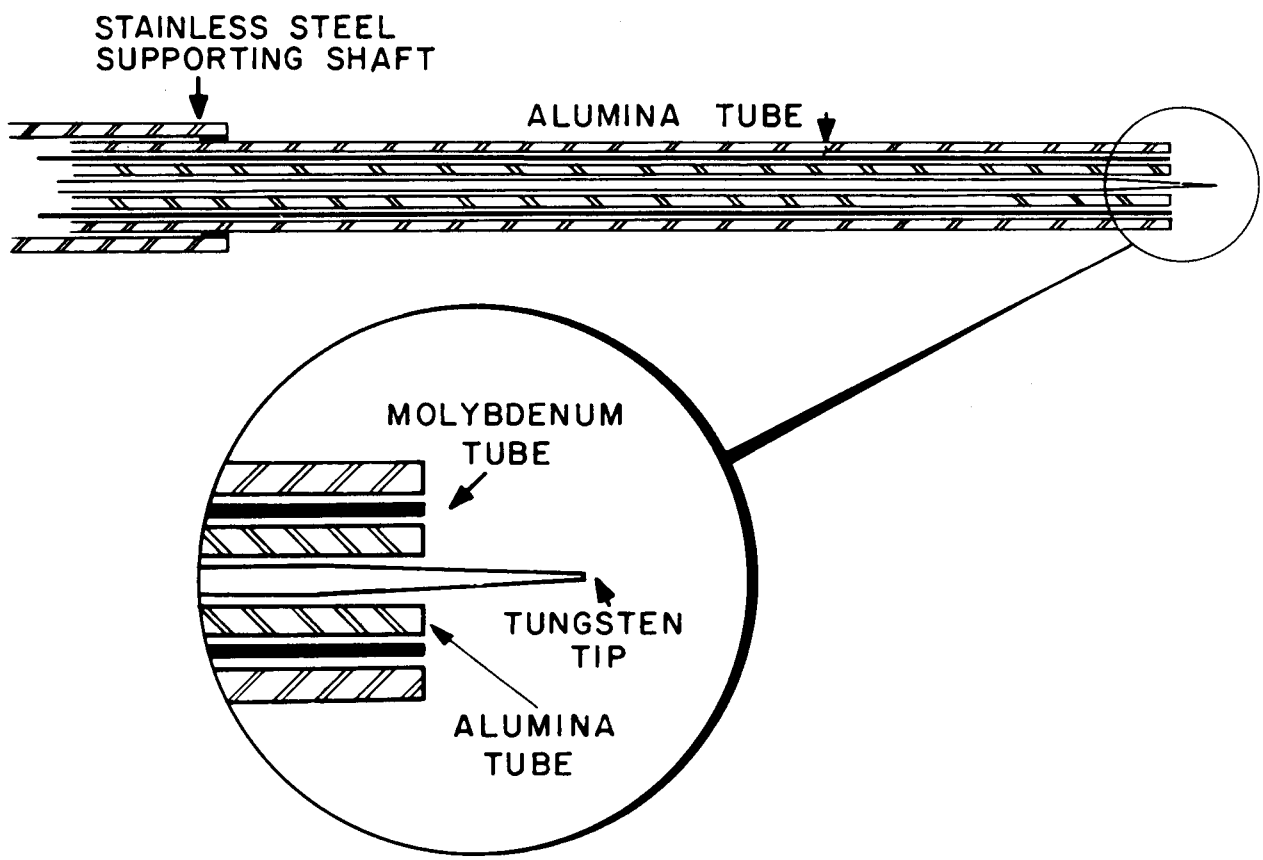

FIG. A.7 TYPICAL DOUBLE SHEATH PROBE

References

(1) S.C. Brown, Basic Data of Plasma Physics, Wiley, New York 1959, P. 227.

(2) F.F. Chen, J. File, and W. Lehmann, Technical Memorandum 68. (NYO 8071) (1959).

(3) D. Bohm, E.H.S. Burhop and H.S.W. Massey, Chapter 2 in Guthrie & Wakerling Characteristics of Electrical Discharges in Magnetic Fields. McGraw-Hill, New York 1949.

(4) See also Mark A. Heald, Matt-17.

(5) A.V. Phelps and S.C. Brown, Phys. Rev. 86, 102 (1952).

(6) N. D'Angelo, Phys. Rev. 121, 505 (1961).

(7) A. Kuckes, R. Motley, E. Hinnov, and J. Hirschberg, Phys. Rev. Letters 6, 337 (1961).

(8) F. Chen, Matt-62.

(9) L. Spitzer, Physics of Fully Ionized Gases, Interscience, New York 1956 P. 82.

(10) ——ibid p. 86.

(11) I.B. Bernstein and R.M. Kulsrud, Physics of Fluids 3, 937 (1960).

(12) Ref. (9) p. 76.

(13) W.H. Cramer, and J.H. Simons, J. Chem, Phys. 26, 1272 (1957).

(14) L.M. Chanin and M.A. Biondi, Phys. Rev. 106, 473 (1957).

(15) J.B. Hasted, Proc. Roy. Soc. (London) A205, 421 (1951).

(16) H.S.W. Massey and E.H.S. Burhop "Electronic and Ionic Impact Phenomena" Oxford University Press, Oxford 1951 p.38.

(17) H. Maier-Leibnitz, and Z. Physik 95, 489 (1935).

(18) Ref. 16 P. 174.

(19) Ref. 3 P. 62

(20) S. Dushman, Vacuum Technique, John Wiley, New York 1949 P. 702.

(21) I. Langmuir, Phys. Rev. 33, 954 (1929)

(22) F.F. Chen, Matt-77

(23) A. Von Engel, Ionized Gases, Oxford University Press, Oxford 1955 P. 137

(24) —ibid P. 143

(25) —ibid P. 141

(26) Salz, Meyerand, Lary, and Walch, Phys. Rev. Letters 6, 523 (1961).